Copyright Warning & Restrictions

The copyright law of the United States (Title 17, United States Code) governs the making of photocopies or other reproductions of copyrighted material.

Under certain conditions specified in the law, libraries and archives are authorized to furnish a photocopy or other reproduction. One of these specified conditions is that the photocopy or reproduction is not to be "used for any purpose other than private study, scholarship, or research." If a, user makes a request for, or later uses, a photocopy or reproduction for purposes in excess of "fair use" that user may be liable for copyright infringement,

This institution reserves the right to refuse to accept a copying order if, in its judgment, fulfillment of the order would involve violation of copyright law.

Please Note: The author retains the copyright while the New Jersey Institute of Technology reserves the right to distribute this thesis or dissertation

Printing note: If you do not wish to print this page, then select "Pages from: first page # to: last page #" on the print dialog screen

ABSTRACT

Agitation Requirements for Complete Liquid Dispersion in Liquid-Liquid-Gas Systems

by
Emad Ahmad Abu-Hakmeh

A number of studies have been published in the literature on the determination of the agitation intensity at which two immiscible liquids become completely dispersed in mechanically agitated vessels. However, no information is currently available on the agitation intensity required for the complete dispersion of two liquids in the presence of an additional gas phase. Therefore, the main objective of this study was to experimentally determine the minimum agitation speed for complete liquid-liquid dispersion, N_{cd}, in liquid-liquid-gas systems as a function of gas flow rate, impeller type, impeller size, and impeller off-bottom clearance. The minimum agitation speed was first determined visually. In order to eliminate the ambiguity of the visual determination method, a novel observer-free method was developed. This method is based on the analysis of the content of dispersed phase in samples taken from the mixture at different agitation speeds. The results indicate that the values of N_{cd} obtained with the proposed method are in close agreement (within 4%) with those obtained visually. The minimum agitation speed, N_{cd}, was found to be strongly affected by the air sparging rate. Higher agitation speeds were required to attain the complete dispersion state at higher air sparging rates. N_{cd}, was also found to be strongly affected by impeller type, impeller size, and impeller clearance for both gassed and ungassed systems.

A mathematical model based on Kolmogoroff's theory of isotropic turbulence was developed to predict the results obtained experimentally under gassed conditions. Provided that the impeller was not flooded, good agreement was found between the experimental values of N_{cd} and the corresponding values predicted by the model.

AGITATION REQUIREMENTS FOR COMPLETE LIQUID DISPERSION IN LIQUID-LIQUID-GAS SYSTEMS

By
Emad Ahmad Abu-Hakmeh

A Thesis
Submitted to the Faculty of
New Jersey Institute of Technology
in Partial Fulfillment of the Requirements for the Degree of
Master of Science in Chemical Engineering

Department of Chemical Engineering,
Chemistry, and Environmental Science

October 1993

APPROVAL PAGE

Agitation Requirements for Complete Liquid Dispersion in Liquid-Liquid-Gas Systems

Emad Ahmad Abu-Hakmeh

Dr. Piero M. Armenante, Thesis Advisor (date)
Associate Professor of Chemical Engineering, NJIT

Dr. Basil C. Baltzis, Committee Member (date)
Associate Professor of Chemical Engineering, NJIT

Dr. Demetri Petrides, Committee Member (date)
Assistant Professor of Chemical Engineering, NJIT

BIOGRAPHICAL SKETCH

Author: Emad Ahmad Abu-Hakmeh

Degree: Master of Science in Chemical Engineering

Date: October 1993

Undergraduate and Graduate Education:

- Master of Science in Chemical Engineering,
  New Jersey Institute of Technology, Newark, NJ, 1993
- Bachelor of Science in Chemical Engineering,
  New Jersey Institute of Technology, Newark, NJ, 1990

Major: Chemical Engineering

Presentations and Publications:

- Armenante, P. M., and E. A. Abu-Hakmeh. "Complete Liquid Dispersion in Agitated Gas-Liquid-Liquid Mixtures.", presented at *The First Conference on Process Engineering*, Florence, Italy, 13-15, May 1993.
- Armenante, P. M., and E. A. Abu-Hakmeh, "Minimum Agitation Speed for Complete Liquid Dispersion in Mechanically Agitated Gas-Liquid-Liquid Systems", presented at the *Engineering Foundation Conference "Mixing XIV"*, Santa Barbara, CA, USA, 20-25, June 1993.

This thesis is dedicated to my sons, Ahmad and Khaldoon Abu-Hakmeh

ACKNOWLEDGMENT

I would like to express my appreciation to all the people who contributed to the successful completion of this thesis. I am thankful to my thesis committee members, Dr. Basil Baltzis and Dr. Demetri Petrides for their patience in reviewing the thesis and for their recommendations. My thesis advisor, Dr. Piero Armenante deserves a very special acknowledgment for his guidance during this research. Completion of this thesis would not have been possible without his constant encouragement and moral support.

I would also like to thank the mixing laboratory members, Mr. Gwo-Ming Chang and Mr. Joseph Chou for their timely help and suggestions.

Finally, I would like to express my deepest gratitude towards my parents and my wife, whose sacrifices and love have made it possible for me to complete this thesis.

TABLE OF CONTENT

LIST OF TABLES

LIST OF FIGURES

LIST OF APPENDICES

A. Figures for Chapter 6

Figure **Page**

B. Experimental Data and Predicted Results

Table **Page**

Table **Page**

C. Plots of V* vs. N

Figure **Page**

Figure **Page**

NOMENCLATURE

B	baffle width (m)
C	impeller off-bottom clearance (m)
C_0	a constant determined for different impeller types and locations
Ct	impeller clearance measured from the liquid surface (m)
D	impeller diameter (m)
d	liquid droplet diameter (m)
H	liquid height in the vessel (m)
H_{smp}	sampling point location measured from the bottom of the vessel (m)
m	experimental value of slope in equation 6.1
N_A	gas flow number, Q/ND^3 (dimensionless)
N_{Bo}	Bond number, $D^2g\Delta\rho/\sigma$ (dimensionless)
N	agitation speed (rpm)
N'_{cd}	the minimum impeller speed for nearly uniform mixing
N_{cd}	minimum agitation speed for complete liquid-liquid dispersion (rpm)
$N_{cd-gassed}$	N_{cd} determined under gassed conditions (rpm)
$N_{cd-ungassed}$	N_{cd} determined under ungassed conditions (rpm)
ΔN_{cd}	$N_{cd-gassed} - N_{cd-ungassed}$ for the same agitation speed (rpm)
$N_{cd-model}$	N_{cd} predicted by the model (rpm)
N_{cd-smp}	N_{cd} determined experimentally (rpm)
N_{cd-vis}	N_{cd} determined visually
N_{Fr}	Froude number, $DN^2\rho_M/g\Delta\rho$ (dimensionless)
N_{Ga}	Galileo number, $D^3\rho_M g\Delta\rho/\mu_M^2$ (dimensionless)
N_p	power number, $P/\rho N^3D^5$ (dimensionless)
N_R	the impeller speed at the vigorous start of gas recirculation, (rpm)

P_G	power input under gassed conditions (watts)
P_0	power input under ungassed conditions (watts)
Q	gas flow rate from the sparger (vvm)
Q_{air}	air flow rate from the sparger (vvm)
R	volume of the phase present in small amount in the sample
Re	Reynolds number, $\rho ND^2 / \mu$ (dimensionless)
S	sample total volume (L)
T	vessel diameter (m)
V*	the volume fraction of the dispersed phase (%)
vvm	volume of sparged gas (L/min) per volume of liquid in the vessel (L)
W	width of impeller blade (m)
$W(N_A)$	a function of the flow number, the power ratio of gassed to ungassed conditions at the same agitation speed (dimensionless)

Greek Letters

α, α_0	constants
ε	total power consumption ($\varepsilon_{LG} + \varepsilon_G$) (watts)
ε_G	the power input due to the bubbling of gas (watts)
ε_{LG}	the power input under gassed conditions (watts)
μ_c, μ_d	viscosities of continuous and disperse phases (N s/m^2)
ρ	mixture density (kg/m^3)
ρ_c, ρ_d	densities of continuous and disperse phases (kg/m^3)
$\Delta\rho$	$\lvert\rho_c - \rho_d\rvert$ (kg/m^3)
σ	interfacial tension (N/m)
τ	shear force per unit area (kg/m sec^2)
ϕ	volume fraction of dispersed phase

CHAPTER 1

INTRODUCTION

Multiphase mixing in agitated vessels is a fundamental unit operation for many chemical, petrochemical, biochemical, and pharmaceutical process industries. In many of these processes, mixing and the operating parameters that control it play a key role in the optimization of the overall process. As a result, multiphase mixing has become a very active area of research and investigation.

A number of studies have been published in the literature for the experimental determination of the minimum agitation speed ($N_{cd-ungassed}$) for complete liquid-liquid dispersion in mechanically agitated vessels. However, no information is currently available for $N_{cd-gassed}$, i. e., the agitation speed required to completely disperse two liquids in the presence of an additional gas phase. This situation is typically encountered in many industrial processes, such as the fermentation of antibiotics in which air is sparged to provide oxygen to the microorganisms and an immiscible nutrient oil is added to stimulate antibiotic production.

Therefore, this study focused on the determination of the minimum agitation intensity at which two liquids, in a mixing vessel, become completely dispersed in the presence of an additional gas phase. At or near this point all phases are in contact with each other, thus promoting mass transfer and interphase reactions, while minimizing the power consumption and the possibility of obtaining stable emulsions.

The specific objectives of this work were: to visually determine the point at which the minimum agitation speed, N_{cd-vis}, for the complete dispersion of two liquids in the presence of an additional gas phase is achieved; to determine the minimum agitation speed, N_{cd-smp}, using a novel method to analyze the experimental data; to develop a mathematical model to predict the minimum agitation speed, $N_{cd-model}$,

under gassed conditions; and finally, to investigate the effect of mixing parameters, particularly impeller size, type, and off-bottom clearance, on the minimum agitation speed for complete dispersion of two liquids under both gassed and ungassed conditions.

CHAPTER 2

LITERATURE SURVEY

2.1 Liquid-Liquid Dispersion

Liquid-liquid dispersion in mechanically agitated vessels finds extensive applications in mixer-settler design in extraction operations. The minimum impeller speed for complete dispersion should be known to enable efficient design of the mixer. The earliest publication which considered the minimum agitation speed for complete dispersion is Nagata's [1] limited study on liquid-liquid systems in an unbaffled flat-bottomed vessel using a centrally mounted four-bladed flat-blade impeller with (T/D) of 3 and a blade width of 0.06T. He obtained the following empirical correlation for N_{cd}:

$$N_{cd} = 6D^{-2/3}\left(\frac{\mu_c}{\rho_c}\right)^{1/9}\left(\frac{\rho_c - \rho_d}{\rho_c}\right)^{0.26} \qquad (2.1)$$

A related phenomenon was studied by Quinn and Sigloh [2]. They found that phase inversion, in most of the water-organic systems they studied, occurred at agitation speeds of two to three times N_{cd} for equal-volume fractions of two immiscible liquids.

Skelland and Seksaria [3] studied the effects of liquid properties, impeller location, impeller type, and multiple impellers on N_{cd}. They proposed the following equation:

$$N_{cd} = C_0 D^{\alpha_0} \mu_c^{1/9} \mu_d^{-1/9} \sigma^{0.3} \Delta\rho^{0.25} \qquad (2.2)$$

where C_0 and α_0 are functions of impeller type and location.

Skelland and Jai Moon Lee [4] correlated the minimum impeller speed needed for nearly uniform liquid-liquid dispersion in baffled vessels, and described the effects of impeller type, size, and location, and the effect of liquid properties on the degree of mixing. They expressed the degree of mixing in terms of the mixing-index concept

developed by Hixon and Tenney [4] in their work on solid-liquid systems. They calculated the composition of each sample as "percentage mixed" by the formula:

$$\text{Percentage mixed} = \frac{R}{S/2} \times 100 \qquad (2.3)$$

where R is the volume of the phase present in smaller amount in the sample and S is the sample total volume. They defined the minimum impeller speed for nearly uniform mixing (N'_{cd}) as the speed corresponding to a mixing index (defined as $\frac{R}{S/2} \times 100$) of 98% at all sampled parts of the vessel.

Skelland and Ramsay [5] obtained an empirical correlation of the minimum agitation speed needed for complete liquid-liquid dispersion in baffled vessels. They correlated their observations from 251 runs, the observations of 35 runs by van Heuven and Beek [6] and the observations from 195 runs by Sekllland and Seksaria [3], with the expression:

$$(N_{Fr})_{min} = C^2 (\frac{T}{d})^{2\alpha} \phi^{0.106} (N_{Ga} N_{B0})^{-0.084} \qquad (2.4)$$

where C and α are functions of impeller type, location, and the ratio (H/T).

In these and most of other studies in the area of liquid-liquid dispersion N_{cd} was determined visually. However, Armenante and Huang [7] developed a new method to experimentally determine N_{cd} by taking samples from the liquid mixture at different agitation speeds and plotting the fraction of the dispersed phase in each sample against the corresponding agitation speed. They found that when connecting the resulting points by straight lines a sharp change in the slope occurred in correspondence with the visually determined minimum agitation speed. They also found that their method was independent of sampling point location and type of agitation. By analyzing their data with the method they developed to determine N_{cd-smp}, they found a good agreement between the values so obtained and those obtained visually.

2.2 Power Requirement in Liquid-Liquid Systems

The power consumed in mixing processes is the energy per unit time which is transferred from the impeller to the fluid. Power is one of the most important fundamental parameters associated with the intensity of mixing and completeness of dispersion. The power consumption in agitated vessels is a function of impeller type, agitation speed, the physical properties of the fluid being mixed, and the geometric characteristics of the impeller and the system. The power required to attain certain mixing conditions was studied by several investigators.

White and Brenner [8] were the first to determine the various power law exponents by dimensional analysis. They defined the drag coefficient group $(\frac{Pg_c}{\rho N^3 D^5})$, called the power number, N_p, and proposed that this dependent variable characterizes the flow pattern. Their final power correlation was given as:

$$\frac{P}{D\mu N^2 T^{1.1} W^{0.3} H^{0.6}} = 0.000129(\frac{\rho N D^2}{\mu})^{0.86} \qquad (2.5)$$

Their equation fitted the data for Reynolds numbers from 10^4 to 10^5 but diverged from the data for impeller Reynolds numbers below 10. They showed that viscosity has a minor effect on the power consumed in turbulent flow regimes.

Rushton, Costich and Everett [9] studied the power characteristics of mixing impellers using five impeller types of diameters from 0.06 m to 1.2 m. They used baffled and unbaffled configurations, vessels of diameters from 0.2 m to 2.5 m, and fluids of viscosity from 1 cP to 40,000 cP. They obtained a correlation, using dimensional analysis, for the power number, N_p, in terms of the impeller Reynolds number, Re. Their correlation is:

$$N_p = \frac{P}{\rho N^3 D^5} = K(Re)^m \qquad (2.6)$$

Bates, Fondy, and Corpstein [10] investigated the effects of geometry on power drawn by impellers. They pointed out that the flow pattern around the impeller

changes as a function of impeller-to-tank geometry. They examined the effects of impeller type, blade angle, blade width and number, tank to impeller diameter ratio, baffle width and number, impellers spacing, and impeller clearance, on power consumption. They found that the power input is a very strong function of the off-bottom impeller clearance.

2.3 Gas-Liquid Dispersion

Nearly twenty five percent of all chemical reactions occur in gas-liquid systems [11]. A considerable percentage of these reactions are carried out in agitated tank reactors. Hydrogenation reactions, where the gas phase (hydrogen) is nearly pure , and oxidation, where the gas (oxygen) is soluble in the liquid, are examples of the many reactions carried out in such systems.

Several investigators have studied two-phase, gas-liquid mixing in agitated vessels in order to optimize the design of agitated tank reactors needed in many industrial processes. The areas of greatest interest for gas-liquid dispersion in agitated tanks are the determination of the minimum agitation speed to attain complete dispersion, the hydrodynamic flow regimes occurring around the impeller and in the vessel, and the determination of the studies of gas bubble size and holdup, interfacial area between the gas and the liquid over which transport occurs, and mass transfer coefficient, k_{la}. Any study in this field is affected by the impeller agitation speed, gassing rate, fluid properties, and tank and impeller geometry.

Many studies of gas-liquid dispersion indicated that a vortex system (low-pressure regions where sparged gas accumulates before being dispersed) exists around the impeller blades during the process of agitation. These low pressure regions are known in literature as ventilated cavities. The type of cavity formed is a strong function of impeller geometry, gassing rate from the sparger, agitation speed, and gas

recirculation rate. Takeda and Hoshino and Takashima and Mochizuki (from Tatterson [11]), were among the first researchers to point out the presence of vortex systems around the impeller blades.

Smith and Verbeek [12] studied the cavity development and cavity regimes around the impeller blades in boiling liquids using Rushton impeller in a system of H = T = 2.5 D and 3 D. They found that the general nature of the gas cavities were similar to those generated in gassed systems.

The six-blade disk style turbine is widely used in aerated systems of standard configuration (Holland and Chapman, from Tatterson [11]) with gas sparging below the impeller in fully baffled turbulent agitated tank. In this configuration the disk forces the gas to pass through the high shear impeller region and this results in efficient break-up of gas flow into bubbles and effective dispersion of the bubbles throughout the tank. Gas dispersion by disk turbines at constant air flow rate from the sparger can be described as follows [13]:

1. At low impeller speed, the buoyant forces of the bubbles dominate over the centrifugal forces, thus the gas is not dispersed and leaves from the center of the vessel;
2. Increasing the agitator speed enlarges the area of gas bubbling at the top of the tank with no bubble movement in the bottom;
3. Higher agitation speeds result in gas circulation in the upper part of the tank with very limited movement in the lower region;
4. Further increase in the agitator speed results in circulation throughout the vessel;
5. Finally, any more increase in the agitation speed produces gross circulation.

The minimum agitation speed for complete gas dispersion had been recently defined by Greaves and Kobbacy (from Tatterson [11]) to occur between stage three and stage four. Greaves and Kobbacy defined complete gas dispersion as the

condition where the sparged gas coalesced with the impeller gas cavities and was then dispersed without recirculation to the impeller. They referred to this phenomenon as "The Efficient Mixing Zone". They also developed a correlation for the impeller speed at the vigorous start of recirculation as:

$$N_R = 0.57\left(\frac{T^{0.97}Q^{0.13}}{D^{2.34}}\right) \qquad (2.7)$$

2.4 Power Requirements in Gas-Liquid Systems

The power drawn by the impeller is a function of the physical properties of the fluid, the geometric characteristics of the system, and the hydrodynamic flow regimes occurring during the process of agitation. The introduction of a gas into a mixture in which a mechanical impeller is rotating produces a mixture of lower average density. Power data of gassed systems are commonly presented in the form of plots of the ratio of gassed condition power to ungassed condition power $(\frac{P_g}{P_0})$ against the flow number N_A which is equal to $\frac{Q}{ND^3}$. The ratio of $\frac{P_g}{P_0}$ drops typically, from 1.0 to a value between 0.3 and 0.6, as N_A approaches 0.035 to 0.05 (from Tatterson [11]).

Michel and Miller [14] correlated gassed power for disk turbine in tanks up to 0.3 m in diameter through the following expression:

$$P_g = C\left(\frac{P_0^{\,2}ND^3}{Q^{0.65}}\right)^{0.45} \qquad (2.8)$$

where C is a function of the impeller geometry. They found the value of C to be 0.08 for disk turbine when units of horse power, revolutions per minute, feet, and cubic feet per minute were used.

Yung et al. [15] found that the Michel-Miller expression was adequate to correlate their data for both disk turbine and flat blade turbine. They found that the Michel-Miller constant was 0.812 and 0.829 for disk turbine and flat blade turbine,

respectively. On the other hand, Gary et al. [16] pointed out that the Michele-Miller correlation yields incorrect predictions at high gas flow rates.

These correlations can be applied under specific conditions. However, the complexity of the gas-liquid hydrodynamics and gas recirculation (Warmoeskerken and Smith) [17] are still standing over the development of a single power curve correlation.

2.5 Liquid-Liquid-Gas Dispersion

Liquid-liquid-gas mixing is essential to a variety of processes such as the use of nutrient oil in the production of antibiotics in gassed fermentors, and gas-liquid reactions with product separation in the immiscible organic liquid phase. The presence of the gas complicates the already complex fluid dynamics of two-liquid mixtures. The presence of a third phase changes the flow behavior and makes the system more difficult to analyze.

Liquid-liquid-gas systems have not been studied to the same extent as other three-phase systems. In addition, no data on the minimum agitation speed required to completely disperse both the gas and one of the liquids into the continuous liquid phase, have been reported in literature.

However, a related phenomenon was studied by Susanto [18]. She studied the effect of the presence of an additional gas phase on the complete suspension of particles in solid-liquid-gas systems. The solid particles in such a system have a fixed, constant diameter, while the droplets produced in liquid-liquid systems, have different diameters. Therefore, the approach in modeling the effect of the presence of gas on liquid dispersion is more complicated than that used for the solid suspension case.

CHAPTER 3

A THEORETICAL MODEL FOR THE PREDICTION OF THE MINIMUM AGITATION SPEED TO ATTAIN COMPLETE LIQUID-LIQUID DISPERSION UNDER GASSED CONDITIONS

According to Kolmogoroff's (from Hinze [19]) theory of isotropic turbulence, turbulent flow (for example in a mixing system) produces primary eddies of similar wavelength or scale to the dimensions of the main flow stream. These large primary eddies are unstable and disintegrate into smaller eddies. Most of the kinetic energy is contained in the large eddies, but dissipation occurs primarily in the smaller eddies.

Here it is assumed that the dispersion of the immiscible liquids is mainly due to microeddies of a critical scale equal to the size of the droplets. Microeddies with lower scale than the critical one do not have the energy necessary to generate droplets from the immiscible liquid being at rest in the top, while microeddies with larger scale have frequencies lower than those of the critical scale and hence have a less probability to generate and disperse new droplets.

Therefore, it can be assumed that the forces responsible for generating new droplets (inertial forces associated with turbulent microeddies) are of the same order of magnitude as the resisting buoyancy forces, i. e. :

Inertial forces		Buoyancy forces	
τd^2	$\propto$	$g \Delta \rho d^3$	(3.1)

Furthermore, it is assumed here that in correspondence of the complete dispersion state, the inertial forces are of the same order of magnitude as the resisting surface tension forces, i. e. :

Inertial forces		Surface tension forces	
τd^2	$\propto$	σd	(3.2)

From equations 3.1, and 3.2 it follows that:

$$d \propto \left(\frac{\sigma}{g\Delta\rho}\right)^{1/2} \tag{3.3}$$

The inertial forces can be represented by Kolmgoroff's expression for the inertial subrange:

$$\tau d^2 \qquad \propto \qquad \rho(\varepsilon d)^{2/3} d^2 \tag{3.4}$$

By rearranging equations 3.1 thorough 3.3, and solving for d one gets:

$$d \propto \frac{\sigma^{3/5}}{\varepsilon^{2/5}\rho^{1/5}} \tag{3.5}$$

By combining equation 3.3, and 3.5, it follows that:

$$\varepsilon \propto \frac{\sigma^{1/4}(g\Delta\rho)^{5/4}}{\rho^{1/2}} \tag{3.6}$$

The power input under gassed conditions in a tank of height H and diameter T is (Susanto [18]) :

$$\varepsilon_{LG} = \left(\frac{4}{\pi}\right)\rho N_p W(N_A) N^3 \frac{D^3}{HT^2} \tag{3.7}$$

where $W(N_A)$ is the power ratio of gassed to ungassed conditions at the same agitation speed. The power input due to the bubbling of the gas is (Susanto [18]) :

$$\varepsilon_G = \frac{\Delta PQ}{\rho V} = \frac{4}{\pi}\frac{gHQ}{D^3}\frac{D^3}{HT^2} \tag{3.8}$$

The total power consumption (ε) is equal to the sum of ε_{LG} and ε_G, hence ε is:

$$\varepsilon = \frac{4}{\pi}\left[\rho N_p W(N_A) N^3 + \frac{gHQ}{D^3}\right]\frac{D^3}{HT^2} \tag{3.9}$$

From equations 3.6 and 3.9, it follows that in correspondence of the minimum agitation speed, $N_{cd-gassed}$, to disperse the liquid phases in the presence of a gas it must be that:

$$\frac{4}{\pi}\left[(\rho N_p W(N_A)) N^3_{cd-gassed} + \frac{gHQ}{D^3}\right]\frac{D^3}{HT^2} = \alpha\frac{\sigma^{1/4}(g\Delta\rho)^{5/4}}{\rho^{1/2}} \tag{3.10}$$

Solving equation 3.10 for $N_{cd-gassed}$, gives:

$$N_{cd-gassed} = \sqrt[3]{\frac{\alpha\frac{4}{\pi}\frac{\sigma^{1/4}(g\Delta\rho)^{5/4}}{\rho^{3/2}}\frac{HT^2}{D^3} - g\frac{HQ}{D^3}}{N_p W(N_A) D^2}} \tag{3.11}$$

Using Armenante and Tsai's expression [20] for $N_{cd-ungassed}$:

$$N_{cd-ungassed} = \alpha \frac{4}{\pi} \frac{\sigma^{1/4}(g\Delta\rho)^{5/4}}{N_p W(N_A) D^2 \rho^{3/2}} \frac{HT^2}{D^3} \tag{3.12}$$

equation 3.11 can be rewritten as:

$$N_{cd-gassed} = \sqrt[3]{\frac{N_{cd-ungassed}}{W(N_A)} - \frac{gHQ}{N_p W(N_A) D^5}} \tag{3.13}$$

Using a truncated series expansion it follows that:

$$N_{cd-gassed} \cong \frac{N_{cd-ungassed}}{[W(N_A)]^{1/3}} \cdot [1 - \frac{1}{3} \frac{gHQ}{N_p W(N_A) D^5}] \tag{3.14}$$

Since $\varepsilon_G << \varepsilon_{LG}$, in most practical cases, then the second term contained in the brackets (in equation 3.14) is much less than 1. Then equation 3.14 can be reduced to the simple form:

$$N_{cd-gassed} \cong N_{cd-ungassed} (\frac{P_0}{P_G})^{1/3} \tag{3.15}$$

Equation 3.15 is similar to that obtained by Susanto [18] for gas-solid-liquid systems:

$$N_{js-gassed} \cong N_{js-ungassed} (\frac{P_0}{P_G})^{1/3} \tag{3.16}$$

where N_{js} is the minimum agitation speed for complete suspension of solid particles.

Equation 3.15 can be rewritten in terms of $\Delta N_{cd-gassed}$, i.e., the incremental agitation speed above that for complete dispersion under ungassed conditions, ($N_{cd-ungassed}$), required to achieve complete dispersion. In terms of $\Delta N_{cd-gassed}$, equation 3.15 can be rearranged as :

$$N_{cd-gassed} - N_{cd-ungassed} = N_{cd-ungassed} (\frac{P_0}{P_G})^{1/3} - N_{cd-ungassed}$$

or

$$\Delta N_{cd-gassed} = N_{cd-ungassed} [(\frac{P_0}{P_G})^{1/3} - 1] \tag{3.17}$$

When the power dissipation under both gassed and ungassed conditions is known, the additional speed requirement, due to the presence of gas, can be determined from equation 3.17.

CHAPTER 4

A NOVEL METHOD FOR THE DETERMINATION OF N_{cd-smp}

A survey of the literature has revealed that the visual method is the commonly used technique to determine the minimum agitation speed, N_{cd}, to completely disperse two immiscible liquids. However, our mixing research group has previously developed a new method for the determination of the minimum agitation speed for complete liquid-liquid dispersion in mechanically agitated vessels (Armenante and Huang [7]). The results they obtained indicated that the new method for determining N_{cd} has some significant advantages over the commonly used visual method, such as the reproducibility of the results obtained independently of the observer and the applicability of the method to situations where visual inspection is impossible. Therefore, in this study, the method developed by Armenante and Huang to experimentally determine the minimum agitation speed was extended to three phase liquid-liquid-gas systems.

The method is based on the collection of samples from the bulk of the mixture at different agitation speeds. The volume fraction of the dispersed phase is then determined by allowing the sample to settle in a graduate cylinder. Then V* (expressed in %) can be calculated as the ratio of the volume of the dispersed phase to the total liquid volume of the sample.

The behavior of the function V* = f(N) was found to be similar to that described by Armenante and Huang. It was observed that when the volume fraction of the dispersed phase, V*, for each experiment was plotted against the agitation speed, N, a sharp change in the slope of the resulting plot occurred just before observing the visually determined minimum agitation speed, N_{cd-vis}. This can be seen in Figures 4.1.a and 4.2.a. Figure 4.1.a shows the case in which a sharp change in slope was

observed, but in which V* never had a maximum value. On the other hand, Figure 4.2.a shows the case in which V* increases until a certain point and then starts to decrease. The situation in which a maximum was observed is a result of the sampling point being located closer the liquid-liquid interface. This can be explained by assuming that the concentration of the dispersed phase in the region in which the sampling point is located is maximum when the complete dispersion state is reached. Higher agitation speeds result in more homogeneous dispersion, thus decreasing the concentration of the dispersed phase in the region of the sampling point. As a result, a maximum in the plot can be observed.

A convenient way to indicate how V* depends on N is to establish a functional relationship between the two variables fitting the experimental data. Armenante and Huang [7] interpolated their data for liquid-liquid systems, with spline curves. In this study their procedure was extended to three-phase liquid-liquid-gas systems. Accordingly, cubic spline curves were used to interpolate the experimental points. The resulting curve, f(N) (consisting of a collection of spline curves), was used for further analysis as described in the following. For the case of no maximum point, the following function was derived from V*=f(N):

$$\Phi(N) = \frac{f''(N)}{f'(N)} \qquad (4.1)$$

where f'(N) and f''(N) represent the first and second derivatives of f(N), respectively. The ratio $\frac{f''(N)}{f'(N)}$ is the rate of change of the slope (f'(N)) with respect to the slope itself. The rate of change in the slope will be maximum (in absolute value) when :

$$\Phi'(N) = 0 \qquad (4.2)$$

The value of N in correspondence of which $\Phi'(N) = 0$ is taken to be the value of N_{cd}. Additional details on the rationale for this approach are given elsewhere (Armenante and Huang [7]).

In order to distinguish the value of N_{cd} so obtained from that obtained using the visual method, the corresponding variables are labeled N_{cd-smp} (for sampling) and N_{cd-vis} (for visual). Since the experimental points increase with N at a declining rate in the neighborhood of N_{cd} the function $\Phi(N)$ must be negative in correspondence of this point. The method for the case of no maximum is illustrated in Figure 4.1.

In the case of V* having a maximum point, N_{cd} was determined by imposing that the derivative of the resulting interpolating function, f(N), is equal to zero. The method for the case of a maximum is illustrated in Figure 4.2.

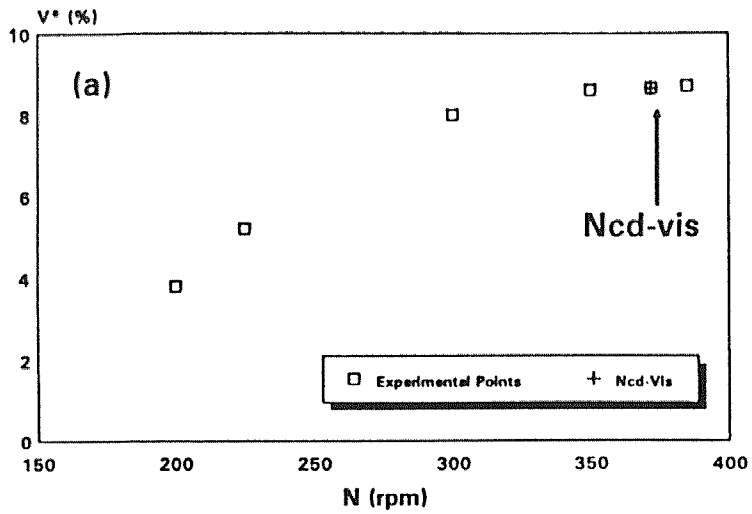

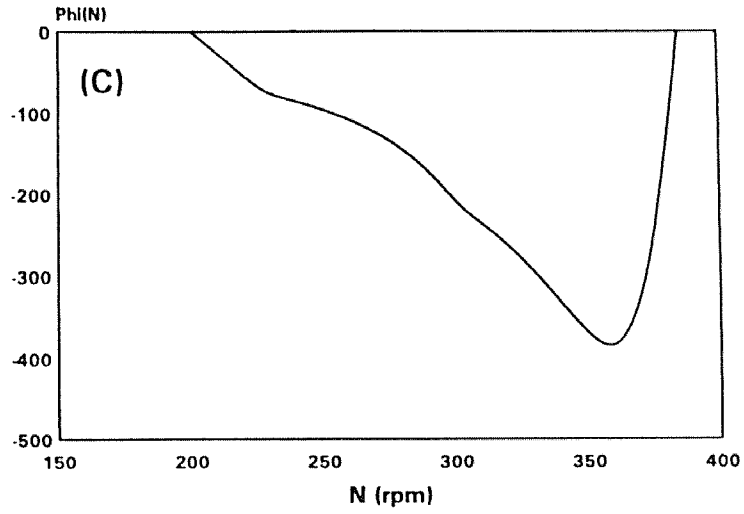

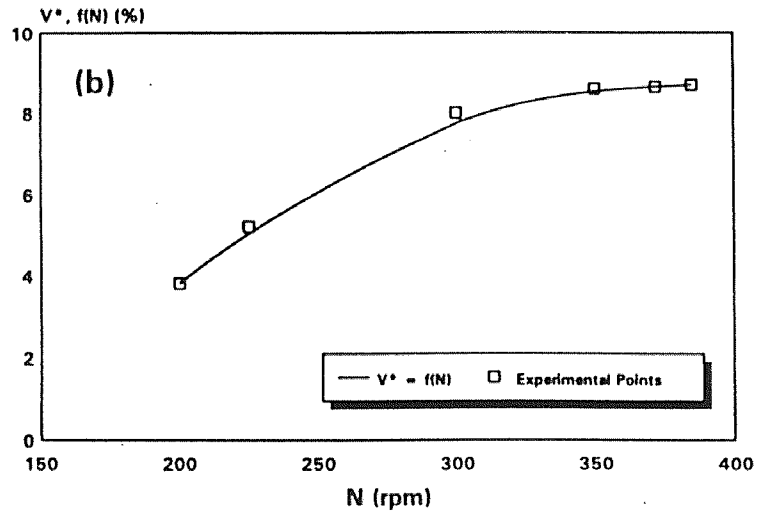

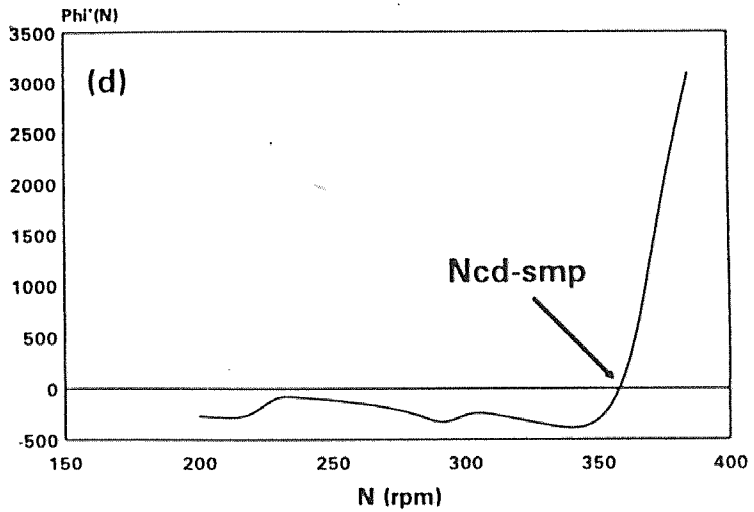

Figure 4.1 Ncd Determination: No-Max Case

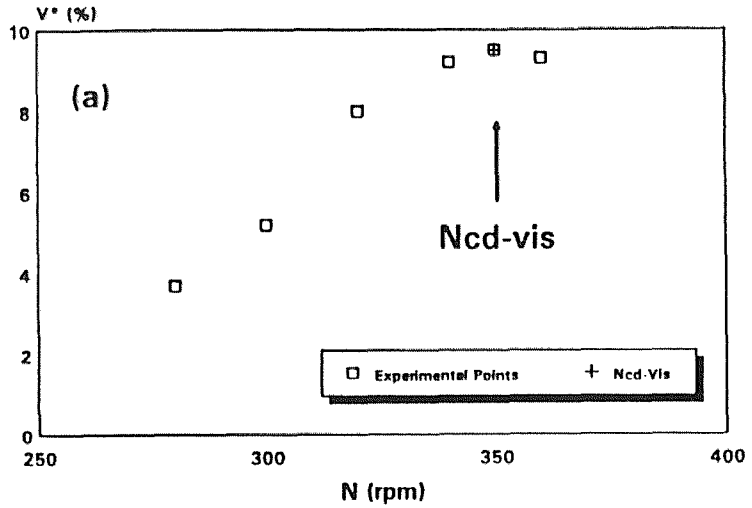

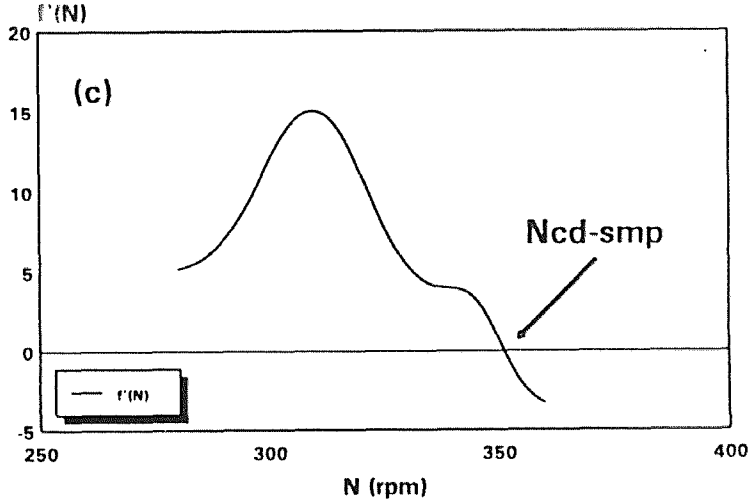

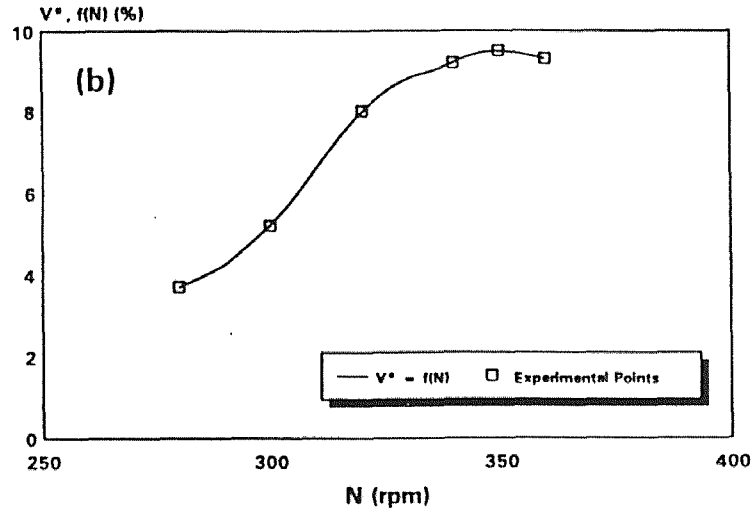

Figure 4.2 Ncd Determination, Max Case

CHAPTER 5

EXPERIMENTAL APPARATUS AND METHOD

5.1 Apparatus for Sampling and Ncd-vis Determination

A schematic of the apparatus used in this part of the work is shown in Figure 5.1. The experimental system consisted of a variable speed reversible motor (GK Heller 12P3225D T7, for use with GK Heller controllers) with a maximum speed of 2000 rpm. The agitation speed was measured using a digital tachometer with a photoelectric pick-up sensor (Cole Parmer, Model 8192-70) and was accurate within ± 1 rpm.

Two fully baffled cylindrical vessels were used. The first vessel was made entirely of plexiglas with an internal diameter of 0.286 m and a baffle width equal to 1/10th of the vessel diameter. The second vessel was also made entirely of plexiglas with a baffle width equal to 1/10th of the vessel diameter, but with an internal diameter of 0.241 m.

Five types of impellers of different diameters were used, namely, disk turbine (DT), 45°pitched blade turbine (PBT) pumping either up or down, flat-blade turbine (FBT), curved-blade turbine (CBT), and propeller turbine (PT). Their shapes and sizes are listed in Table 5.1. Each of the first four types of impellers had six blades and a bore diameter of 0.0127 m. The propeller was of the standard three-blade kind. One impeller was mounted on the shaft in each experiment. The clearance of the impeller off the bottom of the vessel, C, was varied. Air was dispersed through the vessel using a sparger tube having an internal diameter of 0.002 m placed directly beneath the impeller at a distance of 0.04 m off the bottom of the vessel. The air flow rate was measured using an air flow meter (Gilmont, Shielded Compact Flowmeter Size 13). The air flow rate was varied from 0 to 0.44 vvm (i.e., volumetric flow rate of air (L/min) per volume of liquid in the vessel (L)).

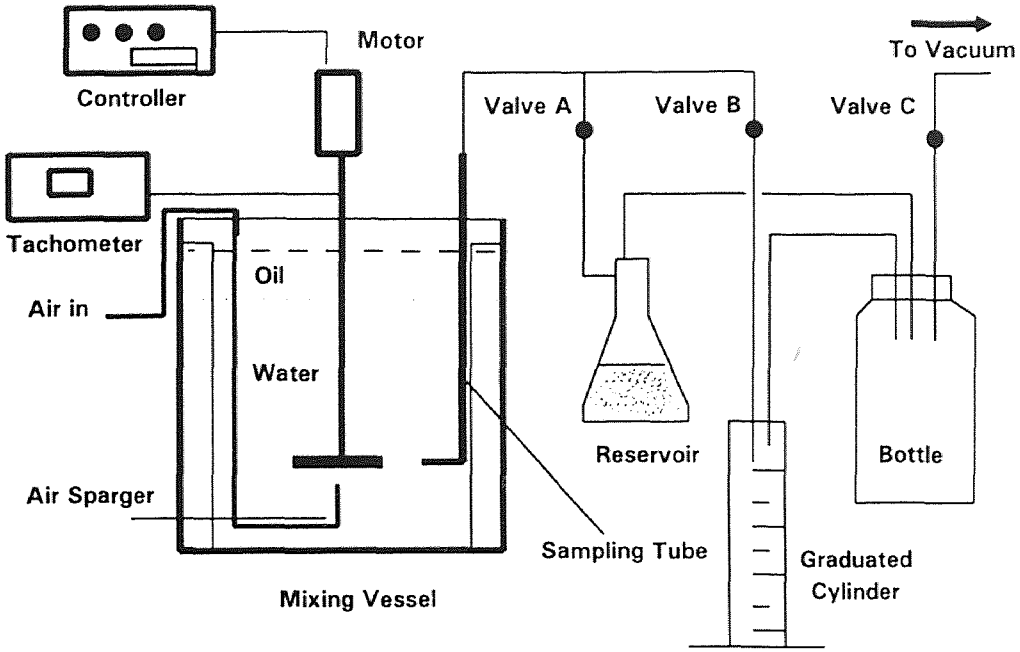

Figure 5.1 Experimental Set-up for Ncd Measurement

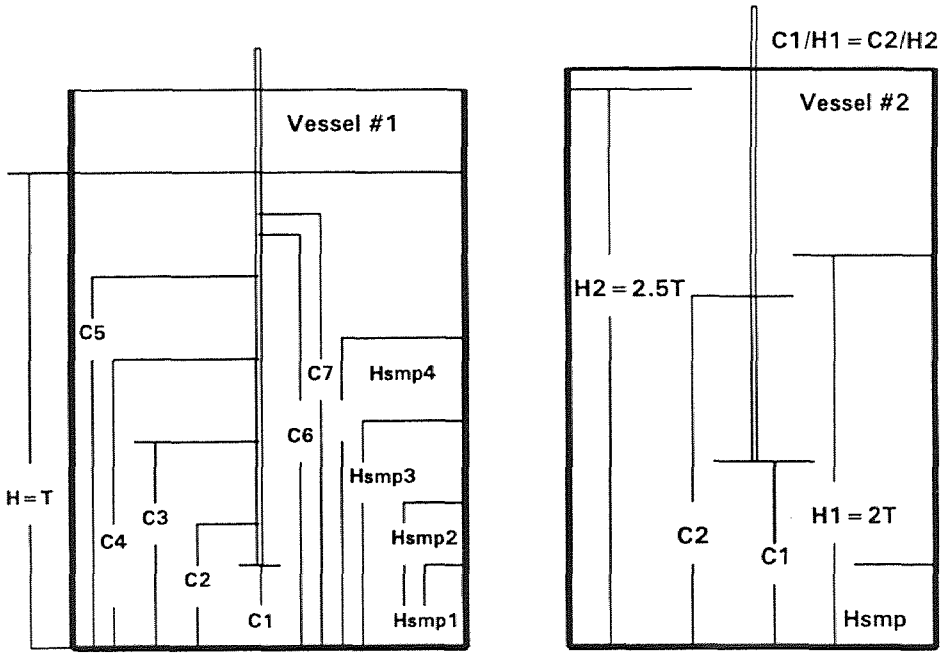

Figure 5.2 Vessel Set-up

The sampling apparatus consisted of a 90° angle glass tube, having an internal diameter of 0.004 m, attached to one of the baffles. The inlet point of the sampling tube was placed in the middle position between two baffles and at a radial distance from the vessel wall equal to 0.05 m. The sampling point location was varied only in the first vessel. A sketch of the vessels used is shown in Figure 5.2. Table 5.2 gives the details of the vessel dimensions, where C1 = 0.065 m, C2 = 0.0762 m, C3 = 0.1016 m, C4= 0.15 m, C5 = 0.186 m, C6 = 0.21 m, and C7= 0.2225 m for the first vessel and C1 = 0.228 m, and C2 = 0.2853 for the second vessel are the off-bottom impeller clearances for which the minimum agitation speed was obtained. The sampling tube was connected to a series of flasks and hooked to a vacuum system. Several valves were used to divert the flow from the vessel to either a reservoir or a graduated cylinder (100 ml in volume). In all experiments, the continuous phase was always distilled water($\rho_{water} = 1000\frac{kg}{m^3}$). The dispersed phase was always mineral oil ($\rho_{oil} = 826\frac{kg}{m^3}$ and $\mu_{oil} = 11.05 cP$).

The viscosity of the oil was determined experimentally using a Cannon-Fenske Viscometer Tube (ASTM D 445), size 100. The temperature at which the determination was carried out was 71.6°F. At this temperature the kinematic viscosity of water (ν_{water}) was taken to be 0.9213 cSt [21]. The time required for water (i.e., the reference fluid) to pass through the viscometer was experimentally measured to be 67.8 s. Then, the viscometer constant, C', was determined using the following equation [22]:

$$C' = \nu_{water} / t_{water} \qquad (5.1)$$

C' was found to be equal to 0.01358855 cSt/s. At the same temperature (71.6°F) the time required by the oil to pass through the viscometer was experimentally measured

to be 984.88 s. The kinematic viscosity of oil (ν_{oil}) was calculated with the following equation [22]:

$$\nu_{oil} = C' t_{oil} \qquad (5.2)$$

ν_{oil} was found to be equal to 13.383 cSt which is equivalent to a viscosity of 11.05 cP.

Table 5.1 Impeller Types and Dimensions

Impeller Type	Impeller Size (m)
DT	0.0635, 0.0762, 0.1016
PBT(↑)	0.0635, 0.0762, 0.1016
PBT(↓)	0.0635, 0.0762, 0.1016
FBT	0.1016
CBT	0.1016
PT(↓)	0.0762

Table 5.2 Vessel Dimensions

	Vessel Diameter,T (m)	Vessel Height, L (m)	Liquid Height, H (m)	Baffle Width, B(m)	H/T	B/T %
1	0.286	0.386	0.286	0.0286	1	10
2a	0.241	0.748	0.482	0.0241	2	10
2b	0.241	0.748	0.6025	0.0241	2.5	10

5.2 Sampling Procedure and Visual Observation Method

The sampling procedure was as follows. The vessel was charged with the liquids. The dispersed phase was always 10% by volume of the total liquid mixture. The combined height of the liquid phases, in the first vessel, was always equal to the vessel diameter. Experiments were conducted in the second vessel at H/T equal to 2 and 2.5. After setting-up the apparatus, the motor was started at an agitation speed well below the minimum speed for complete dispersion. After an equilibration period varying between 10 and 15 minutes, the vacuum system was activated by opening Valve C (see Figure 5.1). Then, Valve A was opened so that the liquid would flow from the tank into the reservoir. This was done to ensure that the liquid initially contained in the sampling tube would not be included in the sample. When 40-60 ml of dispersion

had accumulated in the reservoir, Valve A was closed and Valve B was opened, allowing the flow to be diverted to the graduated cylinder until some 100 ml were collected. The operation typically lasted only about ten seconds. The last bottle in the line was added only to protect the vacuum system from receiving any liquid. The sample so taken was allowed to separate into two phases, and the fraction of the dispersed phase was determined. Then, all liquid samples were returned to the vessel. The same procedure was repeated at higher agitation speeds until no dispersed phase was observed at rest at the top of the continuous phase. In addition, the minimum agitation speed in correspondence of the complete dispersion state was determined in each experiment by visual inspection. The visually determined value for N_{cd}, N_{cd-vis}, was defined as the minimum agitation speed at which no dispersed phase was observed at rest at the top of the continuous liquid phase (Skelland and Seksaria [3]). In most of our experiments small pockets of fluid were observed near the baffle corners and around the impeller shaft. However, the presence of these pockets was neglected when N_{cd-vis} was determined since they were observed even at agitation speeds much higher than N_{cd-vis}.

The same procedure was repeated at different air flow rates. Every case was studied at air flow rates in the range of 0 to 8 L/min (0 to 0.44 vvm), with an increment equal to 0.055*k, where k was 0,1,...8.

5.3 Power Measurement

A schematic of the apparatus used for power measurement is shown in Figure 5.3. The experimental system consisted of a 2.0 hp variable speed motor (G.K. Heller CAY 1030-12-2) with a maximum speed of 1800 rpm. The rotational speed was measured using a digital tachometer with a photoelectric pick-up sensor (Cole Parmer 8192-70) and was accurate within ± 1 rpm. A strain gage (Measurements Group Co.,

CEA-06-187UV-350) was carefully mounted on an aluminum hollow shaft with an internal diameter of 0.00785m. The strain gage was connected with insulated lead wires passing through the hollow core of the shaft to a signal conditioner and amplifier system (2120A system, Measurement Group Co.). A data acquisition system (Lab Tech Notebook) connected to a computer was used to analyze the signals from the strain gage conditioner and the optical sensor. The power drawn was determined using the following equation:

$$P = \omega T = 2\pi NT \tag{5.3}$$

where ω is the angular velocity, T is the torque produced by the impeller, and N is the agitation speed in revolutions per second (rps).

For the systems described in Section 5.2, the power was measured in correspondence of the experimentally determined values for $N_{cd-gassed}$ under both gassed and ungassed conditions. In addition these results were compared to those predicted using the equation for $N_{cd-gassed}$ developed in Chapter 3, i. e. :

$$N_{cd-gassed} = N_{cd-ungassed}\left(\frac{P_0}{P_G}\right)^{1/3} \tag{3.15}$$

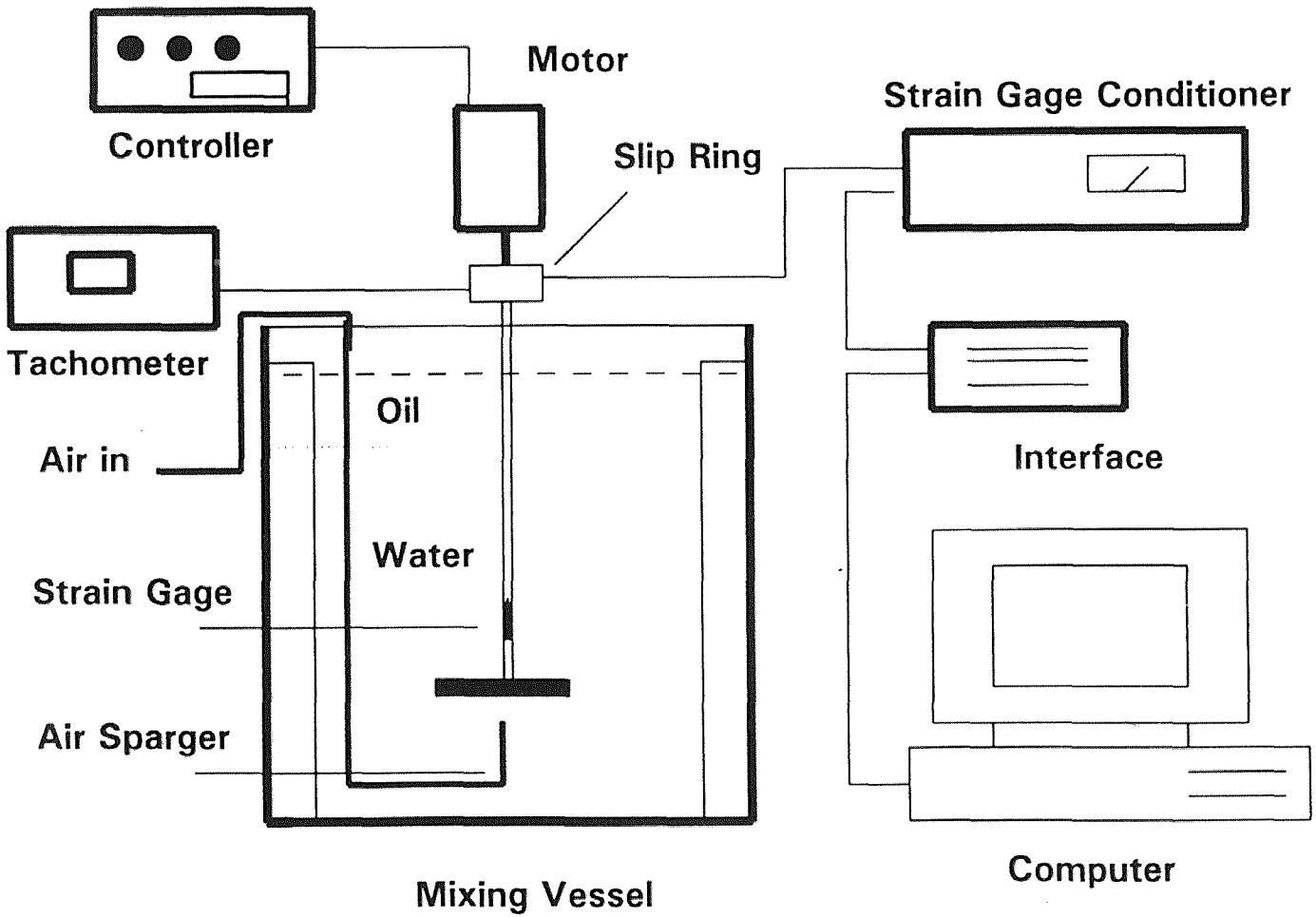

Figure 5.3 Experimental Set-up for Power Measurement

CHAPTER 6

RESULTS AND DISCUSSION

A total of 192 experiments were conducted in which both N_{cd-vis} and N_{cd-smp} were determined for each experiment. The power consumption was measured, as described in Section 5.3, for all cases except those in which pitched-blade turbines pumping up were used, since the motor used for power measurement could not rotate counter clock wise. The results are presented in a tabulated form in Appendix B and in the form of plots of dispersed phase fraction, V* (%) vs. the agitation speed, N (rpm) in Appendix C. Some experiments were carried out, then repeated after a considerable lapse of time to determine the reproducibility of the results for N_{cd-vis}, N_{cd-smp}, and $N_{cd-model}$. The reproducibility for all three values of N_{cd} was determined as follows. Two sets of experiments, each set including runs at 8 different air flow rates, were carried out using DT impeller at C = D = 0.076 m. The second set of experiments was carried out forty three days after the first one. All three values of N_{cd} were determined as described in Chapters 3, 4, and 5. Results for the first set of experiments are shown in Table B.2. The deviations of the results obtained in the second set of experiments from those obtained in the first one were determined for every experimental point. The deviations for those points for which the agitation speed was less than or equal to 500 rpm were found to be similar in all cases but higher than those obtained for when the agitation speed was higher than 500 rpm. Therefore, agitation speeds less than or equal to 500 rpm were considered "low speed" otherwise they were considered "high speed". The results obtained from the reproducibility test are shown in Table 6.1

Table 6.1 Reproducibility of Experimental Results

Minimum Agitation Speed	Repr. (High Speed)	Repr. (Low Speed)
N_{cd-vis}	± 1.8 %	± 4.6 %
N_{cd-smp}	± 2.4 %	± 5.9 %
$N_{cd-model}$	± 1.9 %	± 4.5 %

6.1 Validation of the Sampling Procedure for the Determination of N_{cd}

Each value of N_{cd-smp} was obtained by generating a plot, as described in Chapter 4, containing 5-10 experimental points analyzed using the spline interpolation method. The plots that showed a maximum point were roughly 7 % of the total (14 out of 192). The values of N_{cd-smp}, with or without maximum were plotted against the corresponding N_{cd-vis} values as shown in Figure 6.1. From this figure one can see that a good agreement between N_{cd-vis} and N_{cd-smp} exists. However, the effects of a number of operating parameters on both N_{cd-vis} and N_{cd-smp} were examined in order to test their effect on the proposed method.

6.1.1 Effect of Sampling Point Location on N_{cd-smp}

In order to test the effect of sampling point location plots of V* vs. N were produced for the same system but using four different sampling tube positions off the vessel bottom, H_{smp}. The results so obtained are shown in Figure 6.2. It is obvious that the resulting curves are different, but that the values for N_{cd-vis} and N_{cd-smp} are quite similar dispite the significant change in the sampling point location. Similar results were also obtained for other systems (see Tables B.5, B.6, and B.9 of Appendix B). Therefore, the method is not affected by the sampling point location.

6.1.2 Effect of Air Flow Rate on N_{cd-smp}

To further generalize the validity of the method, the air flow rate was varied from 0 to 0.44 vvm for a given system. The results are shown in Figure A.1. As one can expect, the values of N_{cd-vis} and N_{cd-exp} changed as the air flow rate was increased. However, in all studied cases (see Tables B.1-B.13 of Appendix B) the values of N_{cd-vis} and N_{cd-smp} are still close to each other within 4%.

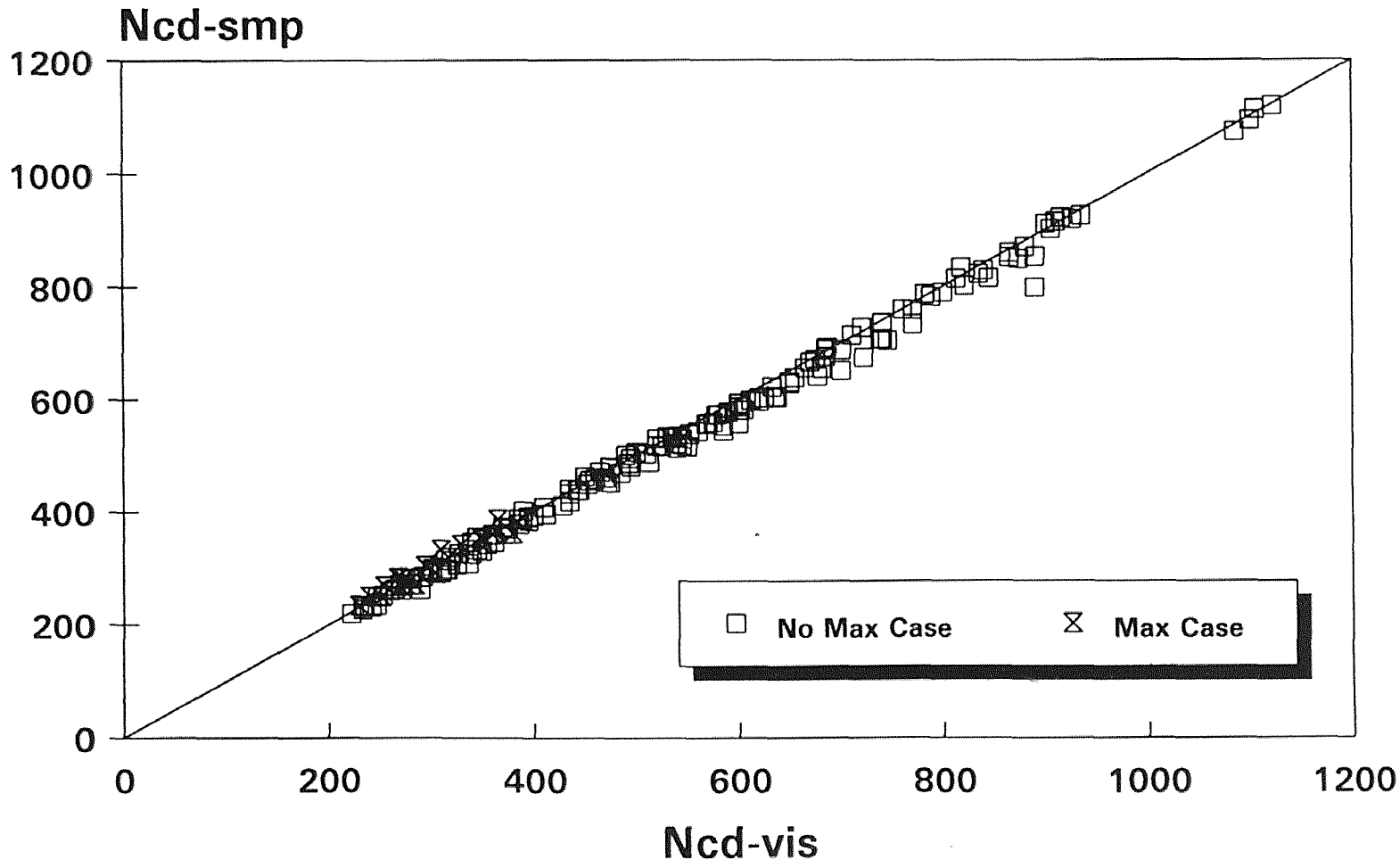

Figure 6.1 Comparison of Ncd-smp with Ncd.vis

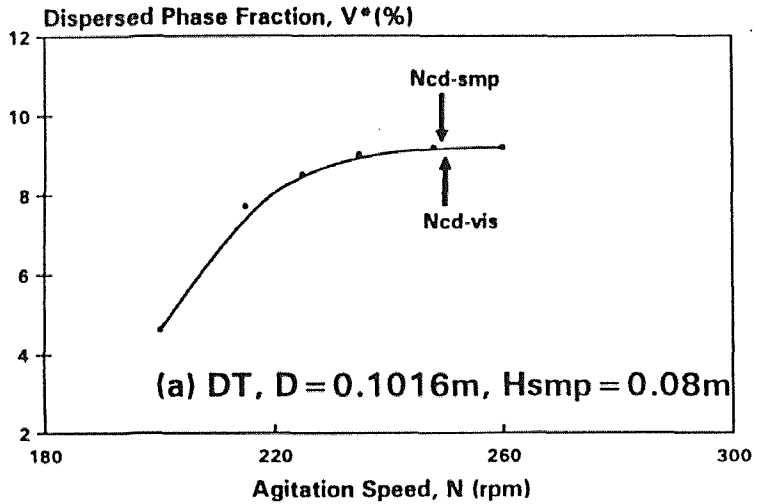

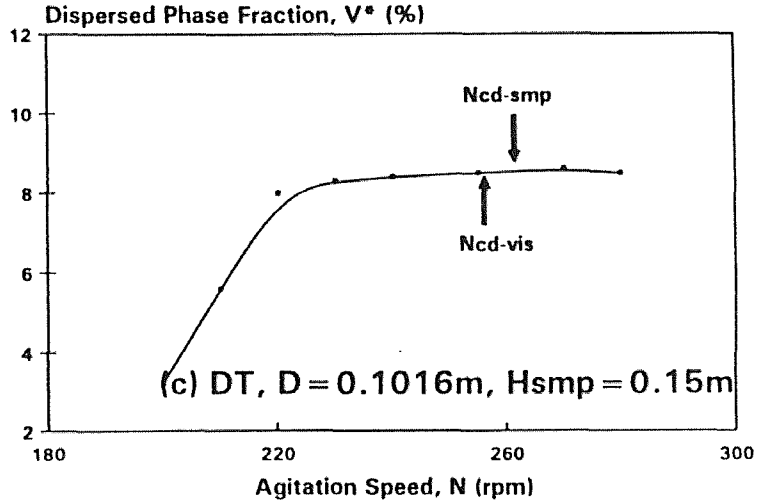

System: 10% oil in water, H = T = 0.286m
C = 0.186m, and Qair = 0.109 vvm

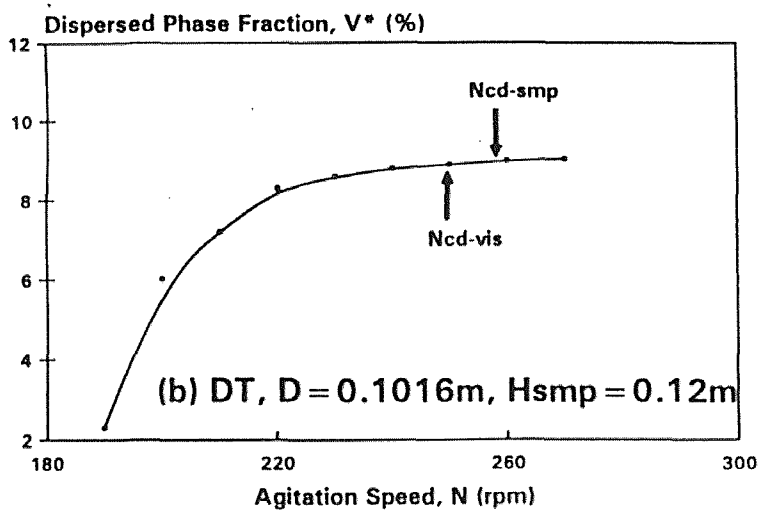

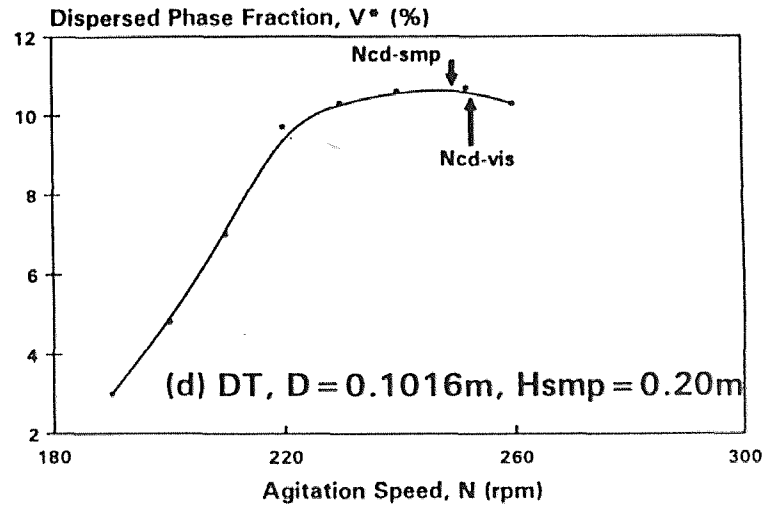

Figure 6.2 Effect of Hsmp on Ncd Values

6.1.3 Effect of Type, Size, and off Bottom Clearance of Impellers on N_{cd-smp}

Figure A.2 shows the effect of impeller type on N_{cd-smp}. Similarly, Figure A.3 shows the impact of the impeller size and Figure A.4 shows the influence of the impeller clearance off the vessel bottom on both N_{cd} values. Even though the values of N_{cd} change from one system to another, the values of N_{cd-vis} and N_{cd-smp} are very similar. This is further evidence that isokinetic sampling is not required for the method.

6.2 Effect of Air Flow Rate and Impeller Type on N_{cd}

Figure 6.3 shows the effect of air flow rate on N_{cd} for five different types of impellers. For each type, a linear relation between N_{cd} and Q_{air} was obtained, i.e. :

$$\Delta N_{cd} = mQ_{air} \qquad (6.1)$$

The slope of this line was found to vary with impeller type as well as size, as shown in Table 6.2. The results shown in Figure 6.3, indicate that when the air flow rate was increased the values of N_{cd} also increased for DT, 45-PBT pumping downward, CBT, FBT, and PT pumping downward. On the other hand, when using 45-PBT pumping upward, it was found that the value of N_{cd} decreased as the air flow rate was increased. In order to explain the reversed relationship between the flow rate of air and the minimum agitation speed, N_{cd}, resulting from the use of 45-PBT pumping upward, the movement of the air bubbles was observed during the dispersion process as follows:

1. A system of water and air (no oil) was used to ease the visual observation of movement of the air bubbles during the process. This system was studied under the same experimental conditions of the system in which oil was included.

2. Q_{air} was set at a value equal to 0.11 vvm and the agitation speed, N, was set at a value equal to 200 rpm. It was observed that the impeller was not able to disperse the

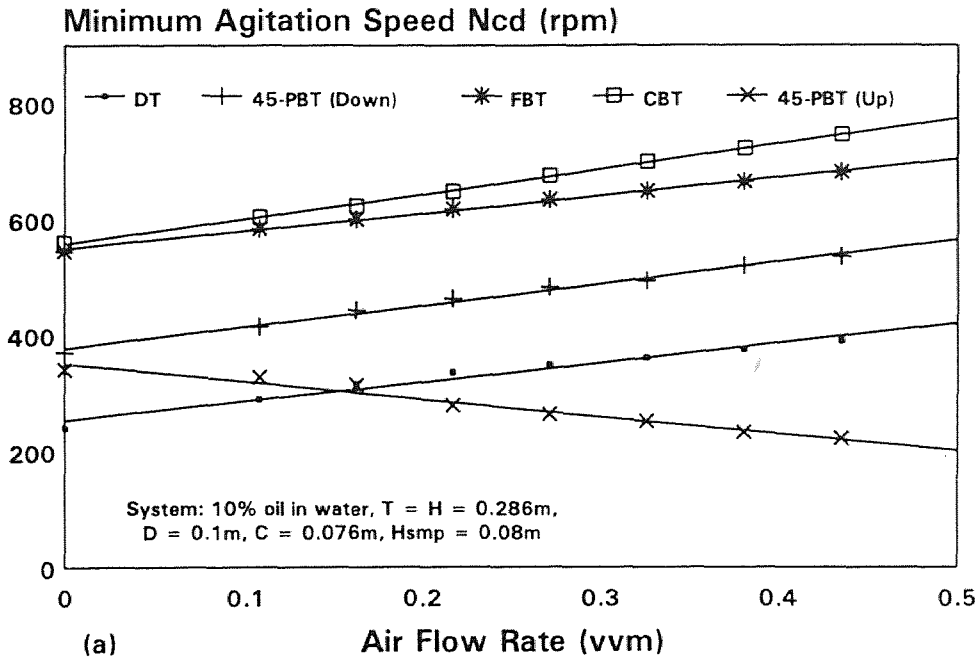

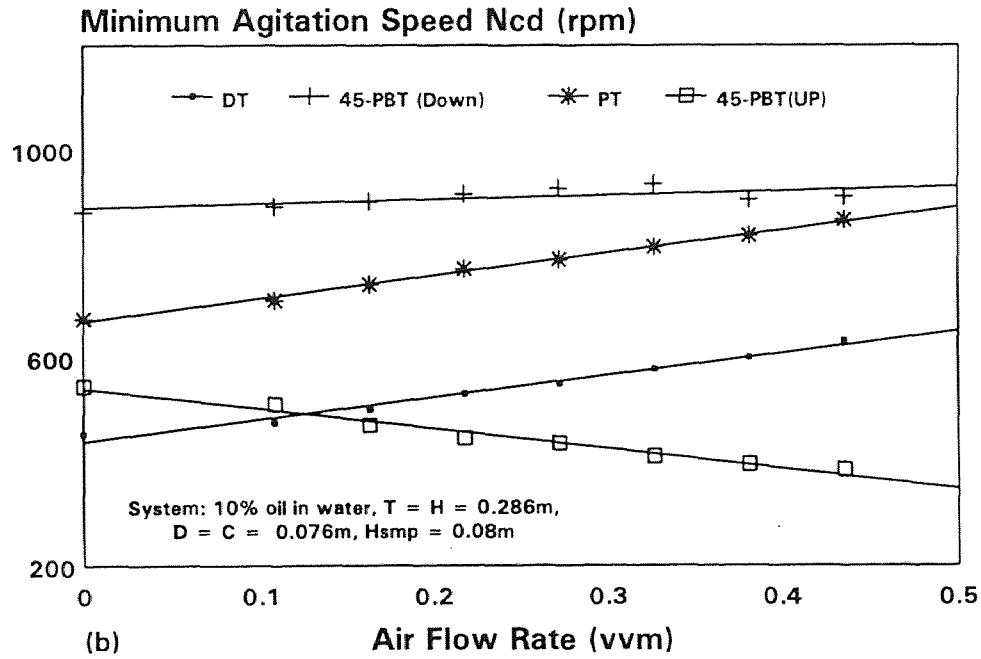

Figure 6.3 Effect of Qair and Impeller Type on Ncd

air properly, (i.e., it was flooded), and the air tended to escape the system from the center of the vessel.

3. Then, N was increased to 260 rpm while Q_{air} was kept constant. It was observed that the air bubbles from the sparger started to fluctuate right and left. However, some of the bubbles were still escaping the impeller without being dispersed, while most of the incoming air flow was broken into small bubbles and was distributed through the vessel without reaching neither the bottom nor the wall of the vessel.

4. When N was increased to 290 rpm, it was observed that the range of fluctuation of the air bubbles from the sparger and the amount of air escaping the impeller were smaller. It was also observed that at this speed the impeller rotation was able to force the bubbles to reach the vessel wall. The position on the wall where the bubbles impacted fluctuated due to the unstable distribution of the sparged air.

5. When N was increased to 328 rpm (the experimentally obtained value of N_{cd} at Q_{air} equal to 0.11 vvm), it was observed that the incoming air stream and the bubbles impacting at the wall of the vessel were approximately stable. The impacting point was found to occur in the range of 0.15 to 0.18 m from the bottom of the vessel. It was also observed that after hitting the wall the air bubbles were deflected in two directions: up and down.

6. At this point N was kept constant at 328 rpm while the value of Q_{air} was increased to 0.22 vvm. It was observed that the impacting position was elevated to 0.165 - 0.2 m from the bottom of the vessel. This could be due to the resulting lower fluid density of the mixture of higher air concentration.

7. Therefore, in order to maintain the same impacting point in correspondence of the complete dispersion state, the acting force on the fluid must be decreased, which can be achieved by decreasing the agitation speed. When N was decreased to 315 rpm (the experimentally determined value of N_{cd} at Q_{air} equal to 0.22 vvm), a behavior similar to the one described in Step 5 was observed.

The equation relating $N_{cd-gassed}$ and Q_{air} derived in detail in Chapter 3 was used to interpret the experimental results, i.e.:

$$\Delta N_{cd-gassed} = N_{cd-ungassed}[(\frac{P_0}{P_G})^{1/3} - 1] \qquad (3.17)$$

Using this equation, the additional agitation speed requirement due to the presence of air could be evaluated, provided that the power consumed under both gassed and ungassed conditions was known. The power consumption under both gassed and ungassed conditions was determined experimentally. However, it was found that this equation worked well for disk turbines but underpredicted the increase in agitation speed due to the presence of air for other types of impeller; the possible reasons behind this are discussed in detail in Section 6.7. An example of the comparison between the experimental data and the predicted results for DT (D = 0.0635 m) is shown in Figure 6.4 (the rest of the figures are shown in Section 6.7, Figures 6.6-6.11, and more details of the results are presented in Appendix B). It can be seen from Figure 6.4 and the rest of the figures that the difference between the predicted value of N_{cd}, $N_{cd-model}$, and the one obtained experimentally increases as the Q_{air} increases. The difference can be partially attributed to errors in the measurement procedure. It was also observed during the experiments that a small portion of air tended to escape the impeller without being dispersed; this case is discussed in detail in Section 6.7.

Table 6.2 Experimentally Obtained Values of Slope m in Equation 6.1 for DT Impeller

Impeller Size (m)	Value of m for C = 0.0762 m	Value of m for C = 0.136 m	Value of m for C/D = 1	Value of m for Ct/D = 1
0.0635	7.7489	6.2096	7.251	5.8225
0.0762	7.8350	6.7456	7.835	7.1862
0.1016	5.3896	3.5869	5.898	3.1602

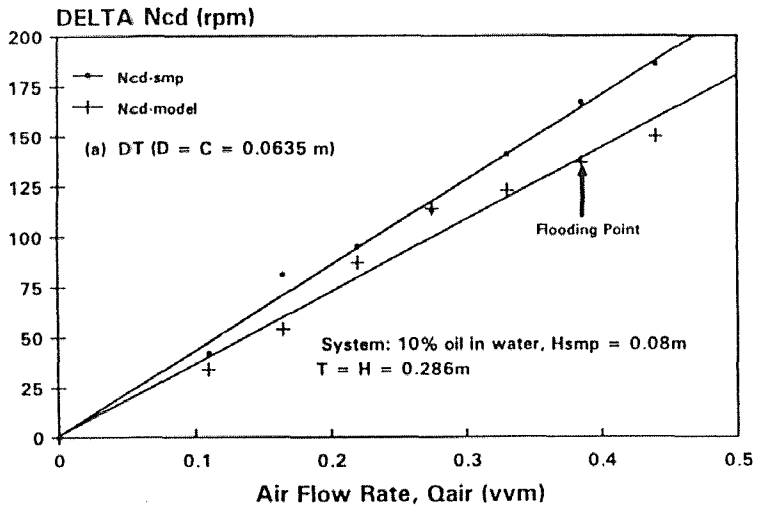

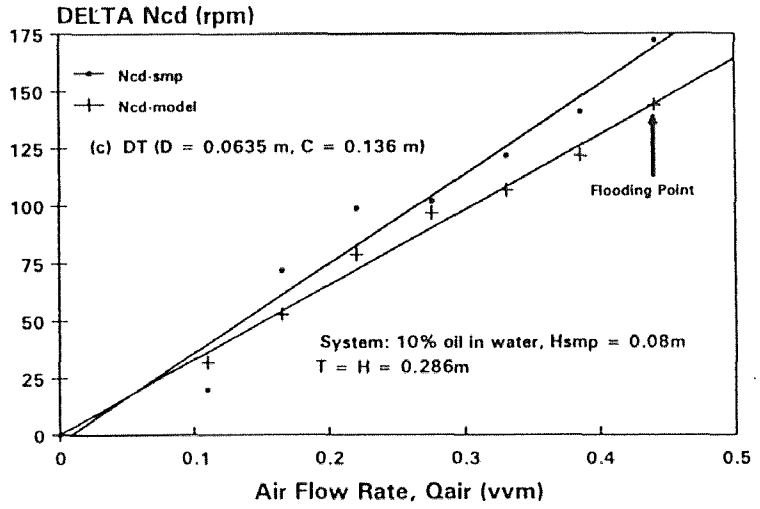

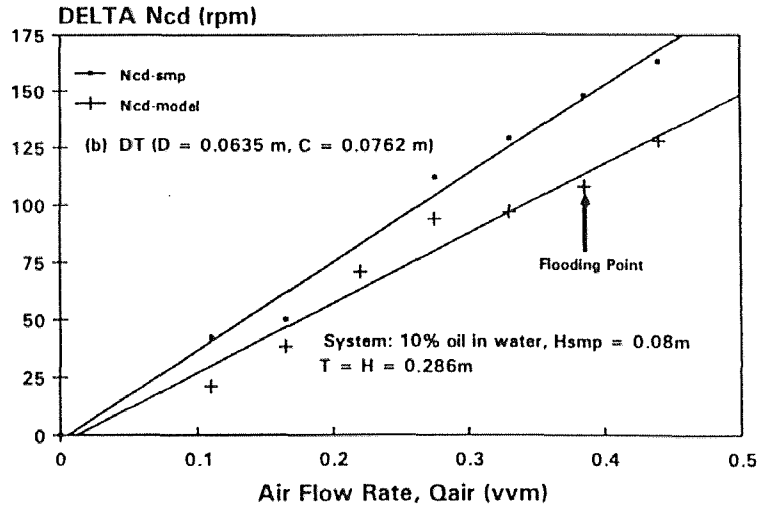

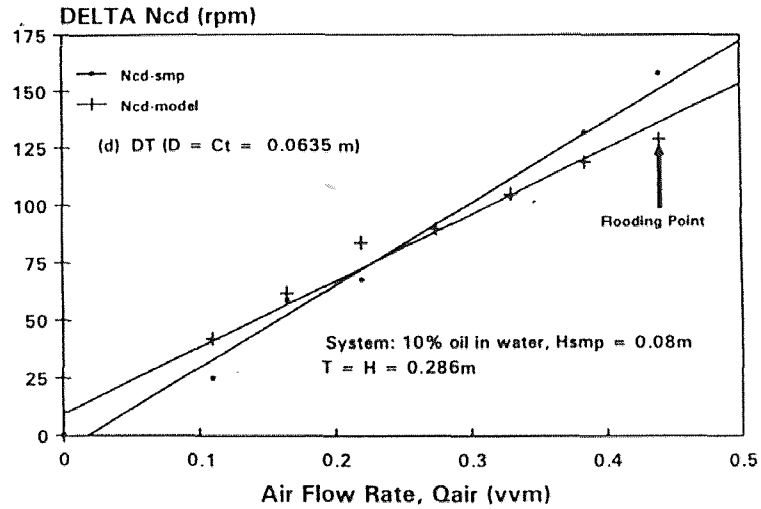

Figure 6.4 Effect of Qair on Delta Ncd for DT, D = 0.0635 m

6.3 Effect of Air Flow Rate on Power Consumption

The power drawn by the impeller was measured for each experiment in correspondence of $N_{cd-gassed}$ under both gassed and ungassed conditions. Power data are tabulated in Appendix B. Figure A.5 shows the effect of the gas flow number (N_A), which is a function of air flow rate, on the ratio of the powers under gassed to ungassed conditions, respectively ($\frac{P_G}{P_0}$). These results are similar in all cases to those shown in Figure A.5. It was found that the ratio ($\frac{P_G}{P_0}$) dropped from 1 at N_A equal to 0 to about 0.5-0.6 at N_A equal to 0.03 to 0.035.

6.4 Effect of Impeller Size on N_{cd}

Two types of impellers with different diameters (0.0635, 0.0762, and 0.1016 m) were tested, namely, DT and 45-PBT pumping either up or down. Experiments were conducted with PBT at: C=0.076 m and at C/D≐1. When DTs were used, experiments were carried out at C equal to 0.0762 m, C=0.136 m, C/D = 1, and Ct/D = 1. Figures A.6, A.7, and A.8 show the results obtained using PBT pumping down, up, and down, respectively. Figure A.9 shows the results obtained for DT at C = 0.0762m. Figure A.10 shows the results obtained at C = 0.136m, Figure A.11 shows the results obtained at C/D = 1, and Figure A.12 shows those obtained at Ct/D = 1.

All these plots show that the dependence of N_{cd} on D followed a power law. Results are shown in Figures A.6 through A.12 and are tabulated in Tables 6.3 and 6.4. It was found that the exponent for D is nearly independent of the aeration rate and similar to that found in two-phase liquid-liquid experiments. It was also found that this exponent was higher for the case in which the clearance of the impeller off the vessel bottom, C, was kept constant than in the case in which the ratio C/D was kept constant. The dependence of N on D predicted by the model (equation 13 Chapter 3) was compared with that experimentally determined. The results are shown in Table 6.4. One can see

that, in general, there is an agreement between the experimental and predicted results, although deviations, at time significant, exist.

Table 6.3 Effect of Impeller Diameter on N_{cd} for PBT

	C = 0.0762 m		C/D=1
Qair (vvm)	Pumping Downward	Pumping Upward	Pumping Downward
0	$N \propto D^{-2.35}$	$N \propto D^{-1.5}$	$N \propto D^{-2.22}$
0.11	$N \propto D^{-2.21}$	$N \propto D^{-1.53}$	
0.165	$N \propto D^{-2.53}$	$N \propto D^{-1.31}$	$N \propto D^{-2.1}$
0.22	$N \propto D^{-1.94}$	$N \propto D^{-1.61}$	
0.275	$N \propto D^{-2.32}$	$N \propto D^{-172}$	$N \propto D^{-1.91}$
0.33	$N \propto D^{-1.78}$	$N \propto D^{-1.43}$	
0.385	$N \propto D^{-1.93}$	$N \propto D^{-1.83}$	
0.44	$N \propto D^{-1.85}$	$N \propto D^{-1.91}$	

Table 6.4 Effect of Impeller Diameter on N_{cd} for DT

Qair (vvm)	C=0.0762 (m)	C = 0.136 (m)	Ct/D=1	C/D=1	Model Prediction
0	$N \propto D^{-2.21}$	$N \propto D^{-2.21}$	$N \propto D^{-1.80}$	$N \propto D^{-1.80}$	$N \propto D^{-1.67}$
0.11	$N \propto D^{-1.91}$	$N \propto D^{-2.21}$	$N \propto D^{-1.82}$	$N \propto D^{-1.37}$	$N \propto D^{-1.67}$
0.165	$N \propto D^{-1.78}$	$N \propto D^{-2.20}$	$N \propto D^{-1.81}$	$N \propto D^{-1.29}$	$N \propto D^{-1.67}$
0.22	$N \propto D^{-1.74}$	$N \propto D^{-2.18}$	$N \propto D^{-1.79}$	$N \propto D^{-1.23}$	$N \propto D^{-1.67}$
0.275	$N \propto D^{-1.72}$	$N \propto D^{-2.15}$	$N \propto D^{-1.79}$	$N \propto D^{-1.15}$	$N \propto D^{-1.67}$
0.33	$N \propto D^{-1.72}$	$N \propto D^{-2.14}$	$N \propto D^{-1.79}$	$N \propto D^{-1.18}$	$N \propto D^{-1.67}$
0.385	$N \propto D^{-1.72}$	$N \propto D^{-2.10}$	$N \propto D^{-1.74}$	$N \propto D^{-1.18}$	$N \propto D^{-1.67}$
0.44	$N \propto D^{-1.72}$	$N \propto D^{-2.12}$	$N \propto D^{-1.73}$	$N \propto D^{-1.24}$	$N \propto D^{-1.67}$

6.5 Effect of Impeller Clearance on N_{cd}

The effect of impeller clearance off the bottom of the vessel on N_{cd} was tested using PBT (D = 0.1016 m) pumping downward and three sizes for DT, i.e.: 0.0635, 0.0762, and 0.1016 m. Figure A.13 shows the results obtained for PBT, Figure A.14 shows the results obtained for DT of 0.0635 m in diameter, Figure A.15 shows the results obtained for DT of 0.0762 m, and Figure A.16 shows the results obtained for DT of 0.1016 m.

The minimum agitation speed, N_{cd}, was found to be a strong function of the impeller clearance, C. In all cases, it was found that N_{cd} had its lowest value when the impeller was placed very close to the liquid-liquid interface. Then, as the impeller was moved farther away from the liquid-liquid interface, N_{cd} increased until it reached its highest value when the impeller clearance, C, off the vessel bottom was equal to the impeller diameter. However, at the same clearance, an increase in the value of N_{cd} was required when the stirred vessel was sparged with air. All plots in Figures A.13-A.16 have similar features. In all cases, these figures show that one or two transition points occur at certain clearance levels. The transition points are represented by the sharp changes in the slopes of the lines connecting the data points. These transition points were found to be a function of the impeller diameter and the air flow rate. It is easier to determine the relationship between the transition points and Q_{air} from Figure A.16 since it includes more data points than Figures A.14 and A.15 and the transition points are more clear than in Figures A.13. From all four plots of Figure A.16, it can be seen that the two transition points are around C = 0.1016 m, and around C = 0.136 m. Comparing the first plot, at Q_{air} = 0 vvm, with the fourth plot, at Q_{air} = 0.44 vvm, it can be seen that the slopes of the two lines connecting the first point with the second and the second with the third are greater for plot having Q_{air} = 0.044 vvm than for those of the plot of Q_{air} = 0 vvm.

It can be concluded that the two transition points should be higher than 0.1016 m, and 0.136 in the first experiment and lower than 0.1016 m, and 0.136 m in the fourth experiment. Furthermore, it could be concluded that the value of Q_{air} determines the impeller clearance at which the flow pattern changes in the agitated vessel. In general, the clearance at which the transition in the flow pattern occurs decreases as the air flow rate increases. This conclusion can de justified as follows. The presence of air causes the liquid in the center of the vessel to move upwards. An increase in the air flow rate

results in faster liquid upwards movement, higher air buoyancy, and lower clearance point in correspondence with the transition point in the flow pattern.

6.6 Effect of the H/T Ratio on N_{cd}

Two vessels with different diameter were used in this part of the work. The first vessel had a diameter equal to 0.286m and the second vessel had a diameter equal to 0.241 m. To eliminate the effect of both the vessel diameter, T, and the liquid height, H, experiments were conducted at a constant value of C/H ratio equals to 0.4755 (at a value of C close to half the liquid height). The results so obtained are shown in Figure A.17. It was found that N_{cd} increased when H/T was increased under both gassed and ungassed conditions.

6.7 Comparison of the Model Results with N_{cd-smp}

In each system, the minimum agitation speed for complete dispersion of the two liquids was determined experimentally under different gassing rates covering the range from 0 to 0.44 vvm. The power consumption was then determined experimentally at every obtained value of N_{cd-smp} under both gassed and ungassed conditions. Then the ratio (P_0 / P_G) was calculated, where P_0 was the power consumption under ungassed conditions and P_G was the power consumption under gassed conditions both determined at the same agitation speed. Finally the value of $N_{cd-model}$ was predicted using the equation derived in Chapter 3, i.e.:

$$N_{cd-gassed} = N_{cd-ungassed}\left(\frac{P_0}{P_G}\right)^{1/3} \qquad (3.15)$$

where $N_{cd-gassed}$ is $N_{cd-model}$ and $N_{cd-ungassed}$ is the constant value of N_{cd} obtained for each system under ungassed conditions. All results are tabulated in Appendix B and a comparison of the values of $N_{cd-model}$ for all tested types of impellers, with the values of N_{cd-smp} is shown in Figures 6.4-6.11. Figure 6.5A shows a comparison of $N_{cd-model}$ with

N_{cd-smp}, Figure 6.5B shows a comparison of $\Delta N_{cd-model}$ with ΔN_{cd-smp}, and the rest of the figures show the effect of air flow rate on both $\Delta N_{cd-model}$ and ΔN_{cd-smp}.

6.7.1 Results for Disk Turbine

The results obtained for the three sizes of DT tested in this study are shown in Figures 6.4, 6.5, 6.6, and 6.7 and presented in detail in Appendix B. In most cases, the results indicate a good agreement between the predicted values of N_{cd} and those obtained experimentally. However, in the case of DT of a diameter equal to 0.1016 m and at an impeller clearance off the vessel bottom less than or equal to the impeller diameter, poor agreement was found between $N_{cd-model}$ and N_{cd-smp}. During the experiments with the larger impeller (D = 0.1016 m, at C $\leq$ D), it was observed that a considerable amount of air tended to escape the impeller to the center of the vessel without being dispersed efficiently. This flooded condition could be due to the low impeller speed and the reduced bottom circulation of DT placed at low clearance. Furthermore, this flooded situation resulted in a mixture of higher density than the density of the mixture in which the air flow could have been dispersed efficiently. Thus, the power consumed under these gassed conditions was found to be higher than the power consumed under efficient gas dispersion conditions. This situation resulted in the poor prediction of N_{cd} by the model.

However, with a little elevation of the clearance point, from 0.1 m to 0.136 m, a good agreement between the values of N_{cd} was obtained despite the decrease in the value of N_{cd} (see Figure 6.7). The reason could be that the flow pattern generated by the impeller was fully developed when the value of the clearance, C, was greater than the impeller diameter, D. Therefore, the air flow from the sparger was almost completely dispersed in the liquid. As a result, the predicted values of $N_{cd-model}$, using the power data obtained under these conditions, were found to be in agreement with the values of

N_{cd-smp}. In addition, a comparison of $N_{cd-model}$ with N_{cd-smp} and a comparison of $\Delta N_{cd-model}$ with ΔN_{cd-smp} are shown in Figure 6.5

In general, the model results for the six-blade disk turbine (as shown in Figures 6.4, 6.5, 6.6, and 6.7) were found to be in agreement with the experimental results with the exception of the case discussed above. This can be credited to the capability of the disc to force the entire amount of the gas to pass through the high shear impeller region which results in efficient break-up of the gas flow into bubbles and effective dispersion of the bubbles throughout the vessel. However, the deviation of the value of $N_{cd-model}$ from the value of N_{cd-smp} could be due to experimental errors in the determination of N_{cd-smp} or could be due to errors in the power measurement due to inefficient dispersion of air. This deviation was found to increase with an increase in the air flow rate; this situation was discussed in detail in Section 6.2 and can be seen clearly from Figures 6.4-6.7.

Excluding the case in which a DT of a diameter equal to 0.1016 m was placed at a clearance level less than or equal to its diameter, the agreement between $N_{cd-model}$ and N_{cd-smp}, for DT, was found to be within 6 % of the value of N_{cd-smp}.

6.7.2 Results for Pitched-Blade Turbine Pumping Downward

The results for PBT are shown in Figures 6.5 and 6.8-6.10 and are available in detail in Tables B.7-B.10. For the case of PBTs of diameters equal to 0.0635 or 0.0762 m (Figures 6.8 and 6.9, respectively) it was found that the deviation of the value of $N_{cd-model}$ from the value of N_{cd-smp} was within 6 %. The deviation in the value of $N_{cd-model}$ for PBT could be due to the unstable flow caused by the mixed-flow pattern exhibited by PBT. It was observed that the air flow rate was never stable while flowing from the sparger to the impeller, especially at air flow rates higher than 0.275 vvm. As a consequence, the air was not distributed equally in the vessel and some of it tended to escape the impeller without being dispersed at all.

A similar behavior was observed for PBT of a diameter equal to 0.1016 m. In this case, however, the deviation was much higher at impeller clearances less than the impeller diameter and at air flow rate higher than 0.11 vvm. This could be due to the low agitation speed and the fluctuation of the air flow direction away from the center of the impeller which affects the air dispersion. In addition, a comparison of $N_{cd-model}$ with N_{cd-smp} and a comparison of $\Delta N_{cd-model}$ with ΔN_{cd-smp} are shown in Figure 6.5

6.7.3 Results for Curved-Blade Turbine, Flat-Blade Turbine, and Propeller Turbine Pumping Downward

The results for these three types of impellers (CBT, FBT, and PT pumping downward) are shown in Figures 6.5 and 6.11 and Tables B.11 and B.12. It was found that the model underpredicted the values of N_{cd}. The deviation from the experimental values was found to increase with the air flow rate. The deviation was found to be in the neighborhood of 6 % at Q_{air} equal to 0.11 vvm and about 16 % at Q_{air} equal to 0.44 vvm. The large deviation in the predicted values of N_{cd} is due to the high values of P_G, in these three cases, which is a result of the failure of these three impellers to disperse the air efficiently. It was observed that a considerable amount of air tended to escape the impeller without being broken into bubbles or being dispersed into the liquid.

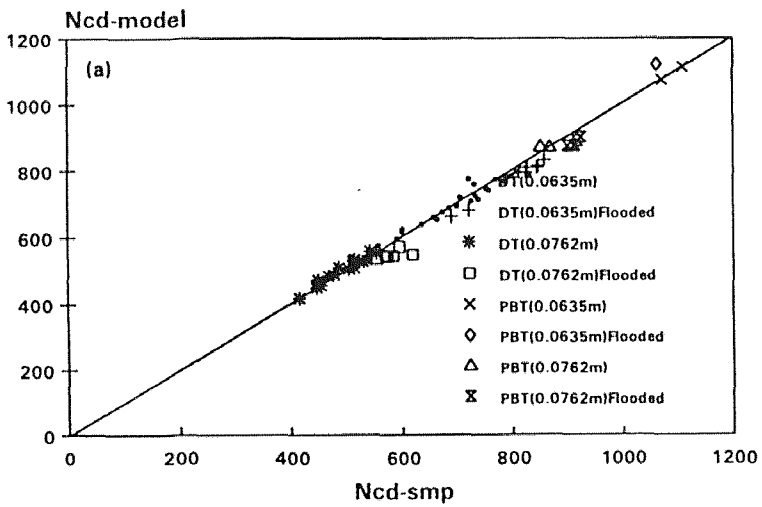

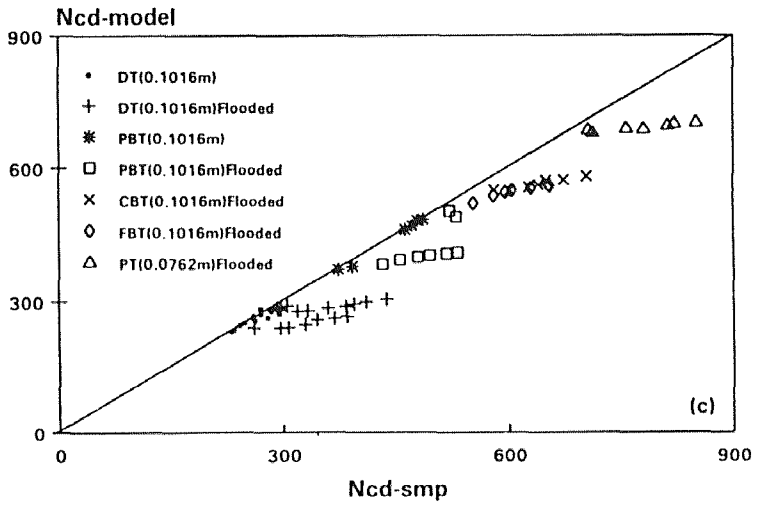

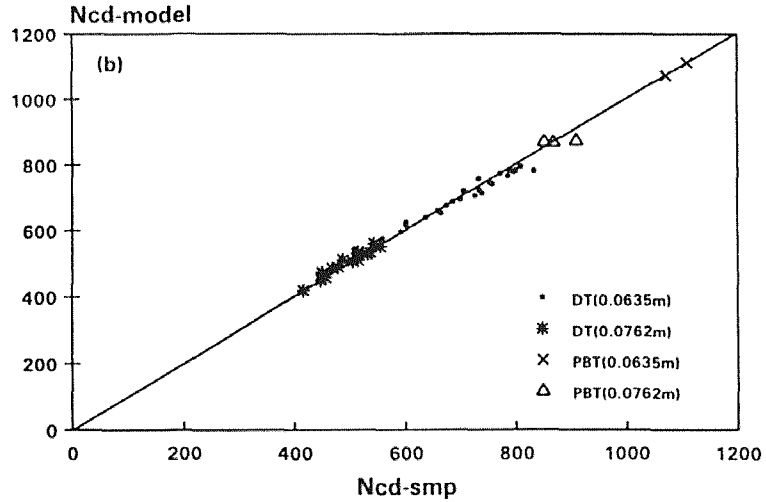

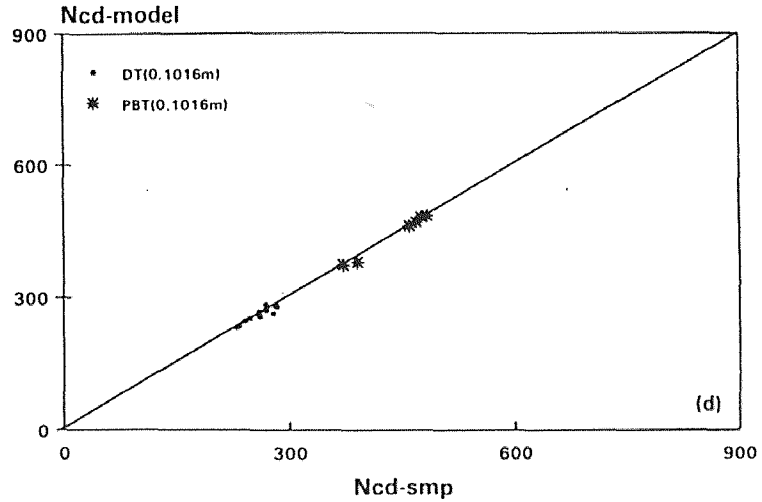

Figure 6.5A Comparison of Ncd-model with Ncd-smp

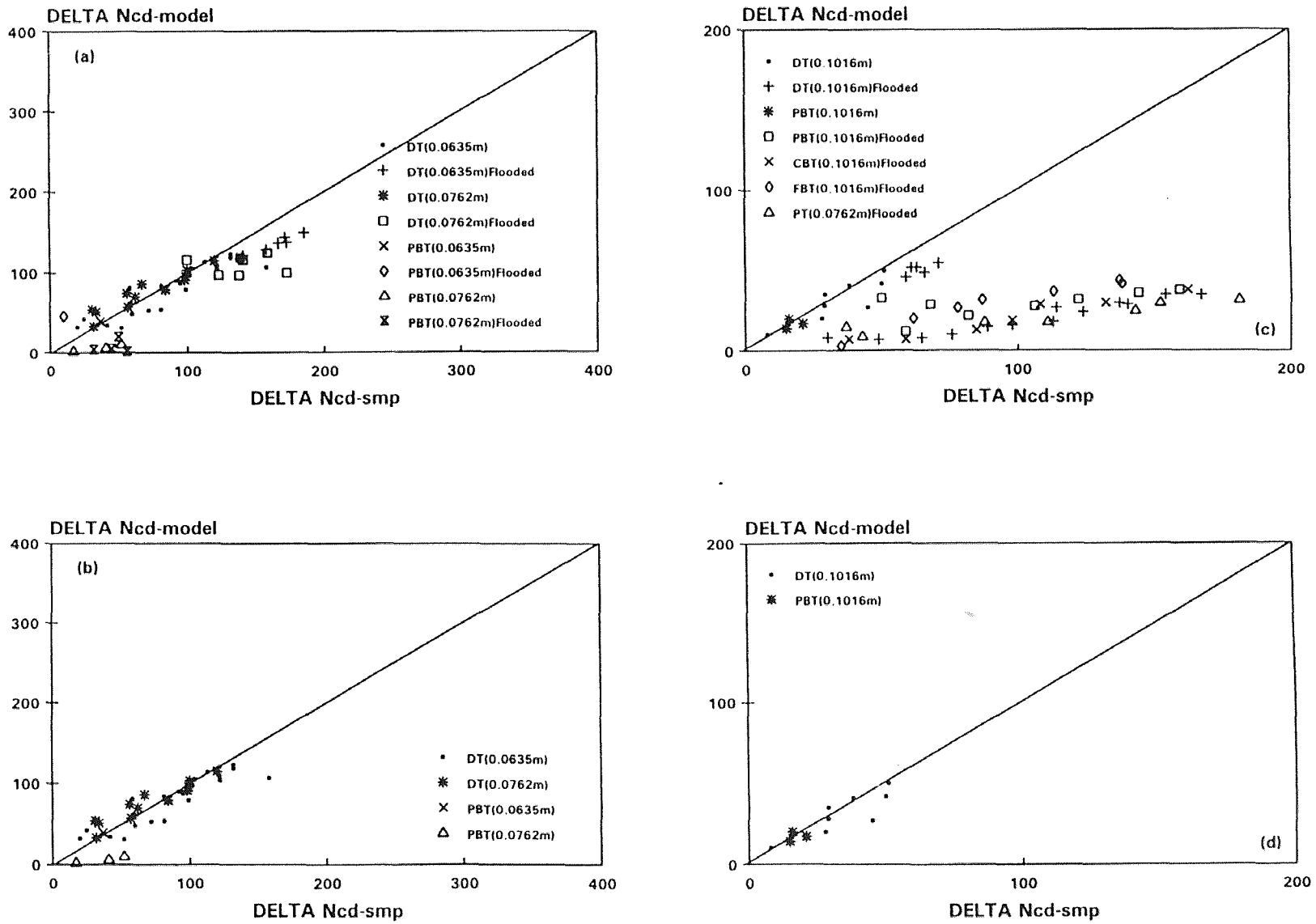

Figure 6.5B Comparison of Delta Ncd-model with Delta Ncd-smp

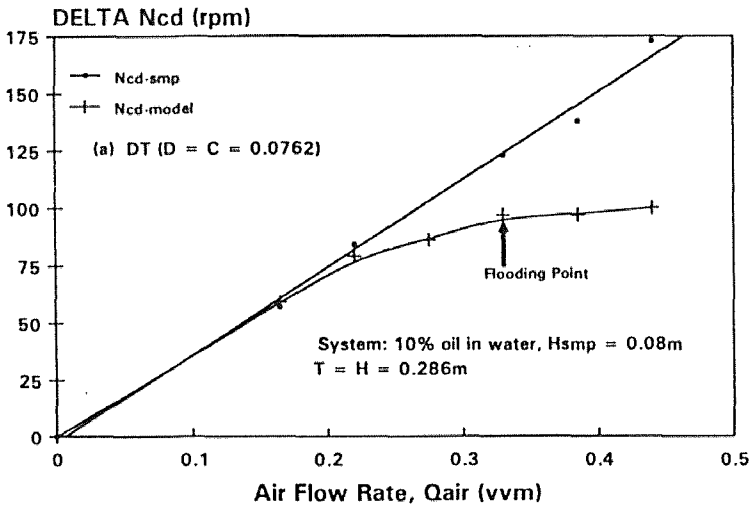

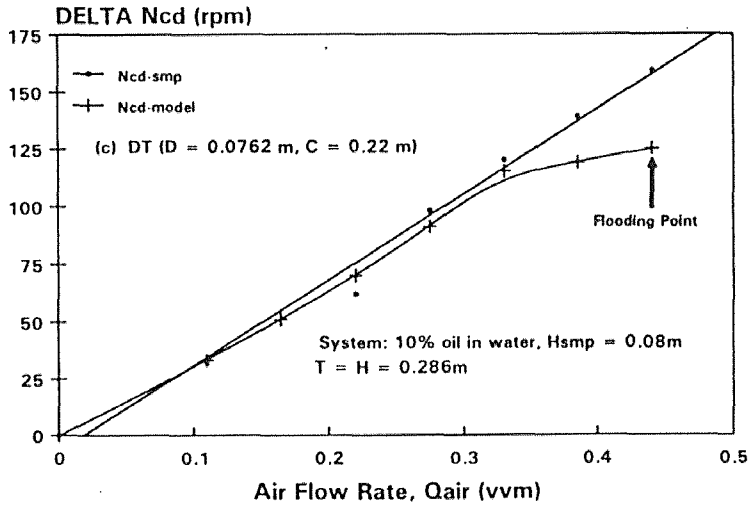

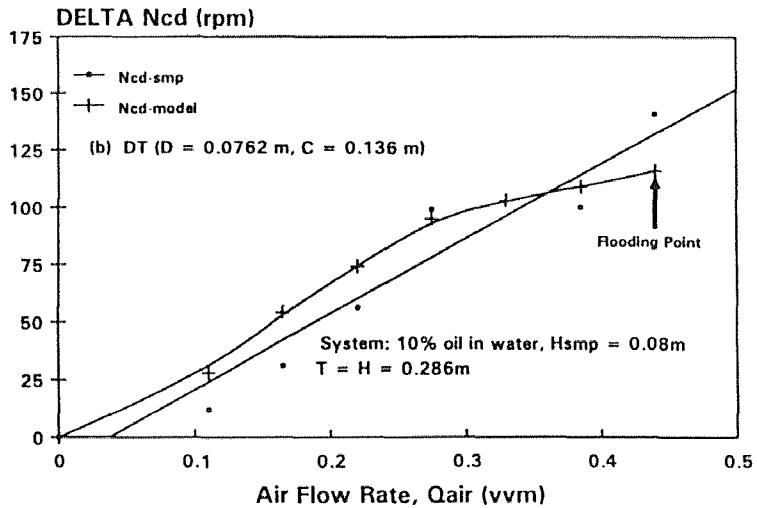

Figure 6.6 Effect of Qair on Delta Ncd for DT, D = 0.0762 m

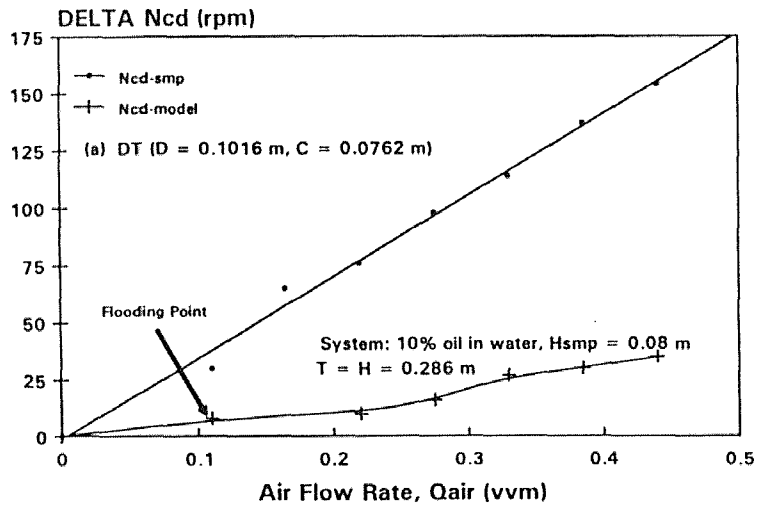

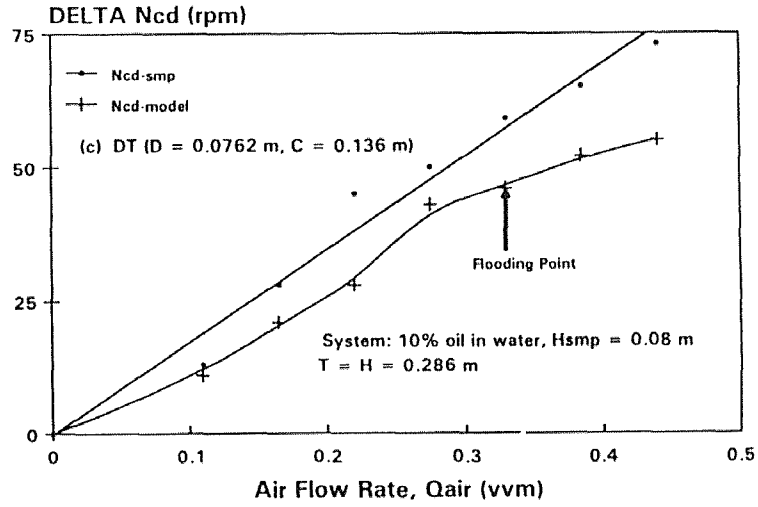

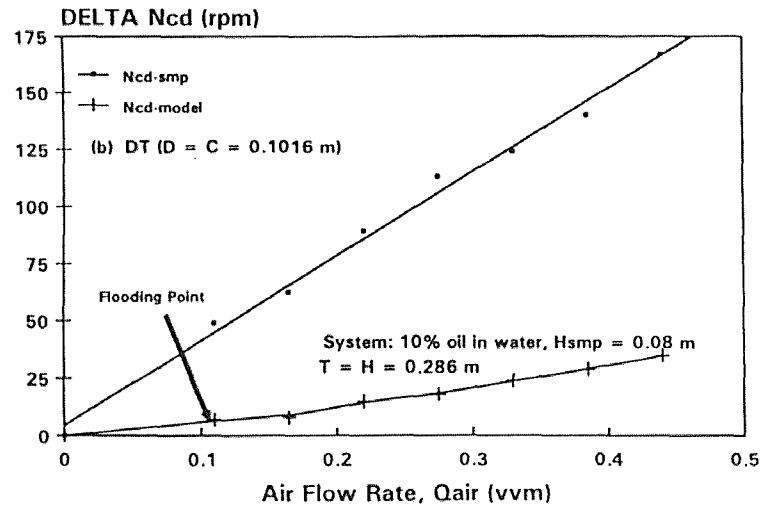

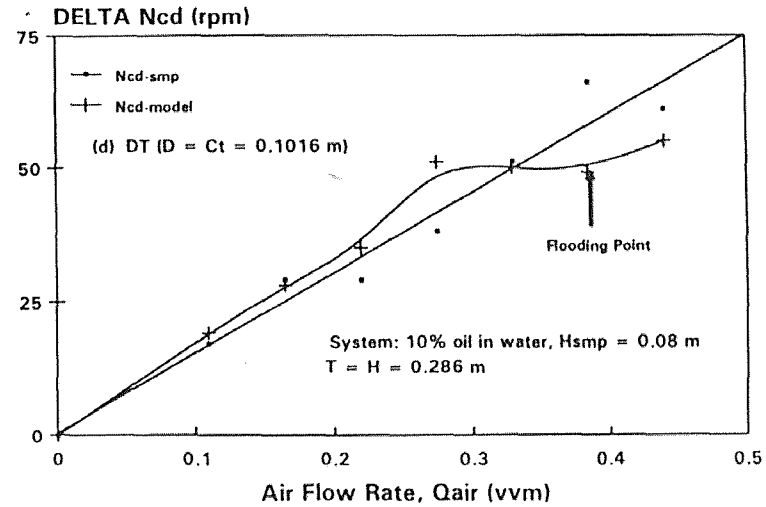

Figure 6.7 Effect of Qair on Delta Ncd for DT, D = 0.1016 m

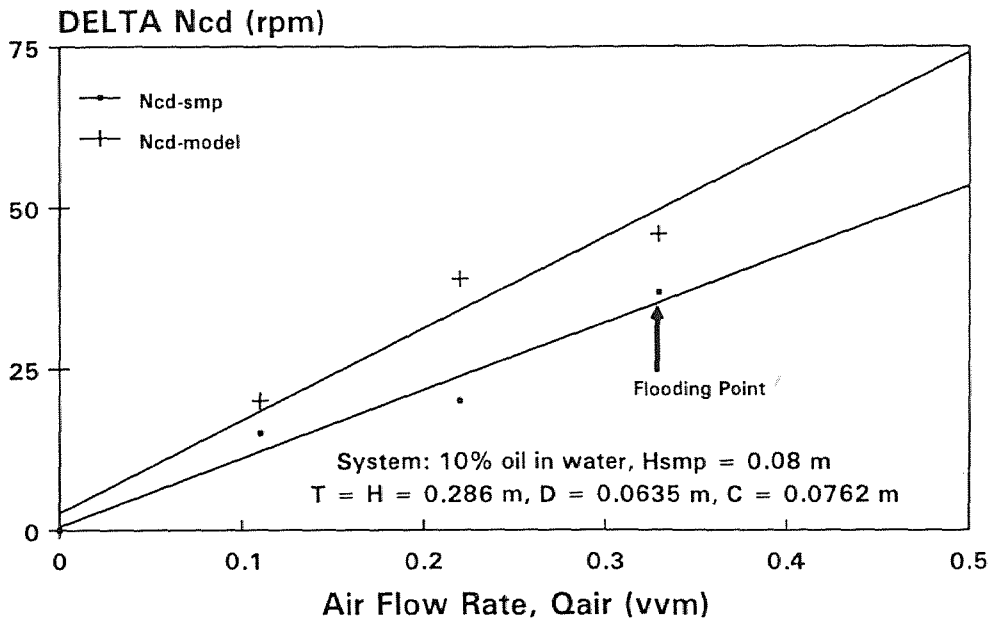

Figure 6.8 Effect of Qair on Delta Ncd for PBT (D = 0.0635 m, DOwn)

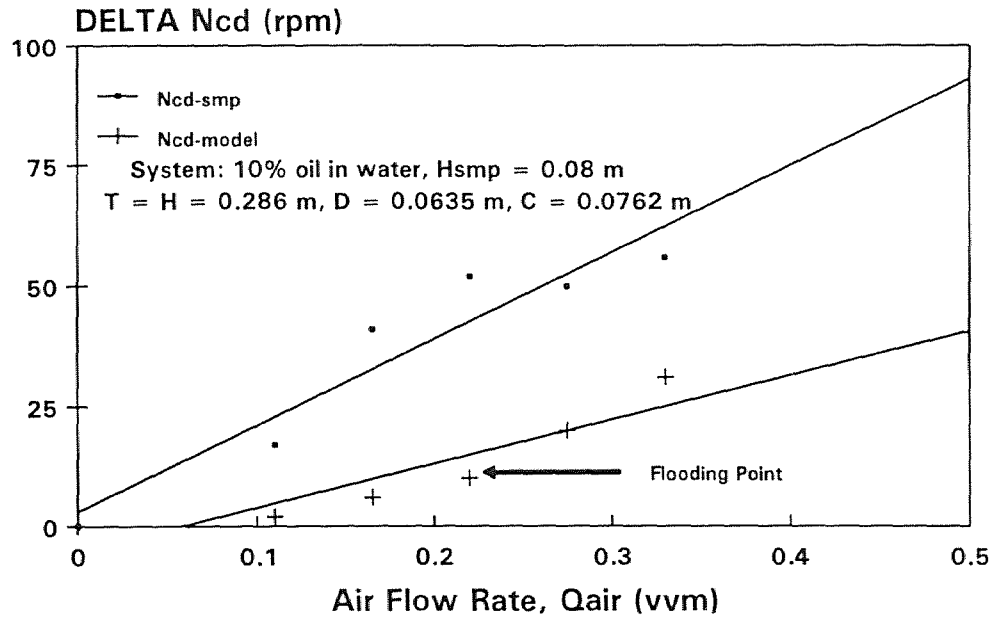

Figure 6.9 Effect of Qair on Delta Ncd for PBT (D = C = 0.0762 m, DOwn)

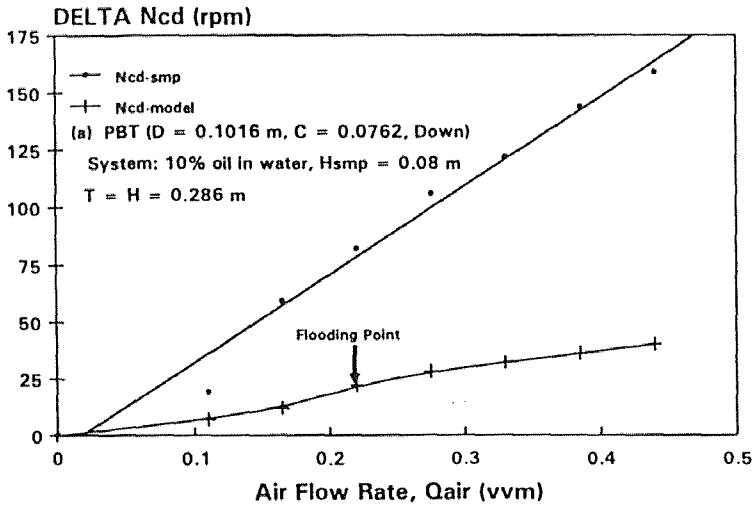

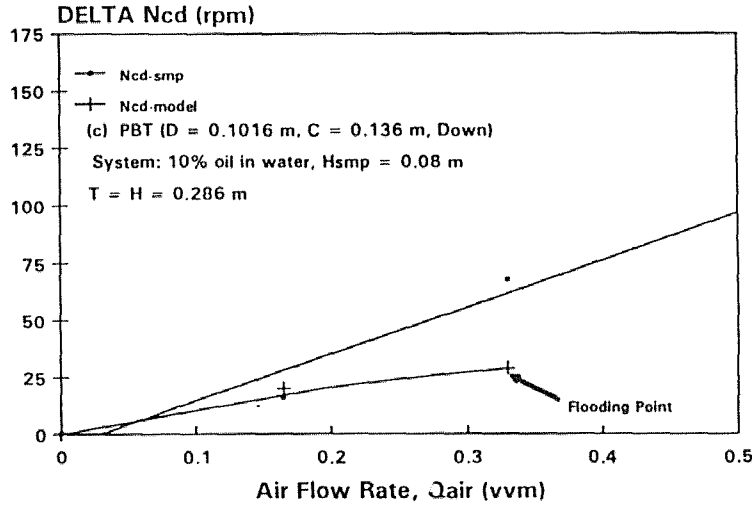

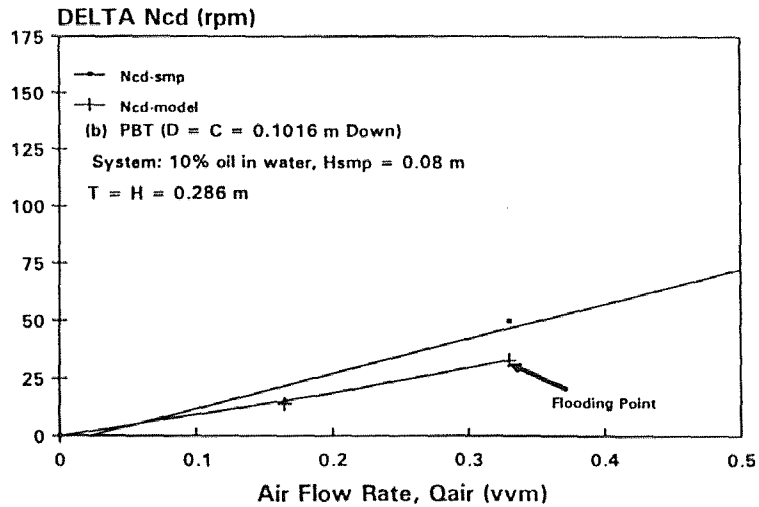

Figure 6.10 Effect of Qair on Delta Ncd (PBT, D = 0.1 m)

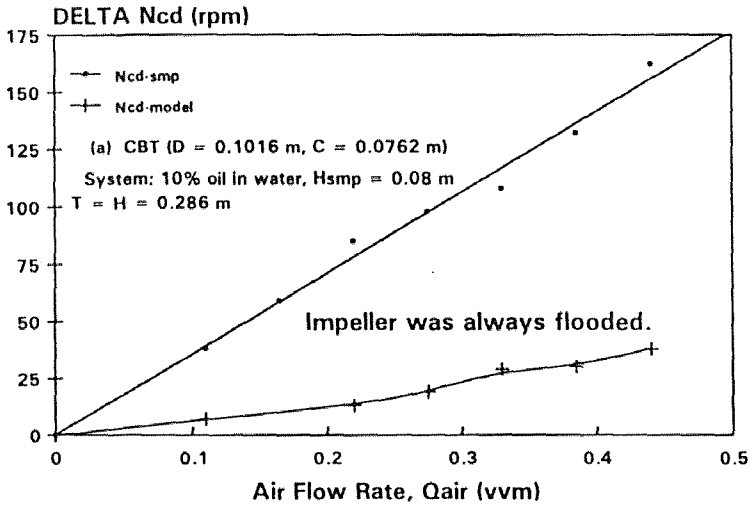

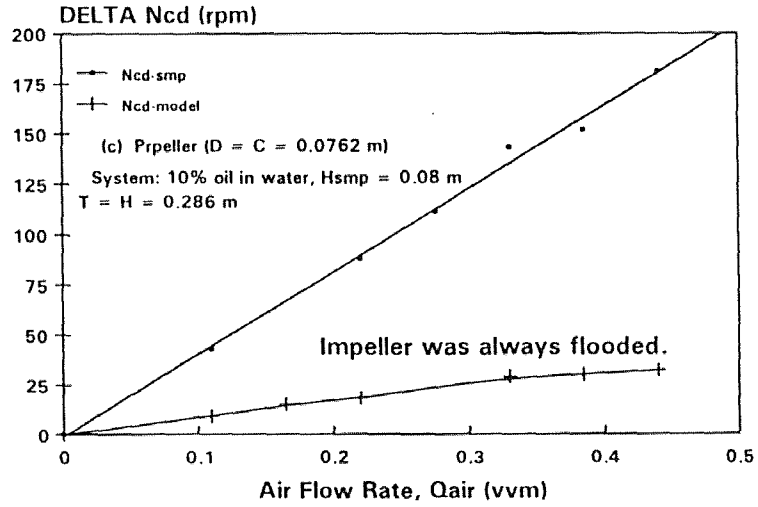

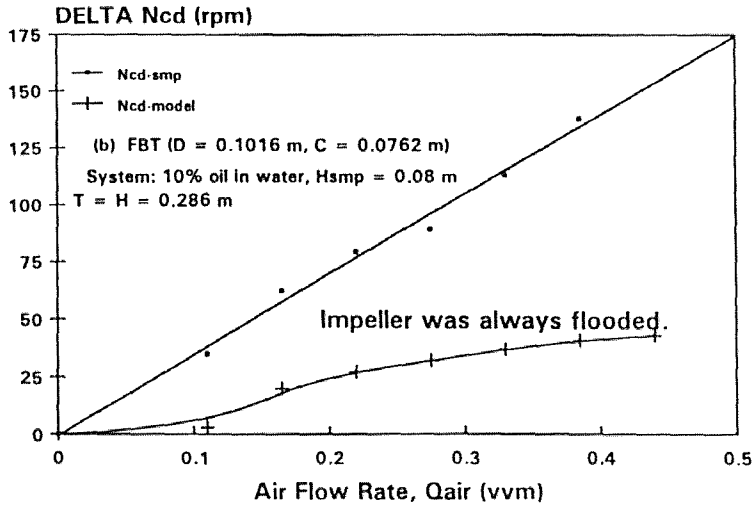

Figure 6.11 Effect of Qair on Delta Ncd for CBT, FBT, and PT

CHAPTER 7

CONCLUSIONS

1. The method earlier developed by our mixing research group to experimentally determine the value of N_{cd} in liquid-liquid systems was found to be also applicable to gassed liquid-liquid systems. The method is based on the analysis of the dispersed phase fraction in samples collected from the bulk of the mixture at different agitation speeds. This method is independent of the observer.

2. The proposed method was tested by collecting experimental data for N_{cd} in gassed liquid-liquid systems as a function of air flow rate, impeller type, impeller size, impeller off-bottom clearance, and sampling point location.

3. It was found that the results obtained using this method are in agreement (within 4%) with those obtained visually for all the cases studied. Therefore, it can be concluded that the proposed method is not affected by either any of the mixing parameter or the isokineticity and the location of the sampling point.

4. N_{cd} was found, to be strongly affected by the air sparging rate. Higher agitation speeds were required to attain the complete dispersion state when the air flow rate was increased and when the impeller pumping direction was opposed to that of the rising air.

5. At air flow rates between 0 vvm and 0.11 vvm, the impellers that were more significantly affected by the presence of air were, in increasing order, DT, PBT(up), Propeller(down), PBT(down), FBT, and CBT. At air flow rates higher than 0.11 vvm, the impellers that were significantly affected by the presence of air were, in increasing order, PBT(up), DT, Propeller(down), PBT(down), FBT, and CBT.

6. It was found that the dependence of N_{cd} on the impeller diameter, D, followed a power law. The results indicated that the exponent for D is similar in both gassed and

ungassed systems. It was also found that this exponent was higher for the case in which the clearance, C, was kept constant than in the case in which the ratio C/D was kept constant.

7. N_{cd} was found to be a strong function of the impeller off-bottom clearance, C. In all cases examined, it was found that N_{cd} had its lowest value when the impeller was placed very close to the liquid-liquid interface. As the impeller was placed farther away from the liquid-liquid interface N_{cd} increased until it reached its highest value at an impeller clearance equal to the impeller diameter.

8. A model based on Kolmogoroff's theory of isotropic turbulence was developed to predict the results obtained under gassed conditions.

9. A good agreement was found between the experimental values of ΔN_{cd} for disk turbine and 45-PBT pumping downward and the corresponding values predicted by the model.

10. The model underpredicted the incremental minimum agitation speed under gassed conditions for CBT, FBT, and propeller turbine pumping downward. This was a result of the failure of these three impeller types to disperse the sparged air efficiently.

APPENDIX A

FIGURES FOR CHAPTER 6

This appendix includes the figures showing the validation of the sampling procedure for the determination of N_{cd} (Figures A.1-A.4). It also includes: a figure showing the effect of Q_{air} on power consumption (Figure A.5), the figures showing the effect of impeller size on N_{cd} (Figures A.6-A.12), the effect of impeller clearance on N_{cd} (Figures A.13-A.16), and the effect of H/T on N_{cd} (Figure A.17).

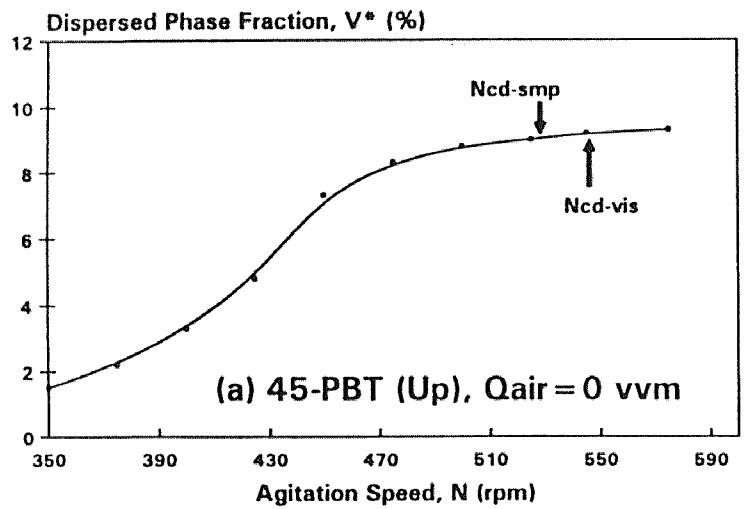

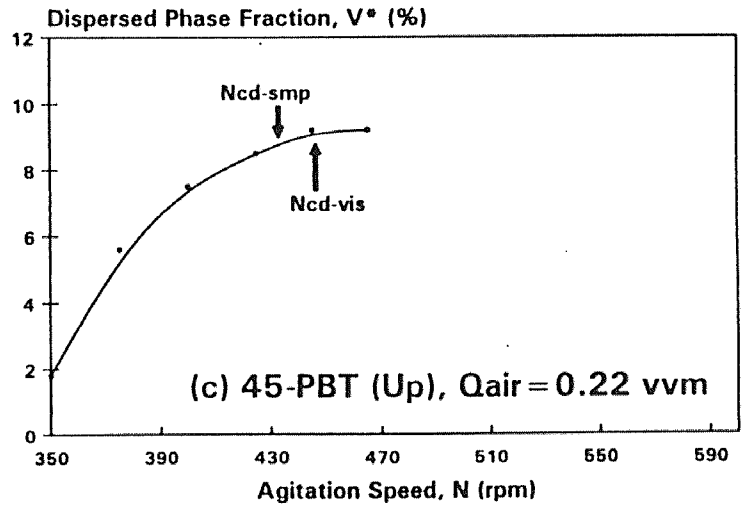

System: 10% oil in water, H = T = 0.286m
C = D = 0.076m, and Hsmp = 0.08m

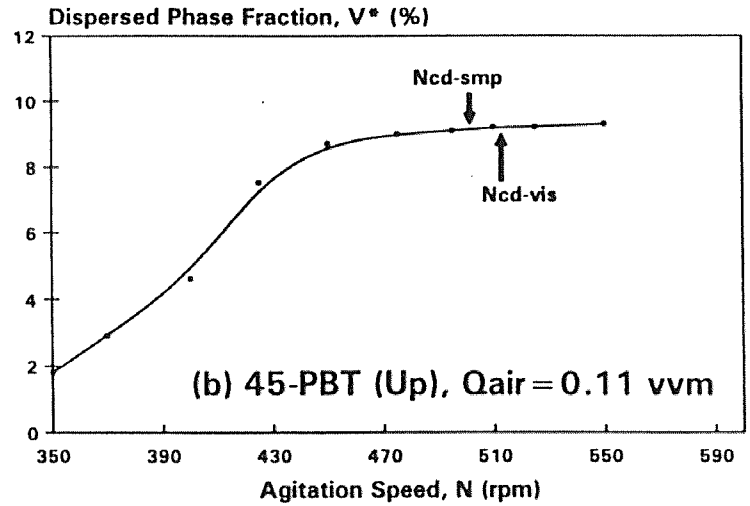

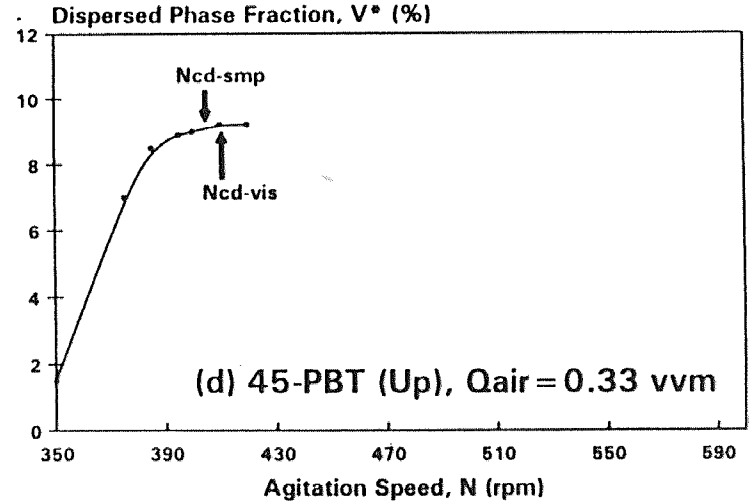

Figure A.1 Effect of Qair on Ncd Values

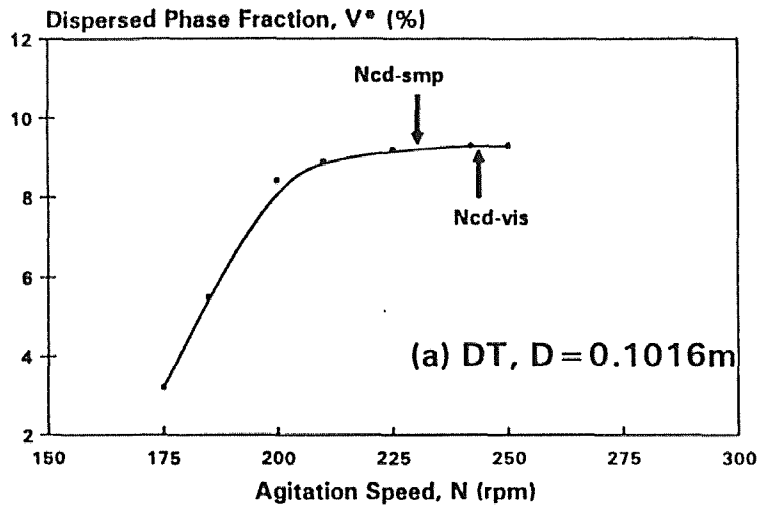

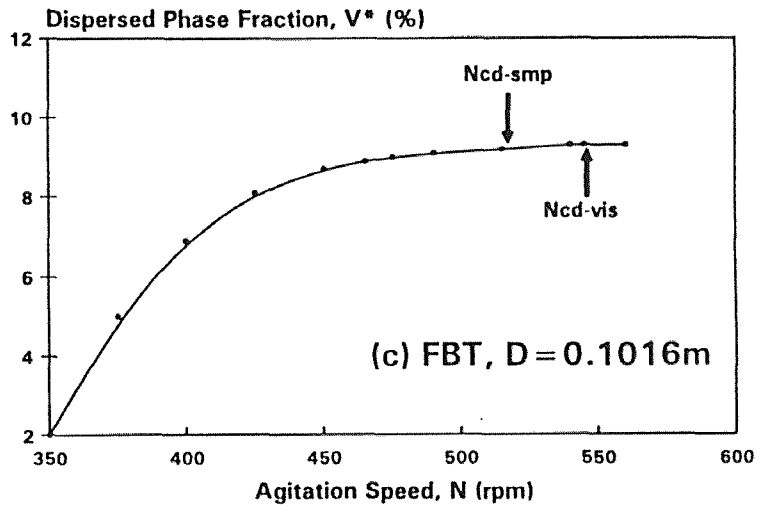

System: 10% oil in water, H=T=0.286m,

C=0.076m, Hsmp=0.08m, and Qair=0vvm

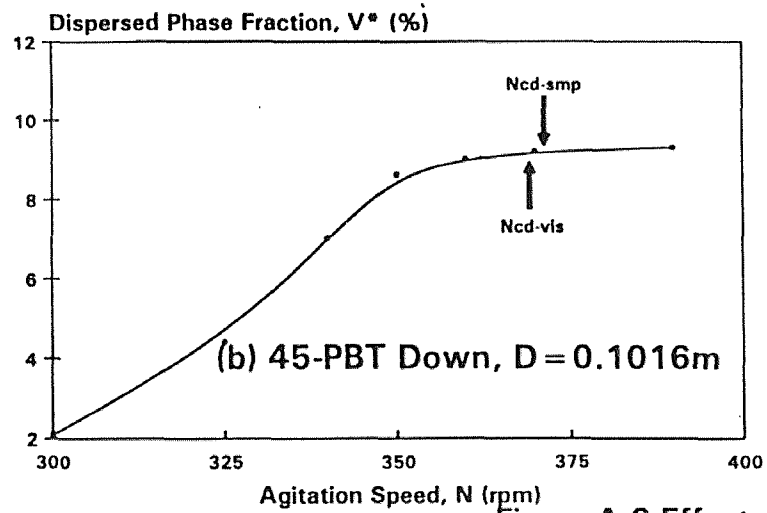

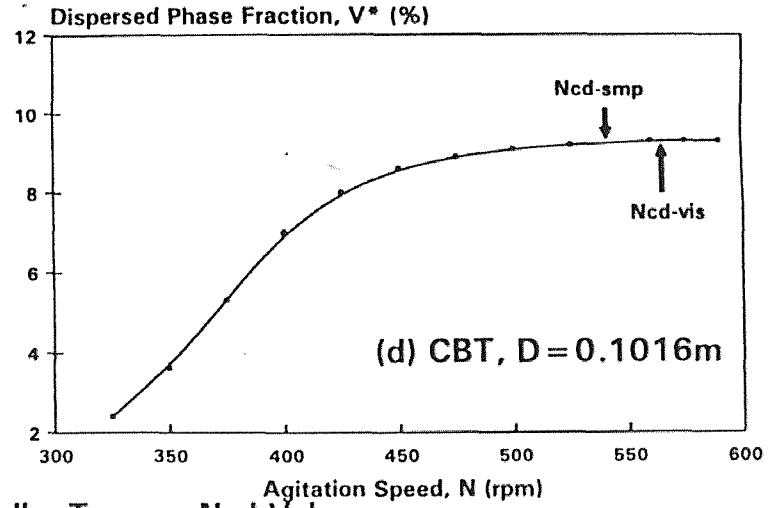

Figure A.2 Effect of Impeller Type on Ncd Values

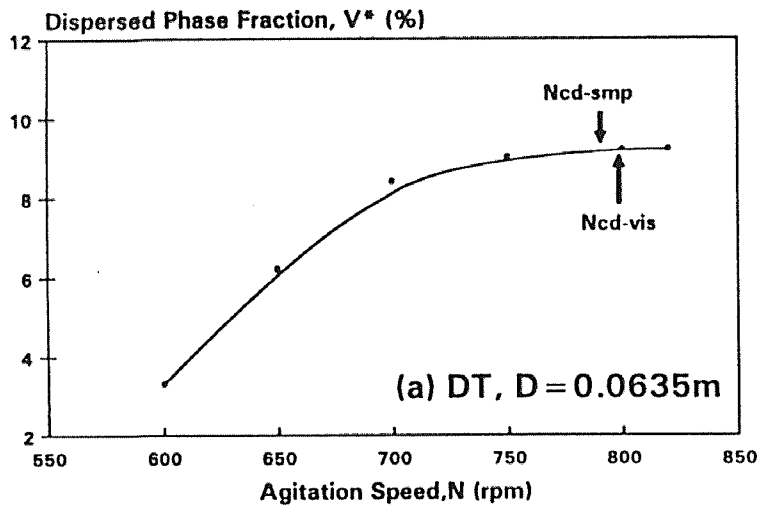

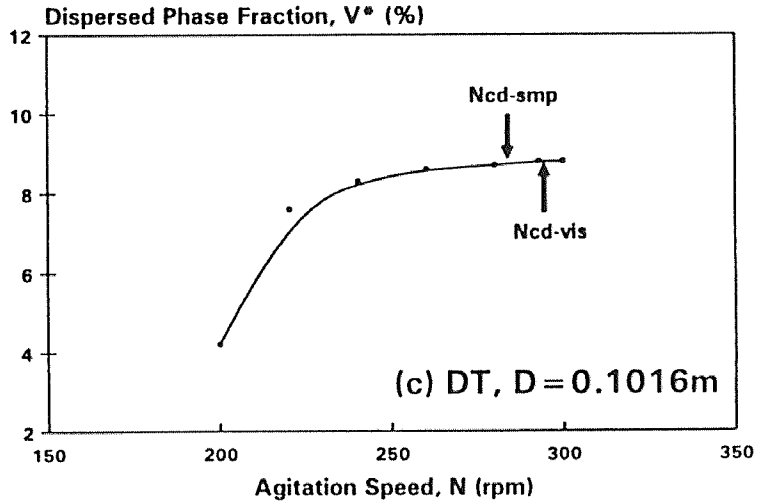

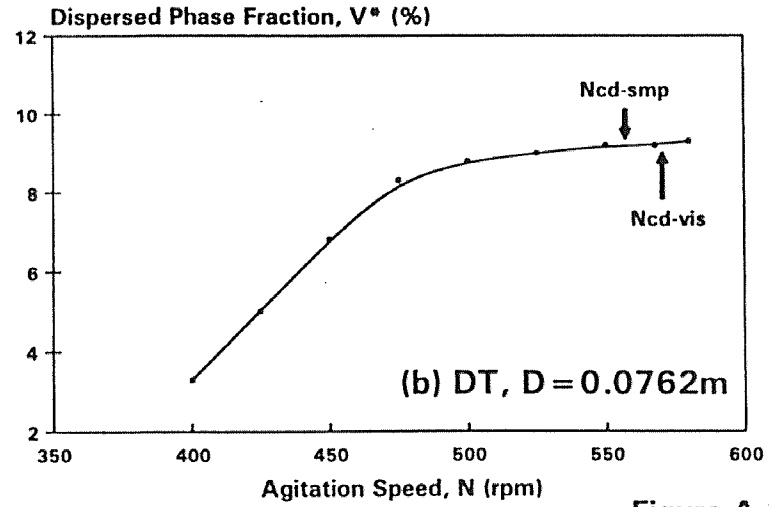

System: 10% oil in water, H = T = 0.286m,
Hsmp = 0.08m, C = 0.136m, Qair = 0.272 vvm

Figure A.3 Effect of Impeller Size on Ncd Values

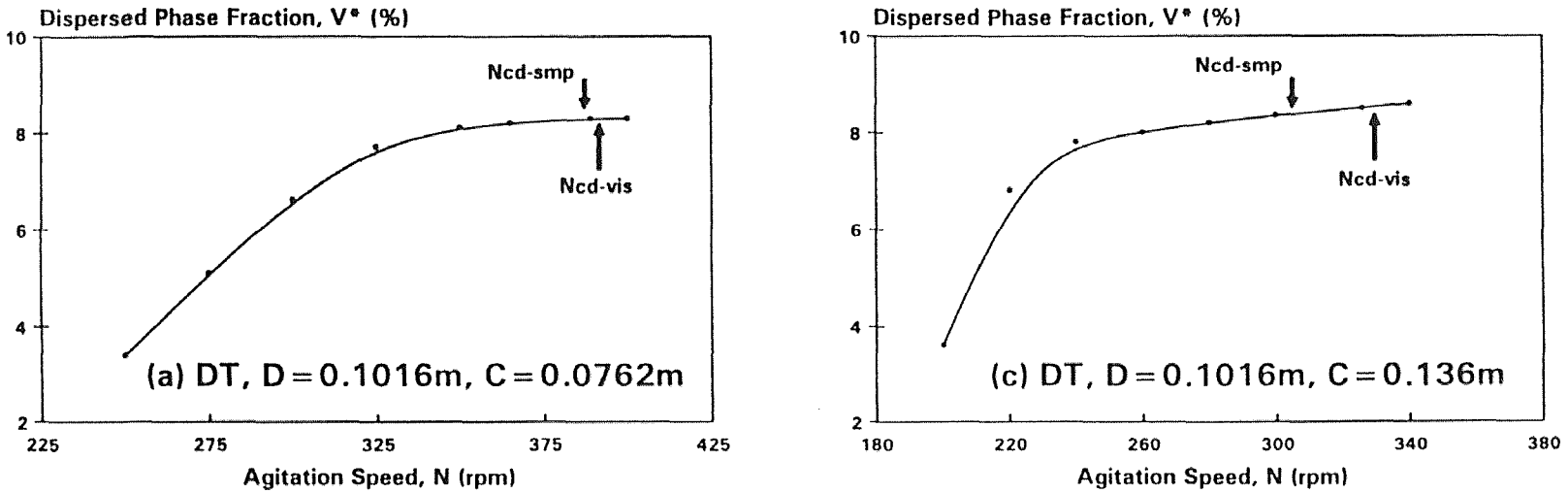

System: 10% oil in water, H = T = 0.286m,
Hsmp = 0.08m, and Qair = 0.435 vvm

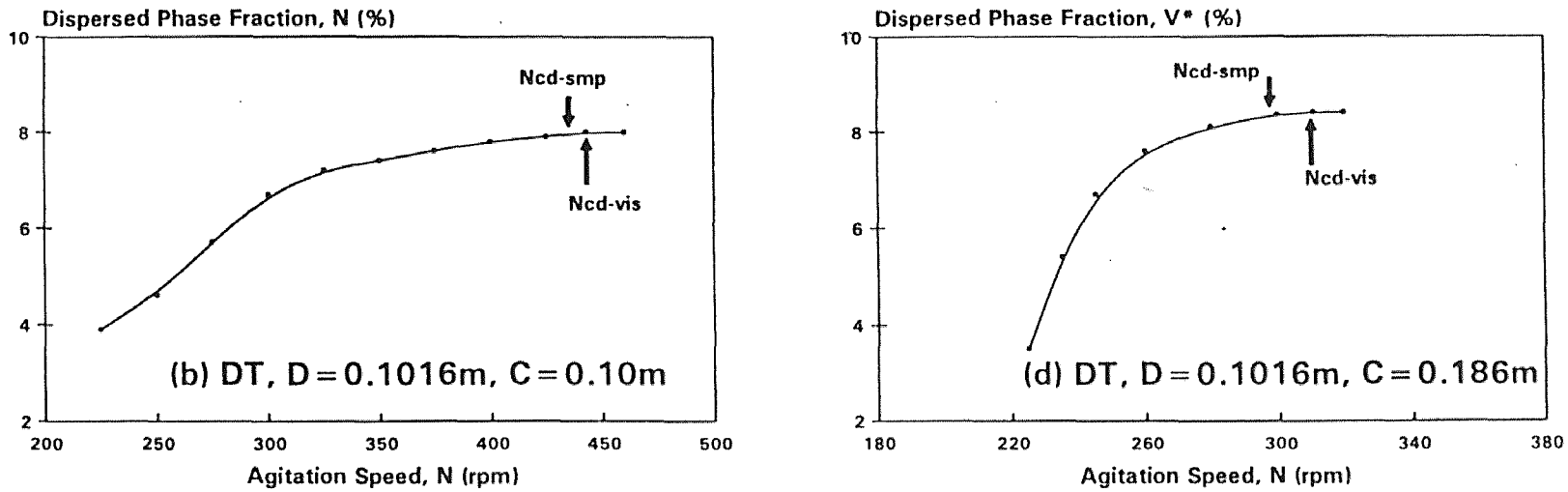

Figure A.4 Effect of C on Ncd Values

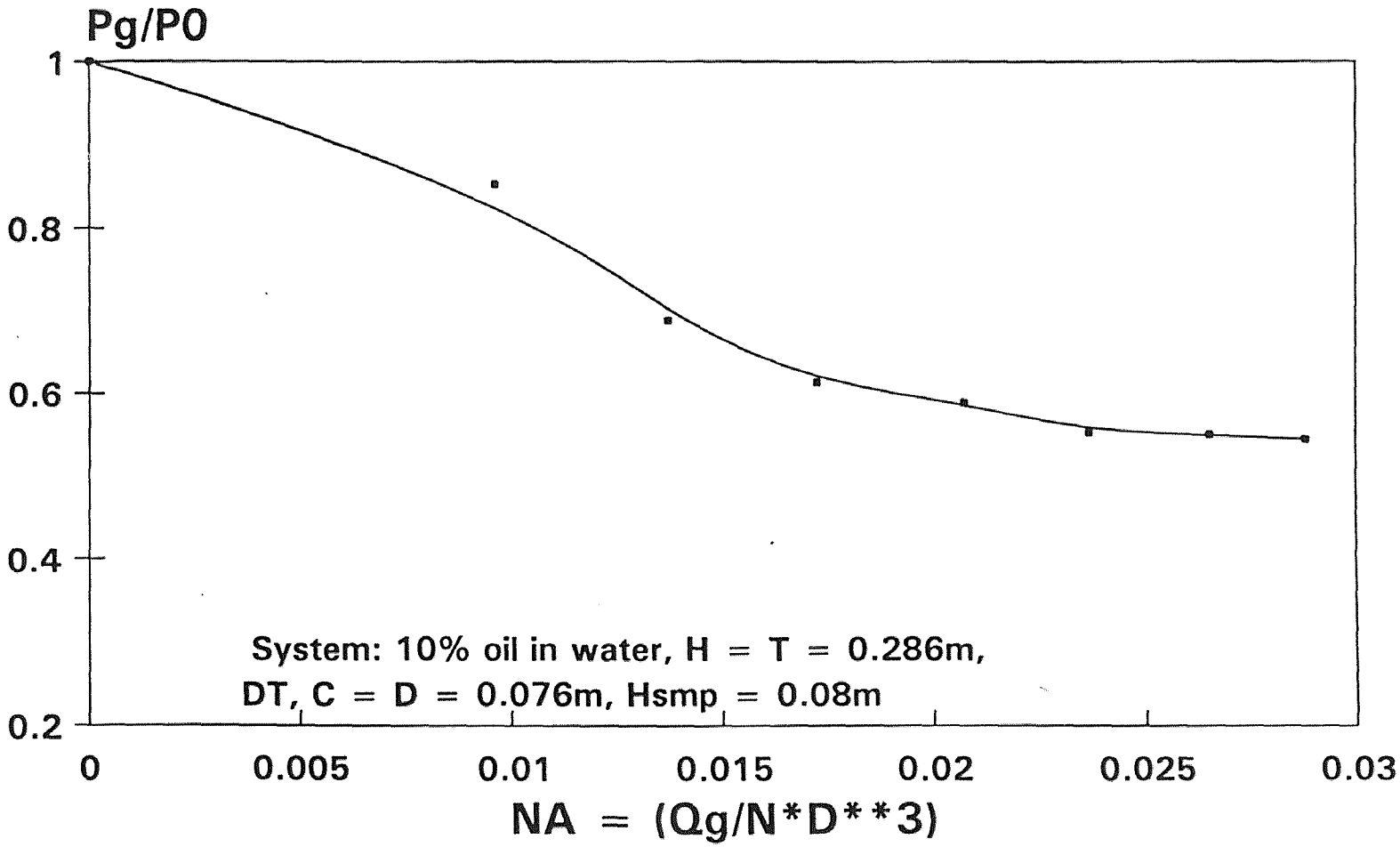

Figure A.5 Effect of Qair on Power Consumption

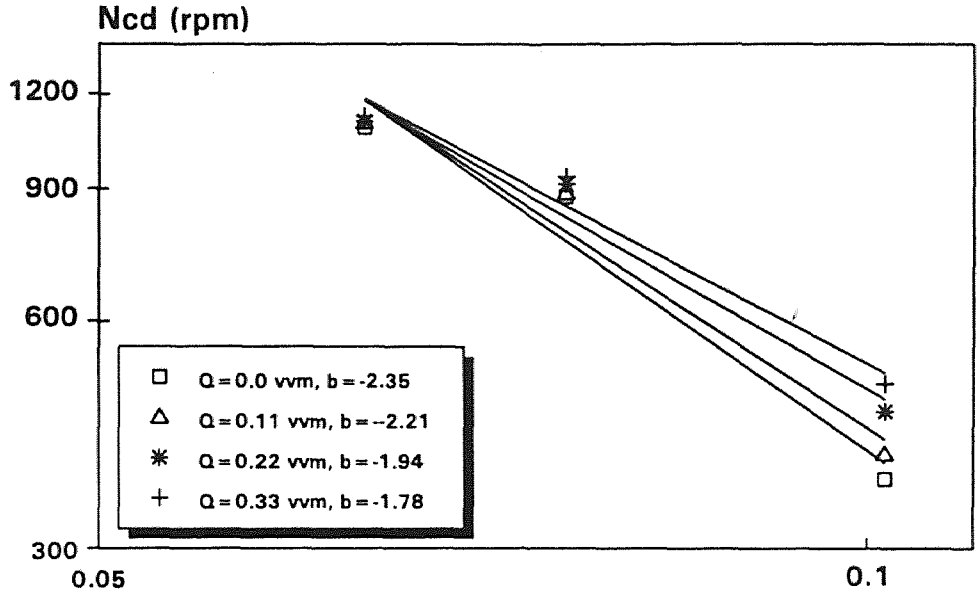

System: 10% oil in water, H = T = 0.286m
PBT (Down), C= 0.076m, Hsmp = 0.08m

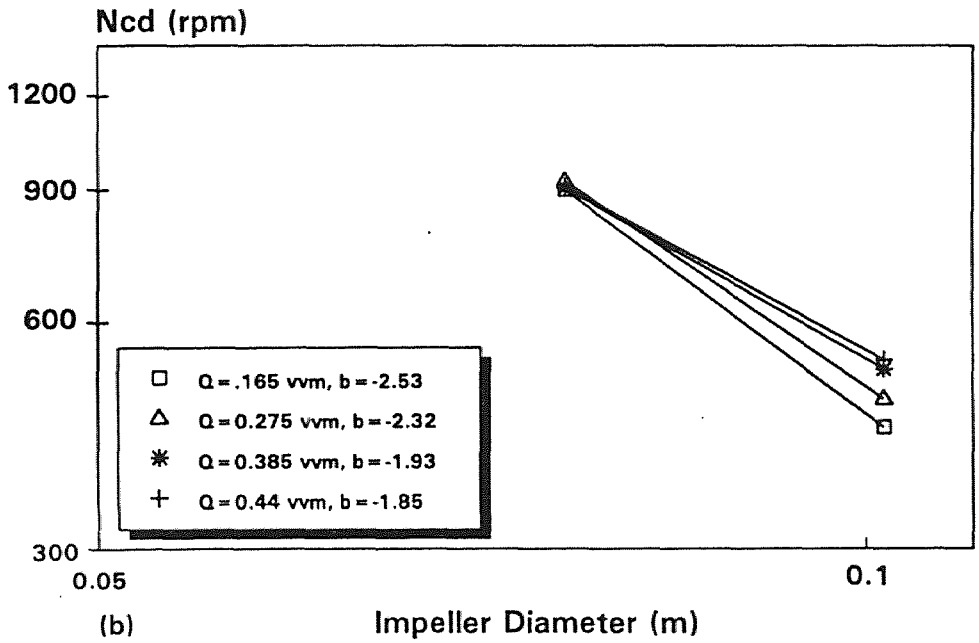

Figure A.6 Effect of D on Ncd, PBT (Down) (Constant C)

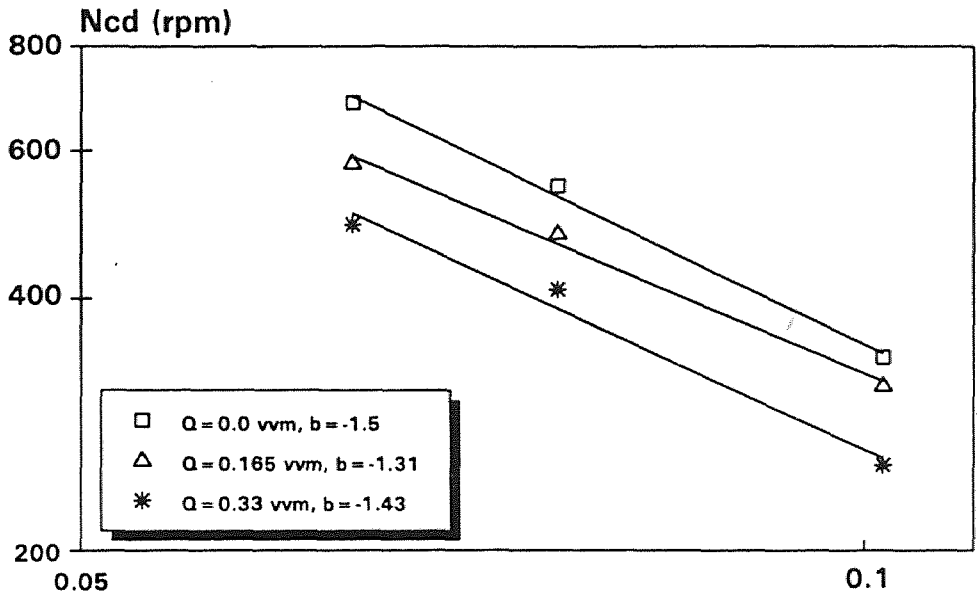

System: 10% oil in water, H = T = 0.286m,
PBT (UP), C = 0.076m, Hsmp = 0.08m

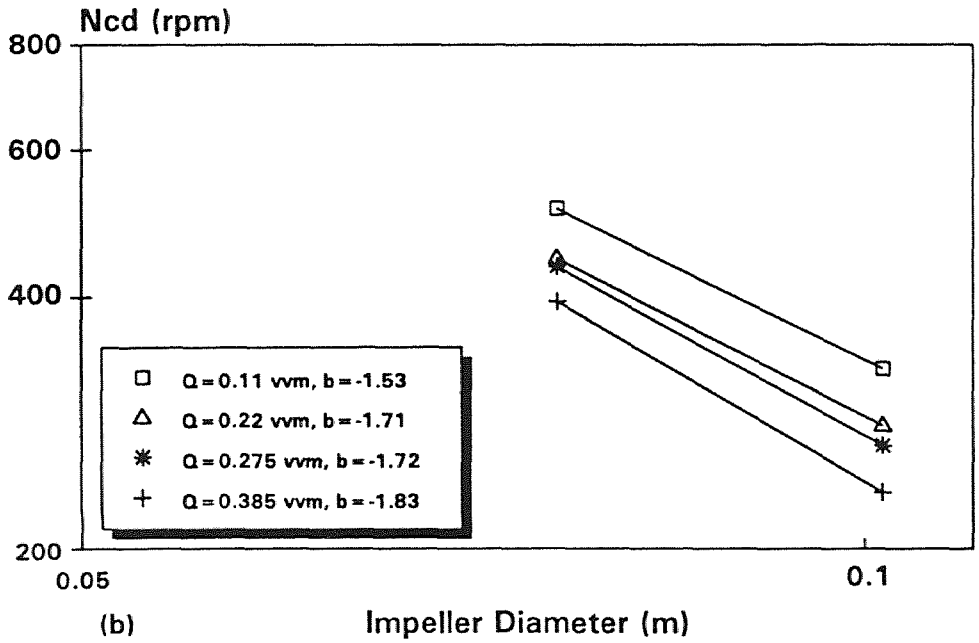

Figure A.7 Effect of D on Ncd, PBT (Up) (Constant C)

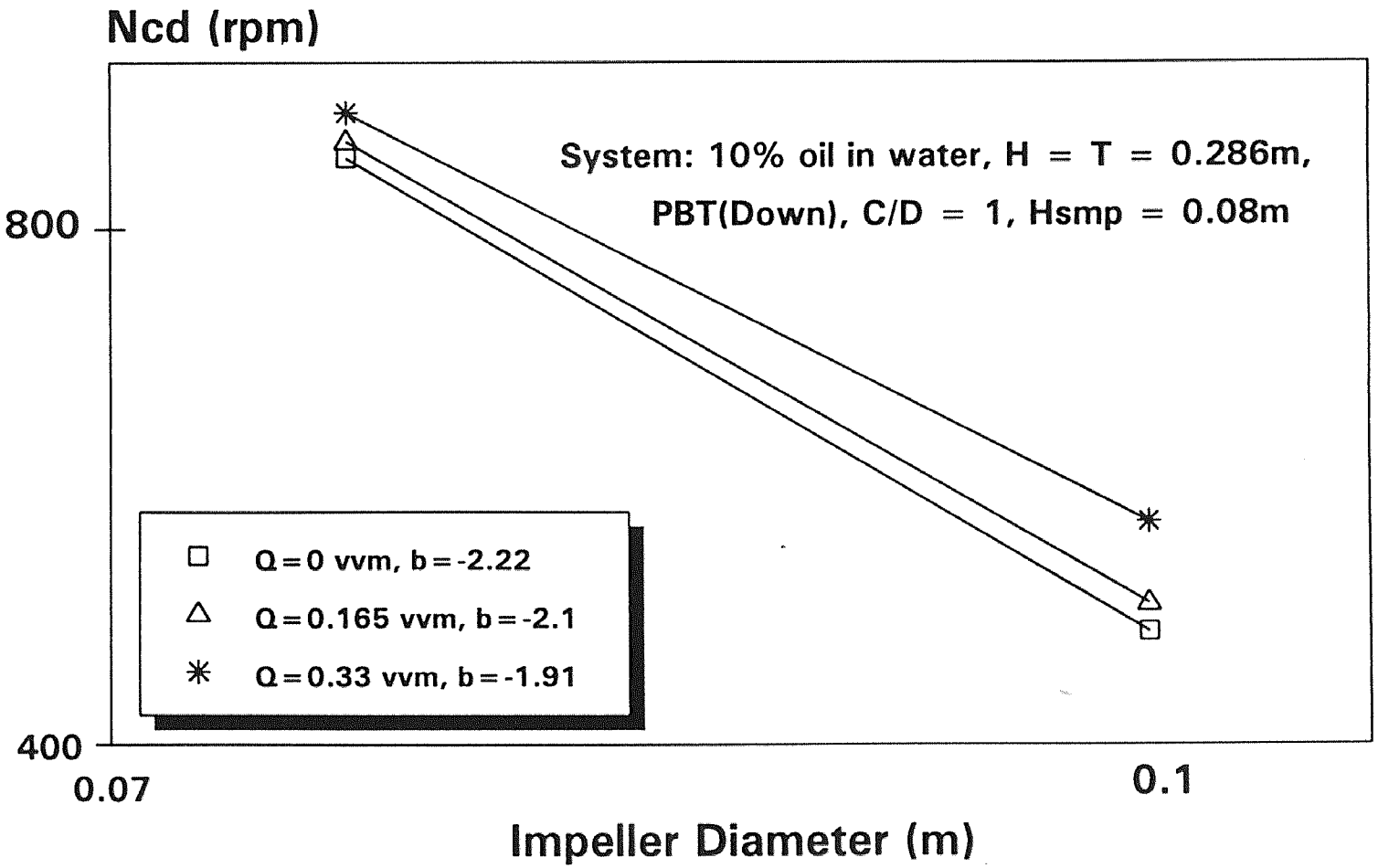

Figure A.8 Effect of D on Ncd, PBT (Down) (Constant C/D)

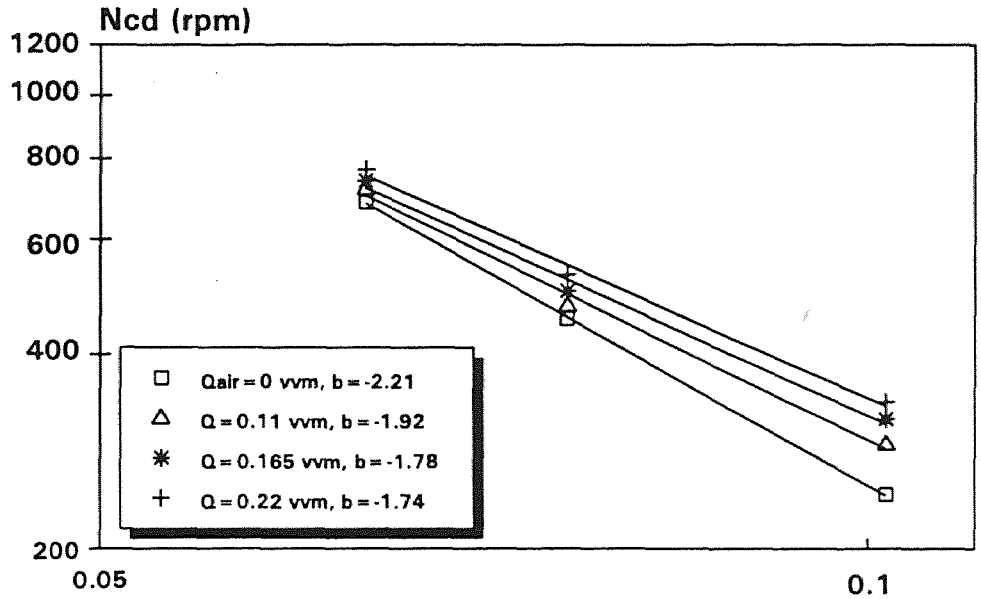

System: 10% oil in water, H = T = 0.286m, DT, C = 0.076m, Hsmp = 0.08m

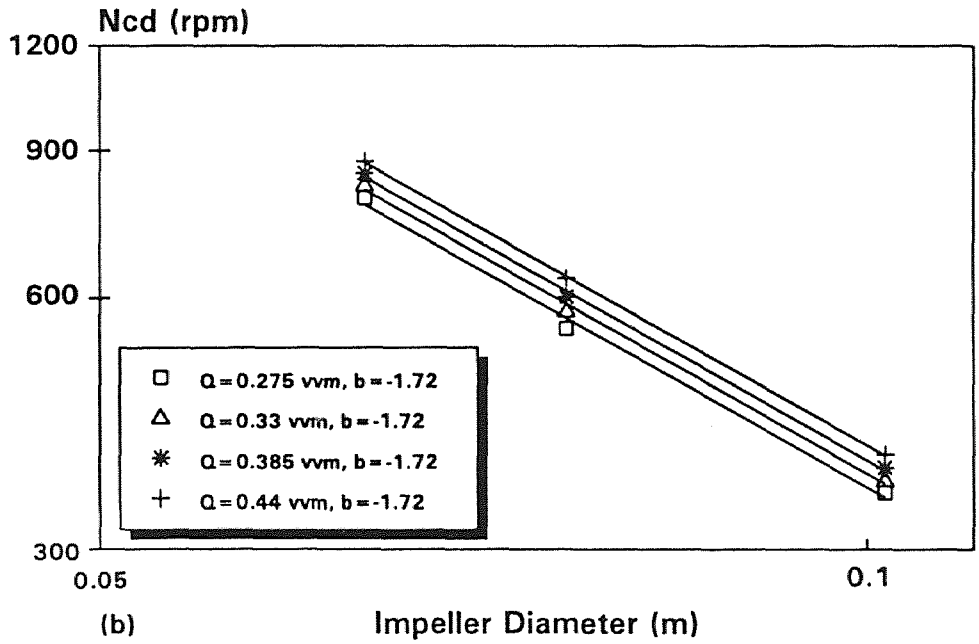

Figure A.9 Effect of D on Ncd, DT (Constant C)

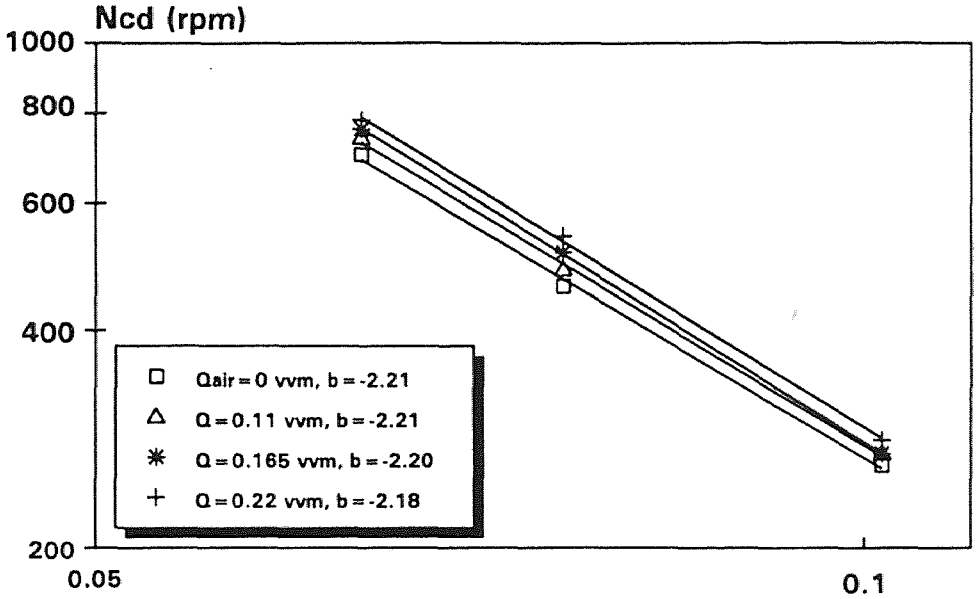

System: 10% oil in water, H = T = 0.286m, DT, C = 0.136m,, Hsmp = 0.08m

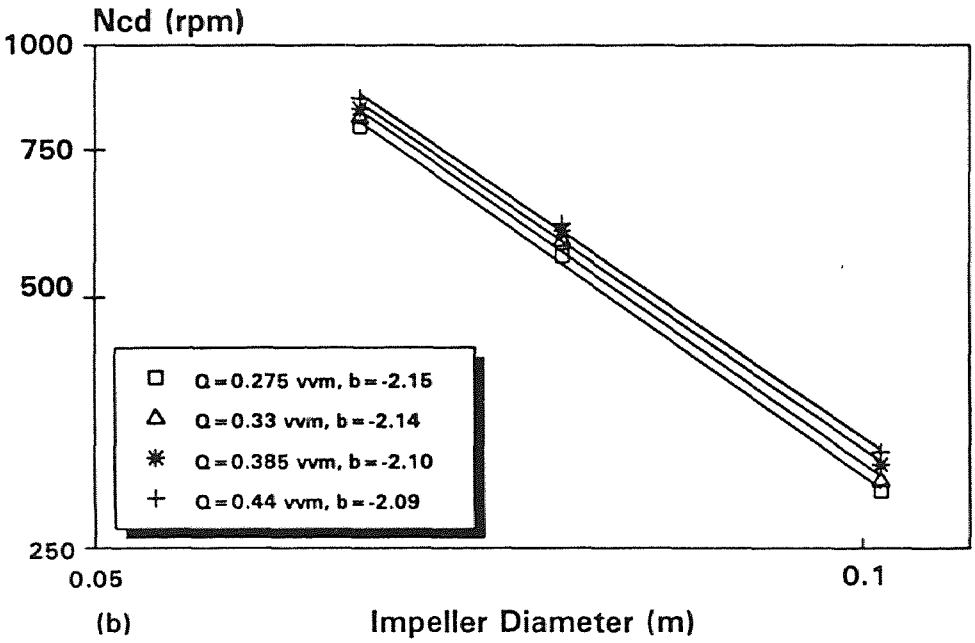

Figure A.10 Effect of D on Ncd, DT (Constant C)

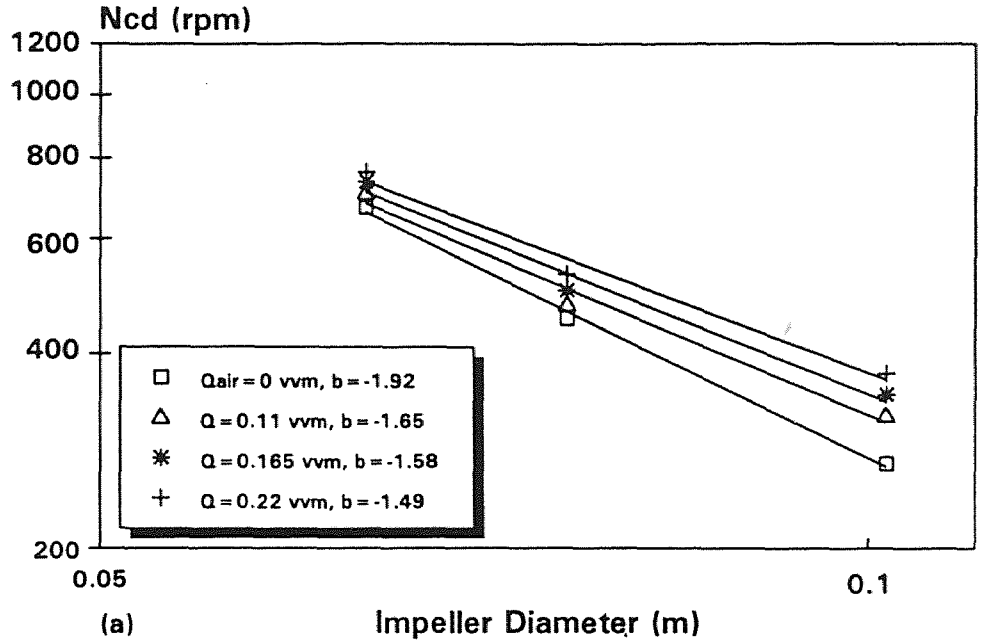

System: 10% oil in water, H = T = 0.286m, DT (C/D = 1), Hsmp = 0.08m

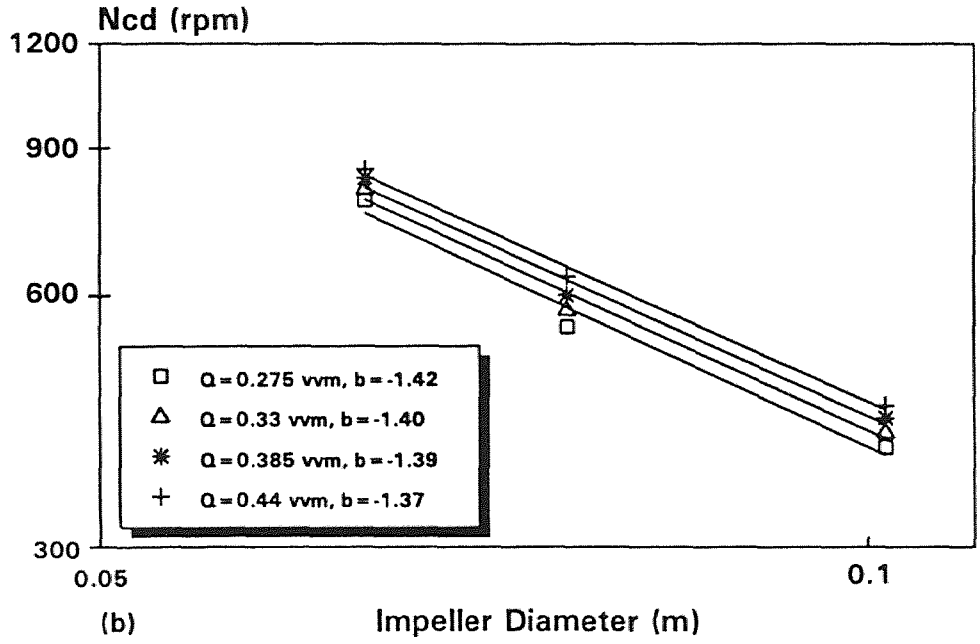

Figure A.11 Effect of D on Ncd, DT (Constant C/D)

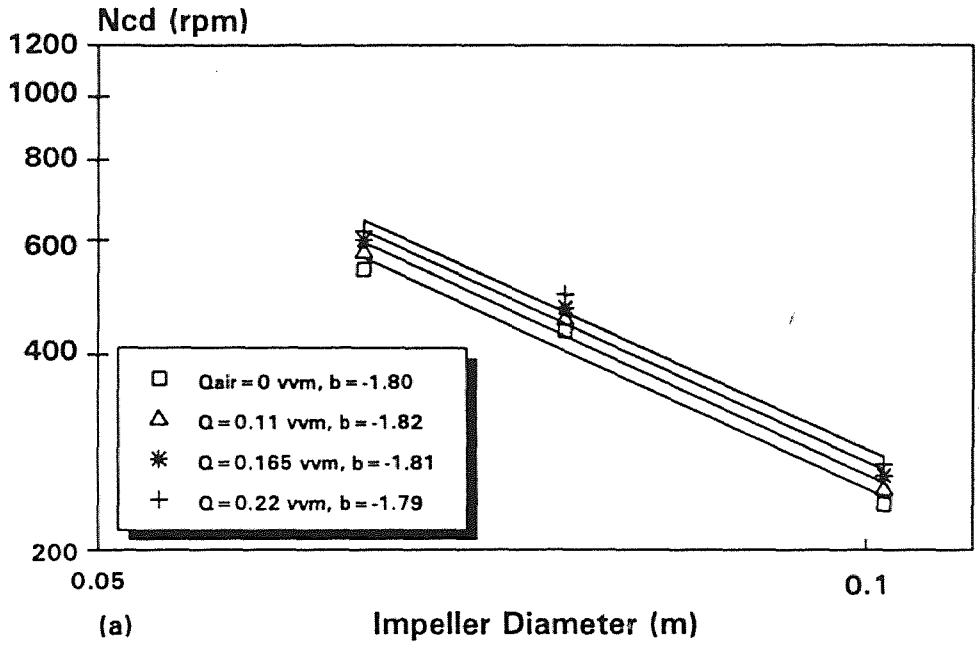

System: 10% oil in water, H = T = 0.286m, DT (Ct/D = 1), Hsmp = 0.08m

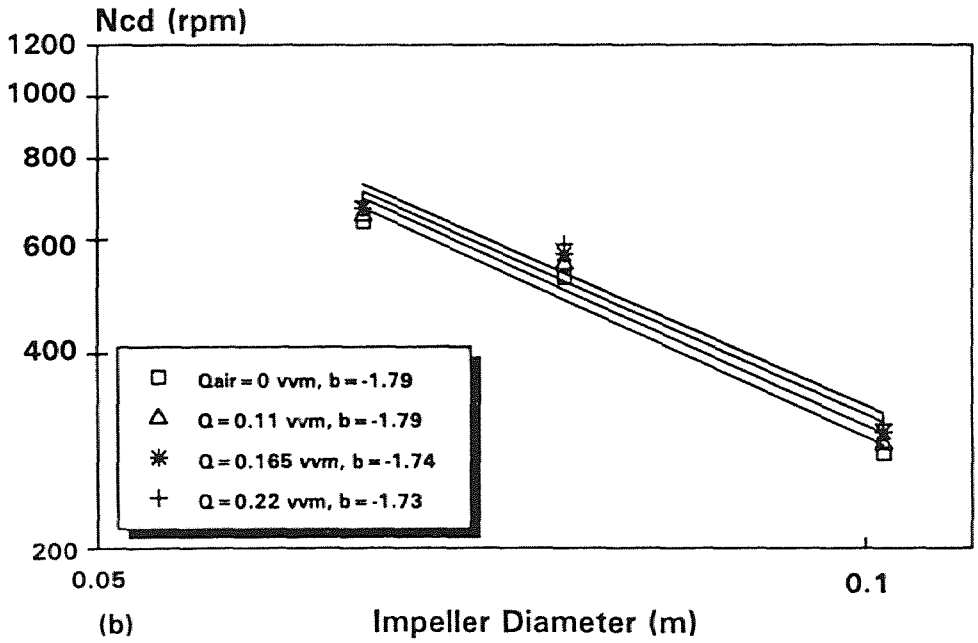

Figure A.12 Effect of D on Ncd, DT (Constant Ct/D)

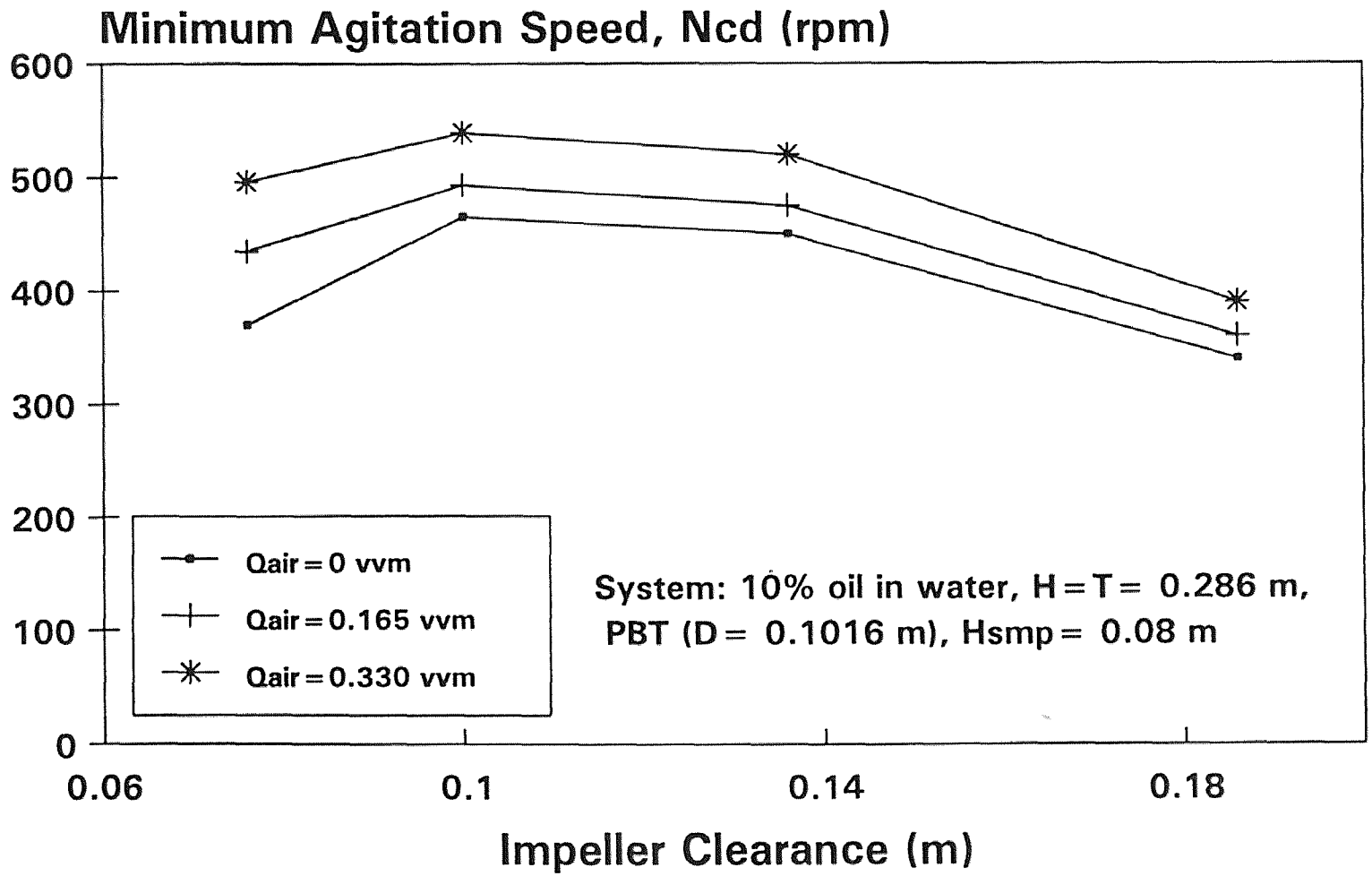

Figure A.13 Effect of C on Ncd,
45-PBT (Down), (D = 0.1016 m)

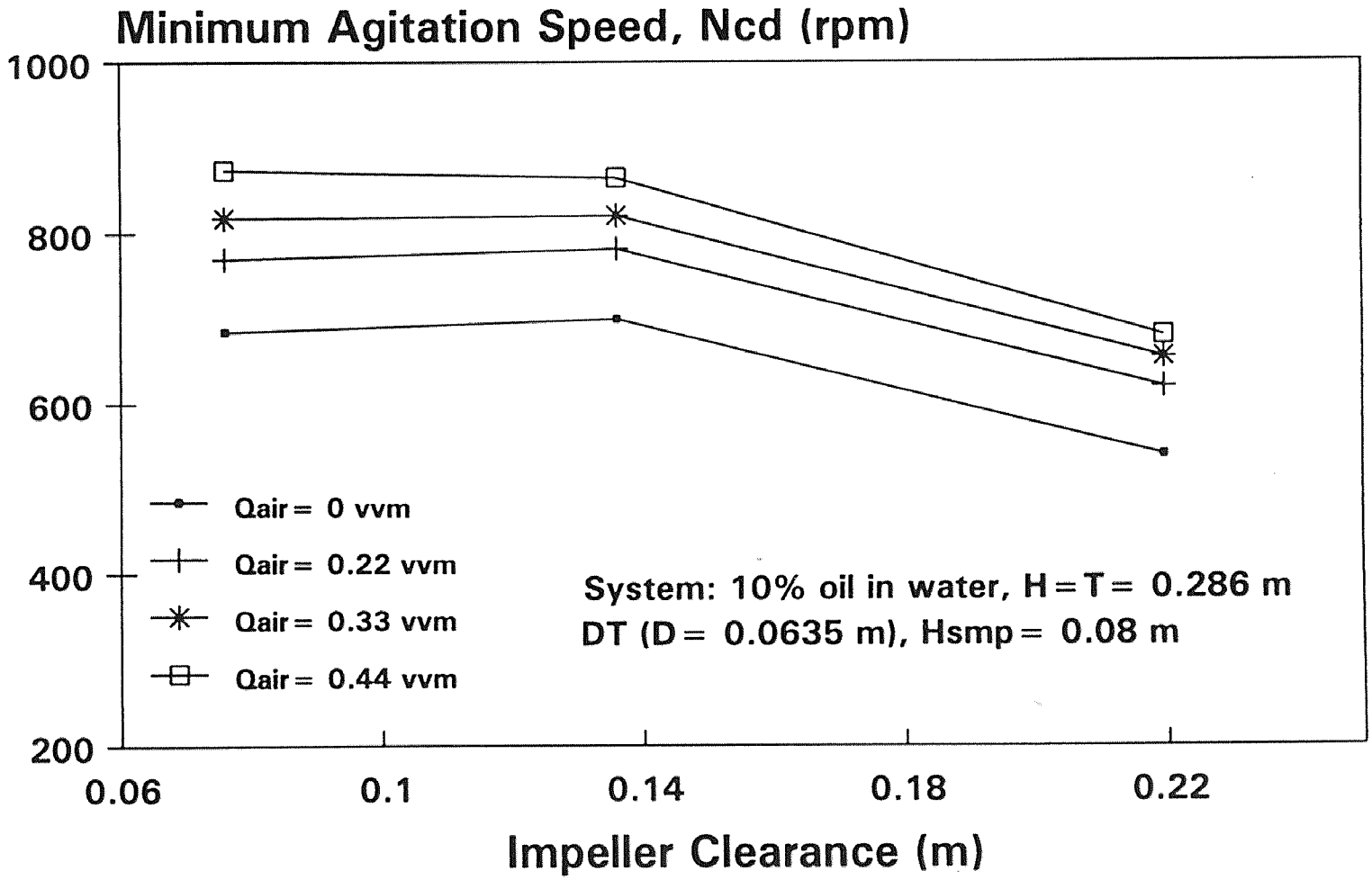

Figure A.14 Effect of C on Ncd, DT (D = 0.0635 m)

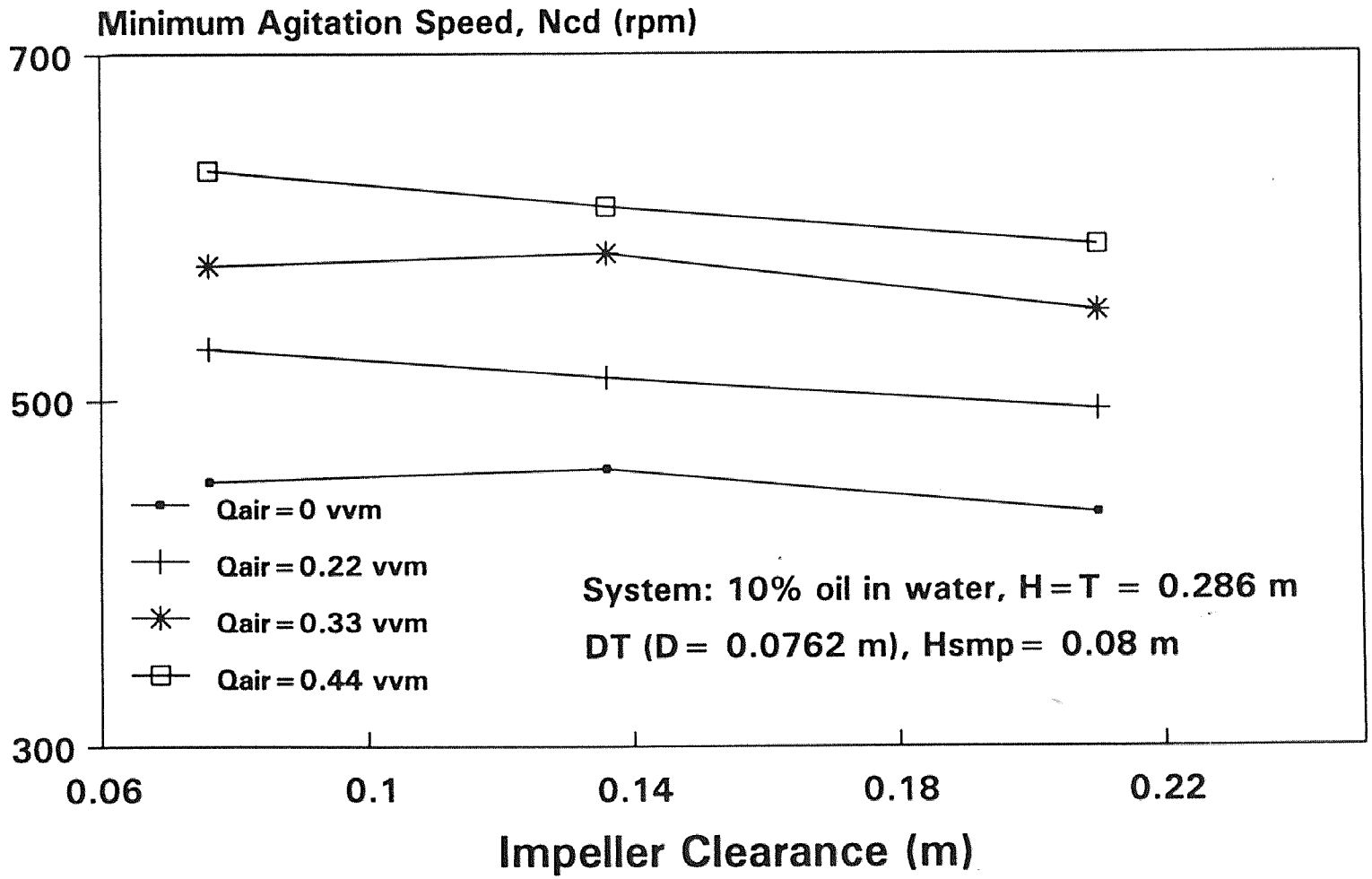

Figure A.15 Effect of C on Ncd, DT (D = 0.0762 m)

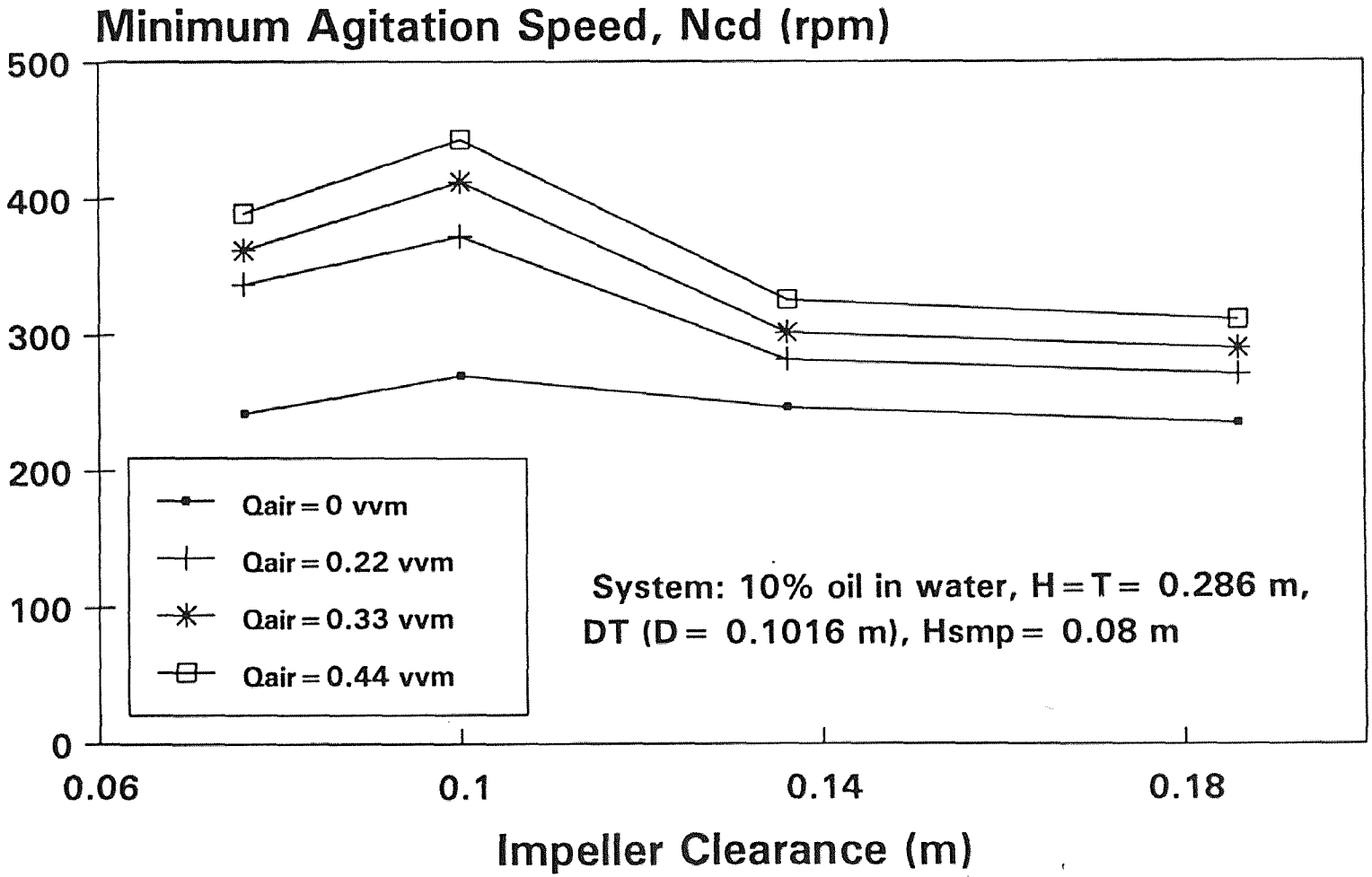

Figure A.16 Effect of C on Ncd,
DT (D = 0.1016 m)

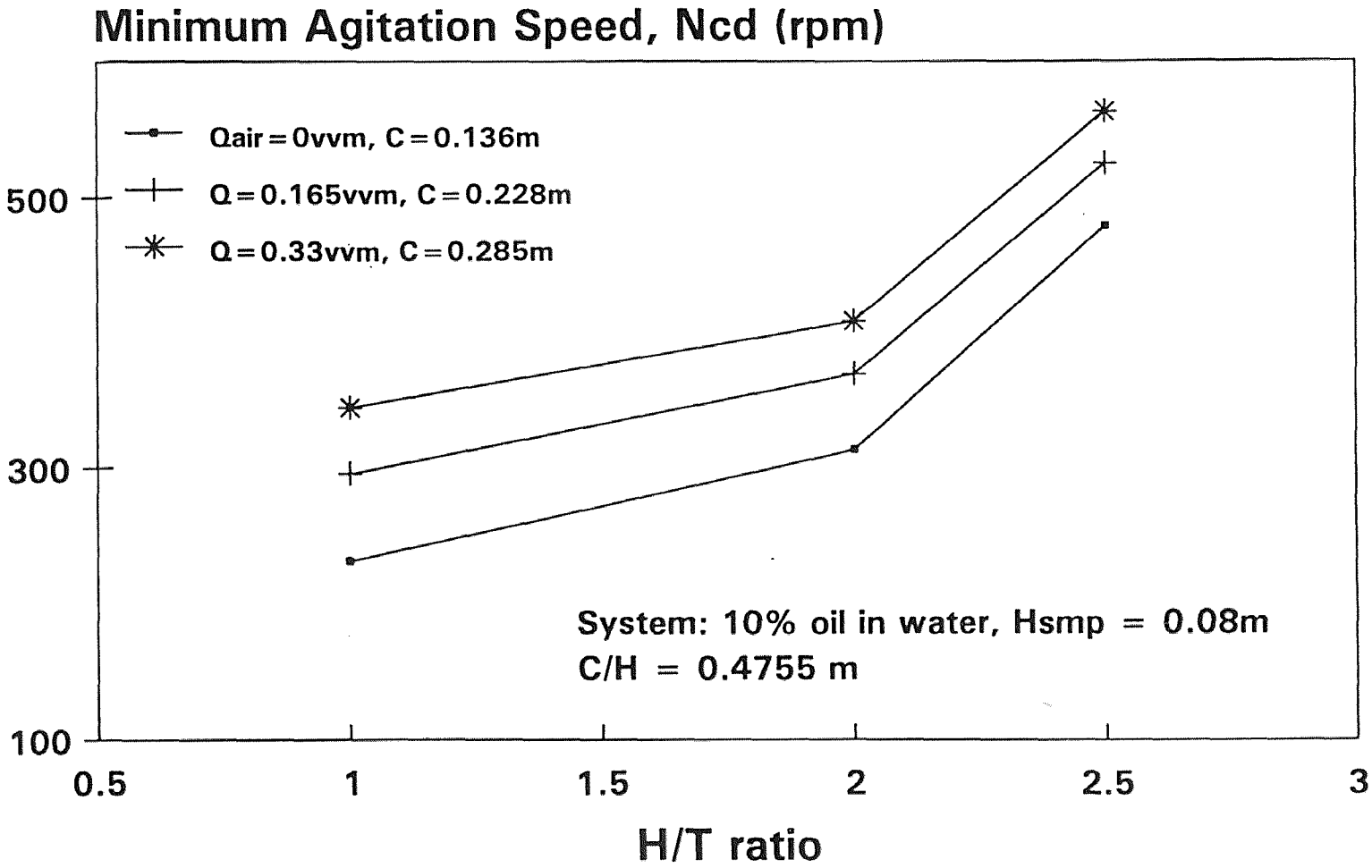

Figure A.17 Effect of H/T on Ncd
DT (D = 0.1016 m)

APPENDIX B

EXPERIMENTAL DATA AND PREDICTED RESULTS

This appendix tabulates the experimental and predicted data for the results obtained under both gassed and ungassed conditions. Results for DTs are shown in Tables B1-B.6 and B.13. Results for 45-PBTs are shown in Tables B.7-B.10. Results for CBT and FBT are shown in Table B.11. Finally, for propeller turbine, results are shown in Table B.12.

Table B.1 Results for Disk Turbine (D = 0.0635 m)

Qair (vvm)	Impeller Clearance, C = 0.0635 m				Impeller Clearance, C = 0.0762 m			
	Ncd-vis (rpm)	Ncd-smp (rpm)	PG/P0	Ncd-model (rpm)	Ncd-vis (rpm	Ncd-smp (rpm)	PG/P0	Ncd-model (rpm)
0	670	659	1.0	659	685	675	1.0	675
0.11	705	701	0.8586	693	720	727	0.8661	706
0.165	735	740	0.7902	713	740	735	0.8032	723
0.22	760	754	0.6870	746	770	733	0.7030	756
0.275	780	772	0.6190	773	790	797	0.6430	779
0.33	805	800	0.5996	782	818	833	0.6360	782
0.385	830	826 (*F*)	0.5670	796	845	814 (*F*)	0.6099	793
0.44	850	845	0.5403	809	874	848	0.5657	813
Qair (vvm)	Impeller Clearance, C = 0.136 m				Impeller Clearance, C = 0.2225 m			
	Ncd-vis (rpm)	Ncd-smp (rpm)	PG/P0	Ncd-model (rpm)	Ncd-vis (rpm	Ncd-smp (rpm)	PG/P0	Ncd-model
0	700	687	1.0	687	540	533	1.0	533
0.11	738	707	0.872	719	575	558	0.795	575
0.165	760	759	0.797	740	600	592	0.716	595
0.22	782	786	0.722	766	620	601	0.643	617
0.275	800	789	0.6734	784	638	602	0.627	623
0.33	821	809	0.646	794	655	637	0.584	638
0.385	840	828	0.612	809	670	665	0.545	652
0.44	865	859(*F*)	0.566	831	686	691 (*F*)	0.522	662

* System: 10 % oil in water, T = H = 0.286 m, Hsmp = 0.08 m. (*F*): The impeller was observed to be flooded at the corresponding air flow rate and at all the air flow rates greater than this.

Table B.2 Results for Disk Turbine (D = 0.0762 m)*

Qair (vvm)	Impeller Clearance, C = 0.0762 m				Impeller Clearance, C = 0.136 m			
	Ncd-vis (rpm)	Ncd-smp (rpm)	PG/P0	Ncd-model (rpm)	Ncd-vis (rpm	Ncd-smp (rpm)	PG/P0	Ncd-model
0	453	448	1.0	448	460	456	1.0	456
0.11	475	450	0.855	472	485	468	0.837	484
0.165	500	505	0.688	507	513	487	0.710	510
0.22	530	532	0.614	527	540	512	0.635	530
0.275	550	515	0.589	534	568	555	0.568	551
0.33	578	571*(F)*	0.553	545	585	543	0.542	559
0.385	601	586	0.555	545	600	556	0.524	565
0.44	633	621	0.544	548	612	597 *(F)*	0.5074	572

* System: 10 % oil in water, H = T = 0.286 m , Hsmp = 0.08 m. *(F):* The impeller was observed to be flooded at the corresponding air flow rate and at all the air flow rates greater than this.

Table B.3 Results for Disk Turbine (D = 0.0762 m)*

Qair (vvm)	Impeller Clearance, C = 0.22 m			
	Ncd-vis (rpm)	Ncd-smp (rpm)	PG/P0	Ncd-model (rpm)
0	435	417	1.0	417
0.11	453	449	0.866	450
0.165	472	451	0.7733	468
0.22	495	479	0.6934	487
0.275	525	515	0.605	508
0.33	552	537	0.528	532
0.385	570	556	0.515	536
0.44	590	576 *(F)*	0.5007	542

Table B.4 Results for Disk Turbine (D = 0.1016 m)

Qair (vvm)	Impeller Clearance, C = 0.0762 m				Impeller Clearance, C = 0.10 m			
	Ncd-vis (rpm)	Ncd-smp (rpm)	PG/P0	Ncd-model (rpm)	Ncd-vis (rpm	Ncd-smp (rpm)	PG/P0	Ncd-model
0	242	231	1.0	231	270	270	1.0	270
0.11	290	261 *(F)*	0.8988	239	320	319 *(F)*	0.9313	277
0.165	317	296	0.899	239	345	332	0.915	278
0.22	337	307	0.882	241	372	359	0.856	285
0.275	350	329	0.821	247	395	383	0.824	288
0.33	362	345	0.721	258	412	394	0.778	294
0.385	375	368	0.693	261	428	410	0.733	299
0.44	389	385	0.652	266	443	437	0.696	305
Qair (vvm)	Impeller Clearance, C = 0.136 m				Impeller Clearance, C = 0.186 m			
	Ncd-vis (rpm)	Ncd-smp (rpm)	PG/P0	Ncd-model (rpm)	Ncd-vis (rpm	Ncd-smp (rpm)	PG/P0	Ncd-model (rpm)
0	247	234	1.0	234	235	231	1.0	231
0.11	260	242	0.866	245	248	248	0.788	250
0.165	270	262	0.775	255	260	260	0.7082	259
0.22	282	279	0.7093	262	271	260	0.6507	266
0.275	293	284	0.605	277	280	269	0.581	282
0.33	302	293 *(F)*	0.587	280	290	282	0.555	281
0.385	315	297	0.549	286	302	297 *(F)*	0.560	280
0.44	326	305	0.534	289	311	292	0.525	286

* System: 10 % oil in water, H = T = 0.286 m , Hsmp = 0.08 m. *(F)*: The impeller was observed to be flooded at the corresponding air flow rate and at all the air flow rates greater than this.

Table B.5 Results for Disk Turbine (D = C = 0.1016 m)

Qair (vvm)	Samplig Point Location, Hsmp = 0.08 m				Sampling Point Location, Hsmp = 0.12 m			
	Ncd-vis (rpm)	Ncd-smp (rpm)	PG/P0	Ncd-model (rpm)	Ncd-vis (rpm	Ncd-smp (rpm)	PG/P0	Ncd-model
0	270	270	1.0	270	263	273	1.0	273
0.11	320	319	0.9313	277	300	297	0.906	282
0.22	372	359 *(F)*	0.856	285	358	357 *(F)*	0.813	293
Qair (vvm)	Sampling Point Location, Hsmp = 0.15 m				Sampling Point Location, Hsmp = 0.2 m			
	Ncd-vis (rpm)	Ncd-smp (rpm)	PG/P0	Ncd-model (rpm)	Ncd-vis (rpm	Ncd-smp (rpm)	PG/P0	Ncd-model
0	268	283	1.0	283	275	270	1.0	270
0.11	310	332	0.906	292	305	290	0.906	279
0.22	365	386 *(F)*	0.813	303	360	358 *(F)*	0.813	290

* System: 10 % oil in water, H = T = 0.286 m. *(F):* The impeller was observed to be flooded at the corresponding air flow rate and at all the air flow rates greater than this.

Table B.6 Results for Disk Turbine (D = Ct = 0.1016 m)

Qair (vvm)	Samplig Point Location, Hsmp = 0.08 m				Sampling Point Location, Hsmp = 0.12 m			
	Ncd-vis (rpm)	Ncd-smp (rpm)	PG/P0	Ncd-model (rpm)	Ncd-vis (rpm	Ncd-smp (rpm)	PG/P0	Ncd-model
0	235	231	1.0	231	235	242	1.0	242
0.11	248	248	0.788	250	250	258	0.795	262
0.22	271	260	0.6507	266	270	264	0.668	276
0.33	290	290	0.555	282	290	264	0.601	285
Qair (vvm)	Sampling Point Location, Hsmp = 0.15 m				Sampling Point Location, Hsmp = 0.2 m			
	Ncd-vis (rpm)	Ncd-smp (rpm)	PG/P0	Ncd-model (rpm)	Ncd-vis (rpm	Ncd-smp (rpm)	PG/P0	Ncd-model
0	240	250	1.0	250	230	234	1.0	234
0.11	255	268	0.795	269	252	248	0.795	252
0.22	273	280	0.668	286	270	267	0.667	267
0.33	295	303	0.610	296	285	269	0.609	275

* System: 10 % oil in water, H = T = 0.286 m. No flooding point was observed under these conditions.

Table B.7 Results for 45-PBTs (D = 0.0635 and 0.0762 m)

Qair (vvm)	D = 0.0635 m, Pumping Downward				D = 0.0635 m, Pumping Upward	
	Ncd-vis (rpm)	Ncd-smp (rpm)	PG/P0	Ncd-model (rpm)	Ncd-vis (rpm	Ncd-smp (rpm)
0	1085	1073	1.0	1073	685	688
0.11	1100	1063	0.946	1093		
0.22	1105	1110	0.898	1112	580	572
0.33	1122	1063 *(F)*	0.883	1119	490	500
Qair (vvm)	D = 0 .0762 m Pumping Downward				D = 0.076 m Pumping Upward	
	Ncd-vis (rpm)	Ncd-smp (rpm)	PG/P0	Ncd-model (rpm)	Ncd-vis (rpm)	Ncd-smp (rpm)
0	880	869	1.0	869	545	529
0.11	890	852	0.994	871	510	502
0.165	900	910	0.98	875	470	459
0.22	915	921 *(F)*	0.979	879	445	437
0.275	926	919	0.935	889	435	439
0.33	935	925	0.8992	900	410	407
0.385	905	901	0.985	873	395	389
0.44	910	914	0.9815	874	385	386

* System: 10 % oil in water, H = T = 0.286 m, C = 0.0762 m, Hsmp = 0.08 m

(F): The impeller was observed to be flooded at the corresponding air flow rate and at all the air flow rates greater than this.

Table B.8 Results for 45-PBT (D = 0.1016 m)

Qair (vvm)	C = 0.0762 m, Pumping Downward				C = 0.0762 m, Pumping upward			
	Ncd-vis (rpm)	Ncd-smp (rpm)	PG/P0	Ncd-model (rpm)	Ncd-vis (rpm	Ncd-smp (rpm)	PG/P0	Ncd-model
0	370	372	1.0	372	340	324	--------	----------
0.11	400	391	0.948	379	328	325	--------	----------
0.165	435	431 *(F)*	0.902	384	315	313	--------	----------
0.22	455	454	0.842	394	280	279	--------	----------
0.275	475	478	0.802	400	265	262	--------	----------
0.33	495	494	0.778	404	253	251	--------	----------
0.385	520	516	0.754	408	233	226	--------	----------
0.44	535	531	0.747	410	222	218	--------	----------
Qair (vvm)	C = 0.1016 m, Pumping Downward				C = 0.136 m, Pumping Downward			
	Ncd-vis (rpm)	Ncd-smp (rpm)	PG/P0	Ncd-model (rpm)	Ncd-vis (rpm	Ncd-smp (rpm)	PG/P0	Ncd-model
0	465	470	1.0	470	450	461	1.0	461
0.165	493	485	0.917	484	475	477	0.8785	481
0.33	539	520 *(F)*	0.814	503	520	529 *(F)*	0.83	490

* System: 10 % oil in water, H = T = 0.286 m , Hsmp = 0.08 m. (*F*): .The impeller was observed to be flooded at the corresponding air flow rate and at all the air flow rates greater than this.

Table B.9 Results for 45-PBT (D = Ct = 0.1016 m)*

Qair (vvm)	Hsmp = 0.08 m, Pumping Downward				Hsmp = 0.12 m, Pumping upward			
	Ncd-vis (rpm)	Ncd-smp (rpm)	PG/P0	Ncd-model (rpm)	Ncd-vis (rpm	Ncd-smp (rpm)	PG/P0	Ncd-model
0	340	345	1.0	345	345	354	1.0	354
0.165	360	358	0.8945	358	355	341	0.876	370
0.33	390	400*(F)*	0.732	383	386	377 *(F)*	0.721	395

* System: 10 % oil in water, H = T = 0.286 m. *(F)*: .The impeller was observed to be flooded at the corresponding air flow rate and at all the air flow rates greater than this.

Table B.10 Results for 45-PBT (D = Ct = 0.1016 m)*

Qair (vvm)	Hsmp = 0.15 m, Pumping Downward			
	Ncd-vis (rpm)	Ncd-smp (rpm)	PG/P0	Ncd-model (rpm)
0	330	341	1.0	341
0.165	350	350	0.864	358
0.33	380	360*(F)*	0.703	384

Table B.11 Results for Curved Blade and Flat Blade Turbines

Qair (vvm)	Curved Blade Turbine, (CBT), D = 0.1016 m				Flat Blade Turbine, (FBT), D = 0.1016 m			
	Ncd-vis (rpm)	Ncd-smp (rpm)	PG/P0	Ncd-model (rpm)	Ncd-vis (rpm)	Ncd-smp (rpm)	PG/P0	Ncd-model
0	560	542	1.0	542	545	517	1.0	517
0.11	605	580	0.9623	549	585	552	0.978	520
0.165	625	601	0.965	549	602	579	0.893	537
0.22	650	627	0.933	555	620	595	0.86	544
0.275	677	640	0.898	561	636	604	0.833	549
0.33	700	650	0.855	571	650	630	0.815	554
0.385	722	674	0.8522	572	665	655	0.793	559
0.44	745	704	0.817	580	681	654	0.785	561

* System: 10 % oil in water, H = T = 0.286 m , Hsmp = 0.08 m, C = 0.076 2 m

* Impeller was always flooded.

Table B.12 Results for Propeller Pumping Downward

Qair (vvm)	Propeller Pumping Downward (D = 0.0762 m)			
	Ncd-vis (rpm)	Ncd-smp (rpm)	PG/P0	Ncd-model (rpm)
0	675	670	1.0	670
0.11	710	713	0.963	679
0.165	740	707	0.936	685
0.22	770	758	0.922	688
0.275	788	781	0.923	688
0.33	813	813	0.898	695
0.385	835	822	0.876	700
0.44	865	851	0.871	702

Table B.13 Results for DT (H/T = 2.0 and 2.5)

	H = 0.48 m, H/T = 2.0, C = 0.228 m		H = 0.6 m, H/T = 2.5, C = 0.2853 m	
Qair (vvm)	Ncd-vis (rpm)	Ncd-smp (rpm)	Ncd-vis (rpm)	Ncd-smp (rpm)
0	320	314	483	479
0.165	370	370	523	522
0.33	415	409	560	563

* System: 10 % oil in water, Hsmp = 0.08 m, T = 0.24 m
D = 0.1016 m

APPENDIX C

PLOTS OF V* vs. N

This appendix includes the experimental data in the form of plots of the dispersed phase fraction, V* (%), vs. the agitation speed, N (rpm). These plots include the following systems:

DT of 0.0635 m in diameter (Figures C.1 C.4)

DT of 0.0762 m in diameter (Figures C.5-C.7)

DT of 0.1016 m in Diameter (Figures C.8-C.17 and Figures C.32 and C.33)

45-PBT of 0.0635 m in diameter (Figures C.18 and C.19)

45-PBT of 0.0762 m in diameter (Figures C.20 and C.21)

45-PBT of 0.1016 m in diameter (Figures C.22-C.28)

CBT of 0.1016 m in diameter (Figure C.29)

FBT of 0.1016 m in diameter (Figure C.30)

Propeller of 0.0762 m in diameter (Figure C.31)

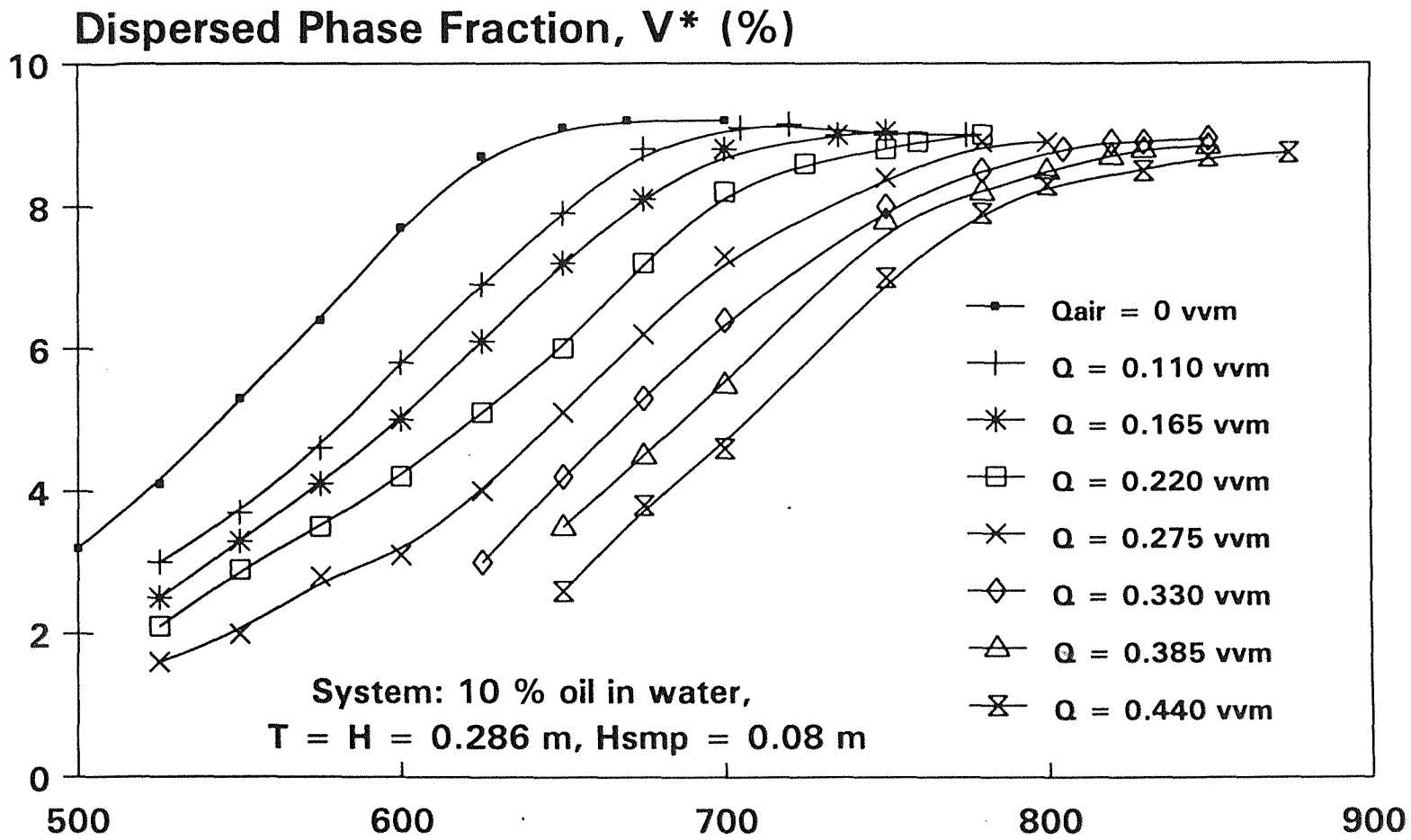

Figure C.1 DT (C = D = 0.0635 m)

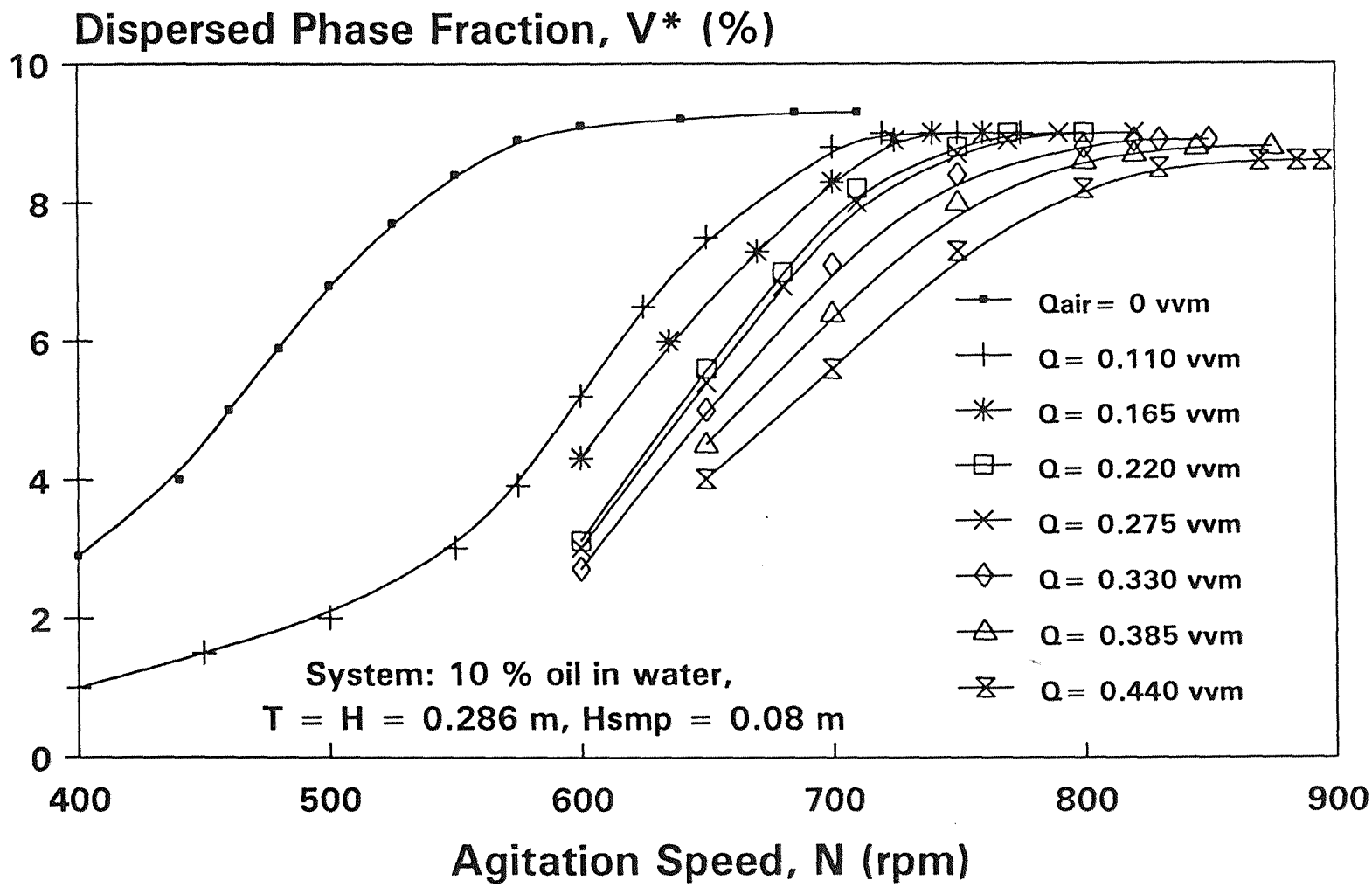

Figure C.2 DT (D = 0.0635 m, C = 0.0762 m)

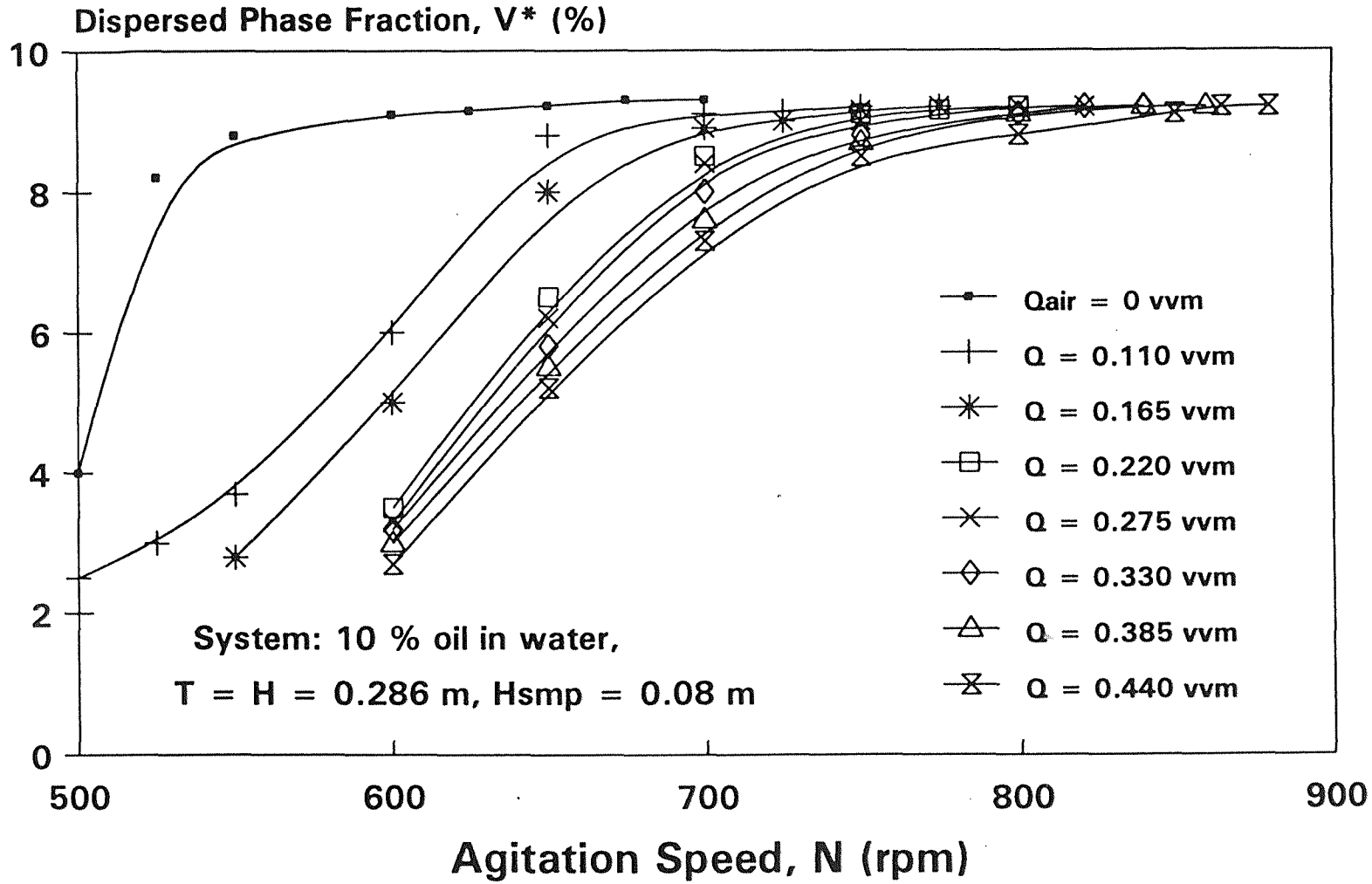

Figure C.3 DT (D = 0.0635 m, C = 0.136 m)

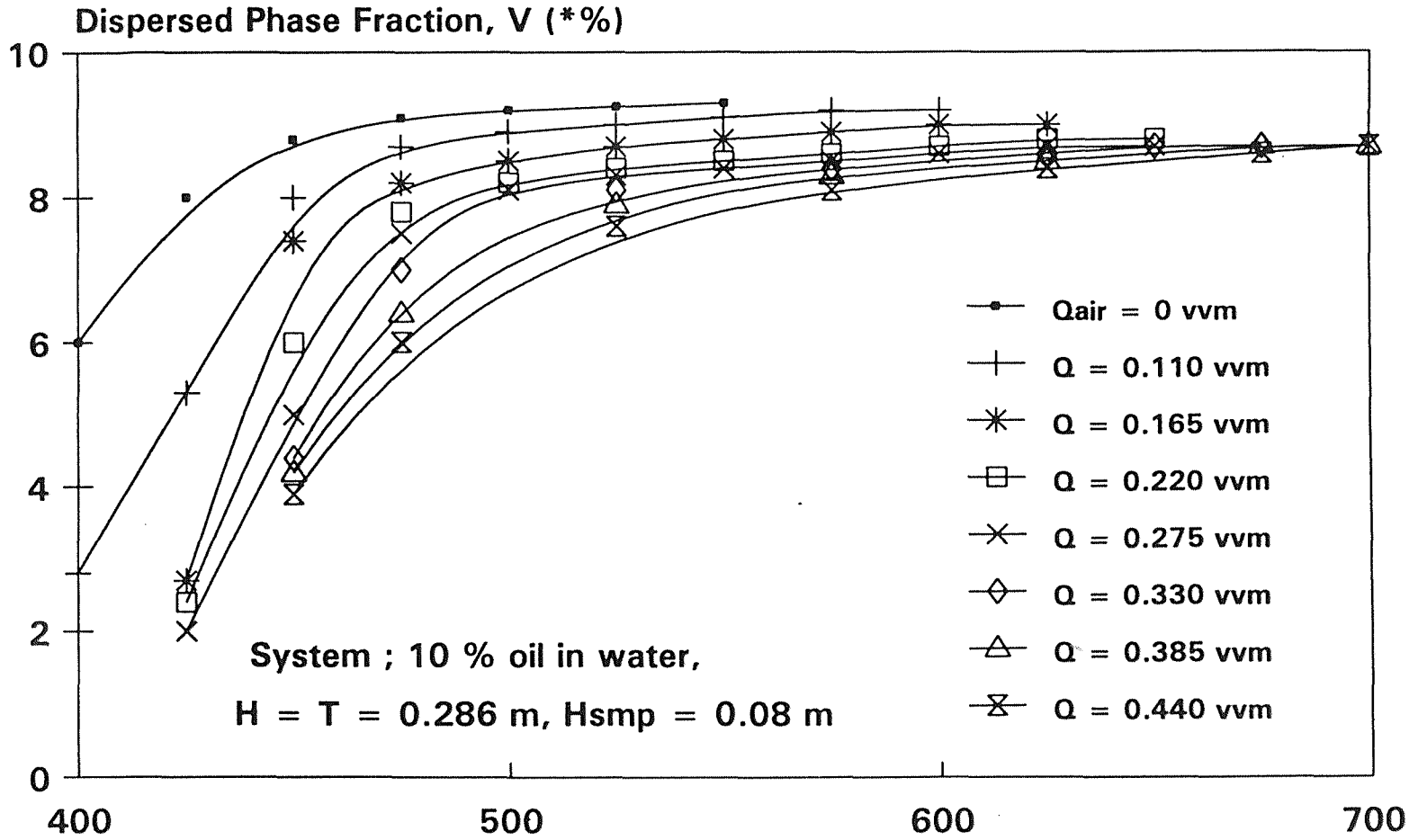

Figure C.4 DT (D = Ct = 0.0635 m)

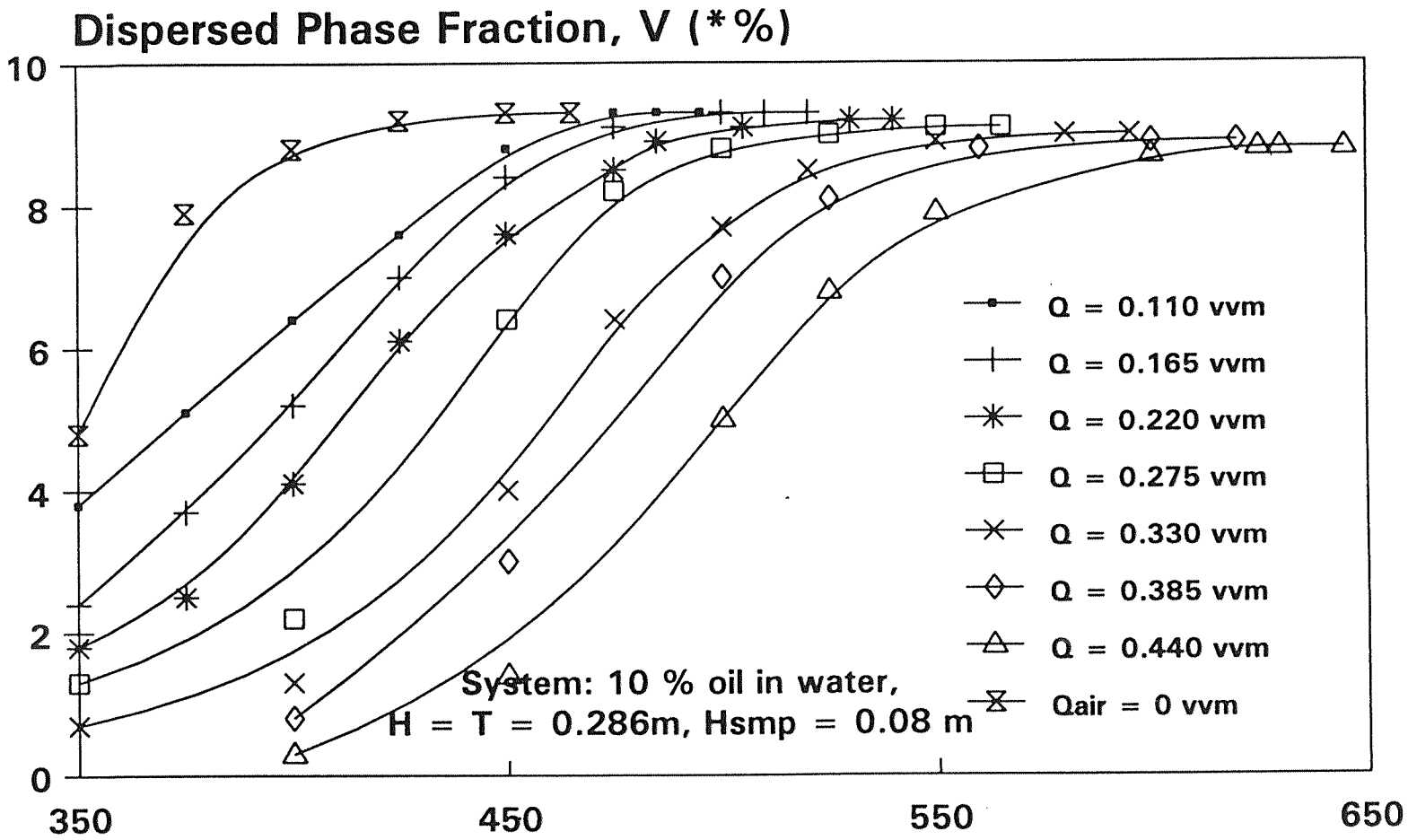

Figure C.5 DT (D = C = 0.0762 m)

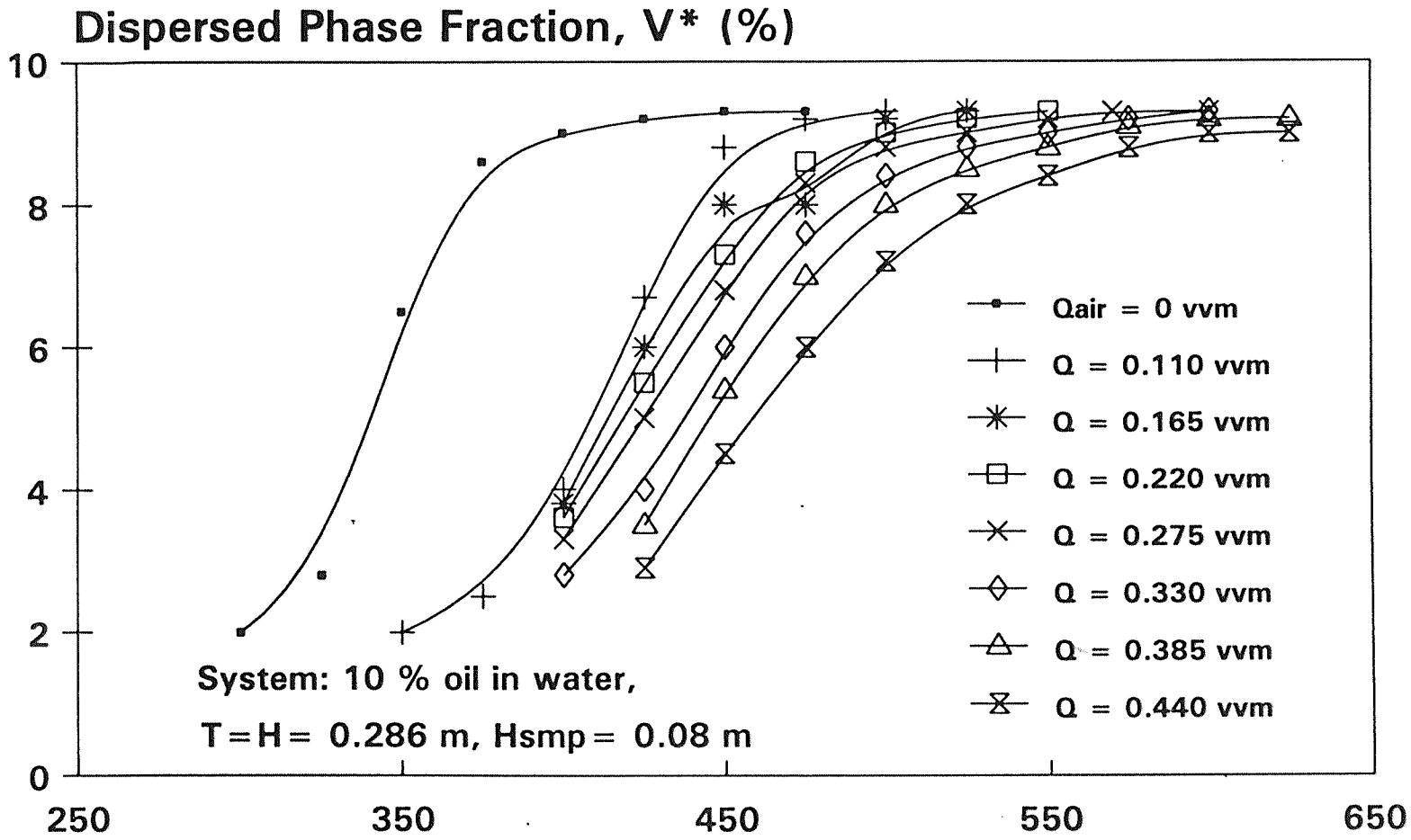

Figure C.6 DT (D=0.0762 m, C=0.136 m)

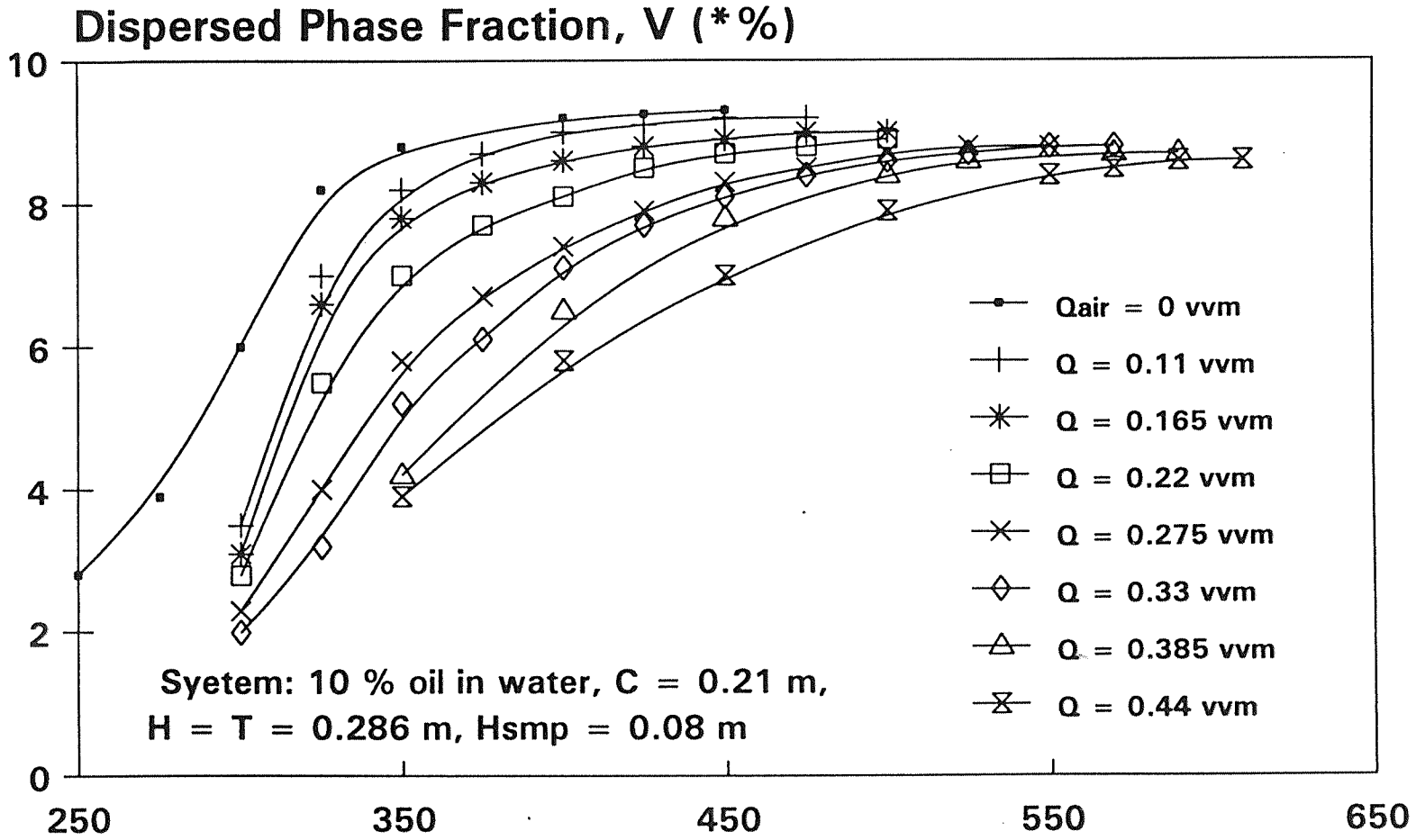

Figure C.7 DT (D = Ct = 0.0762 m)

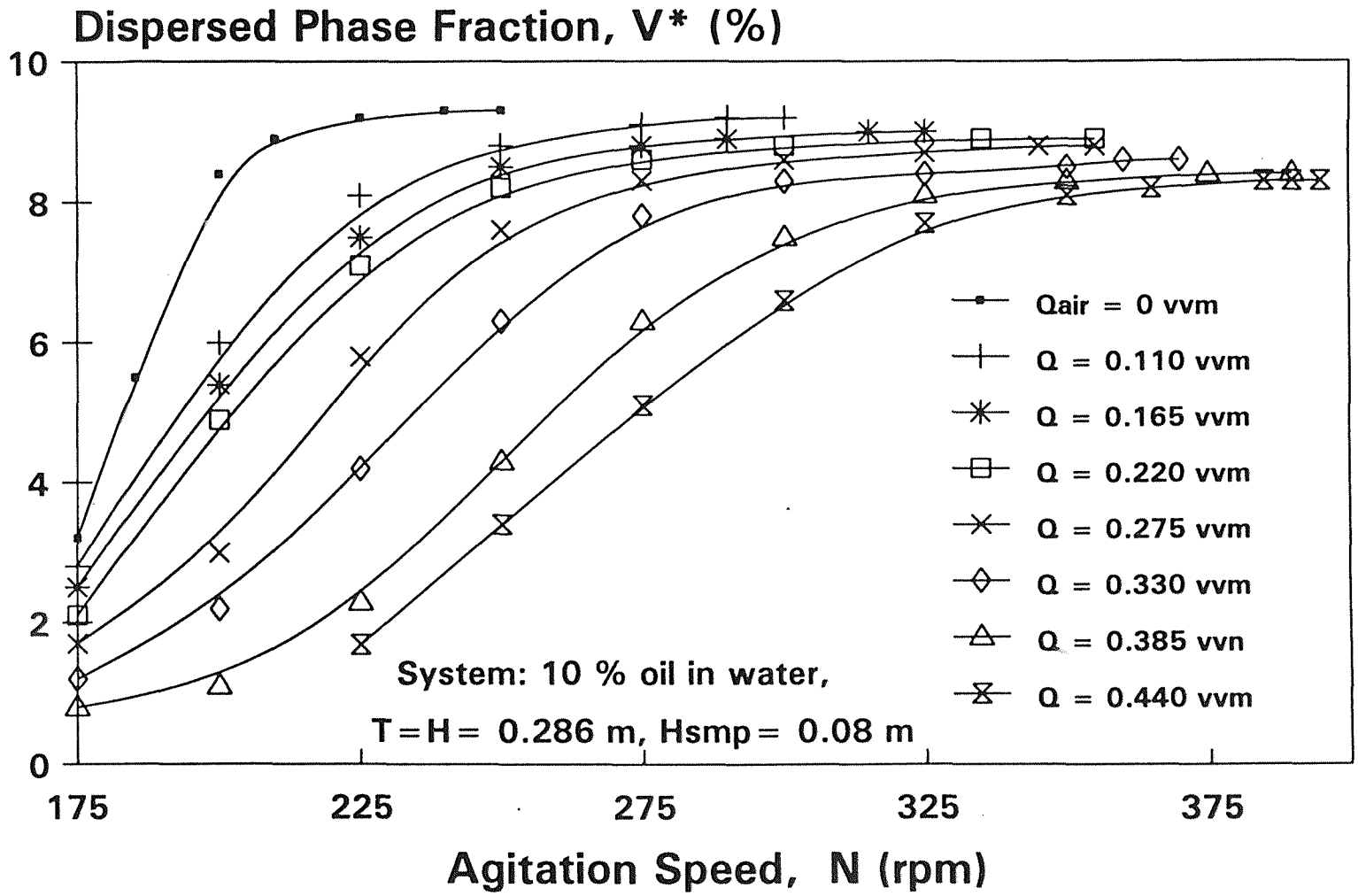

Figure C.8 DT (D= 0.1016 m, C= 0.076 m)

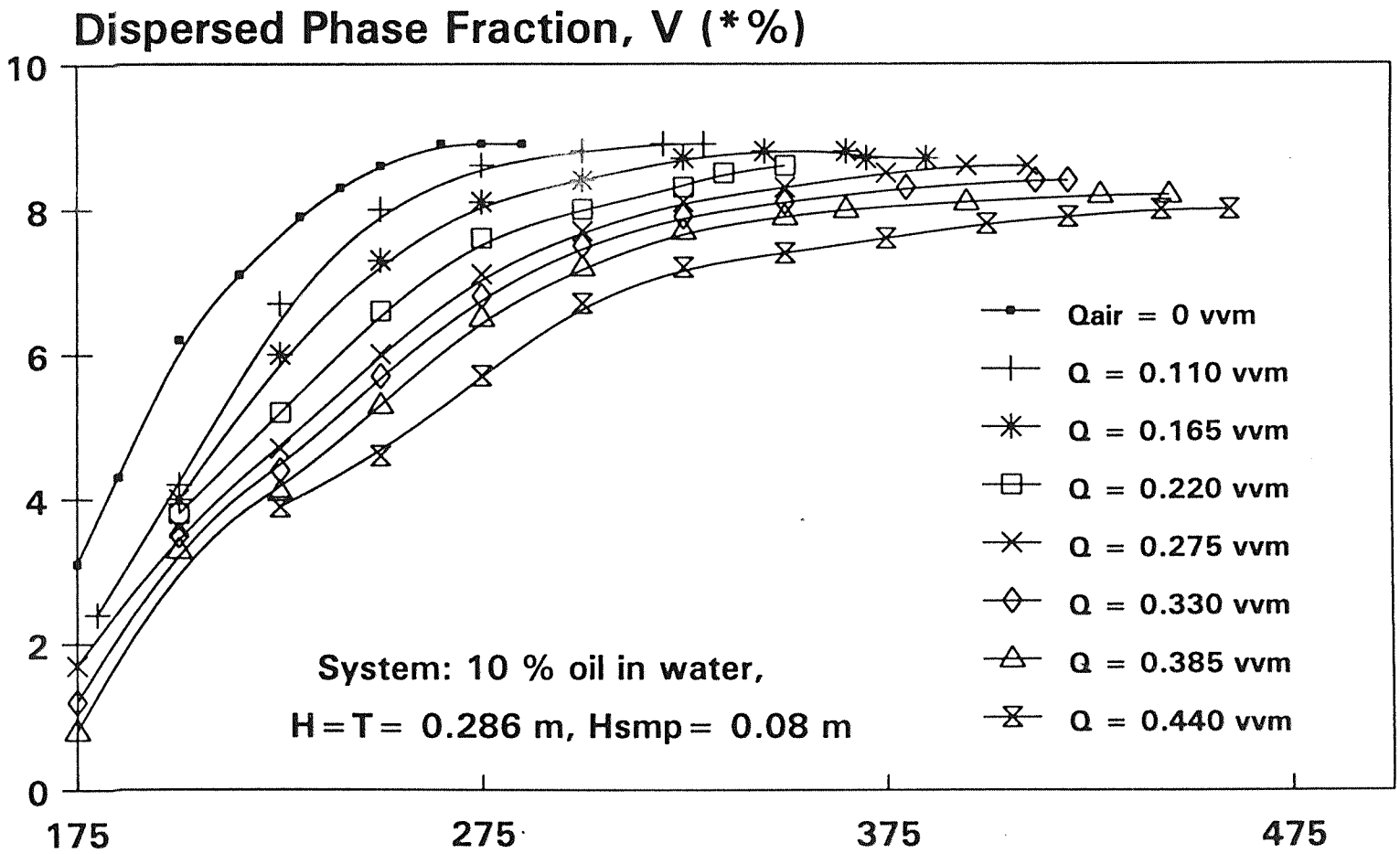

Figure C.9 DT (D=C= 0.1016 m)

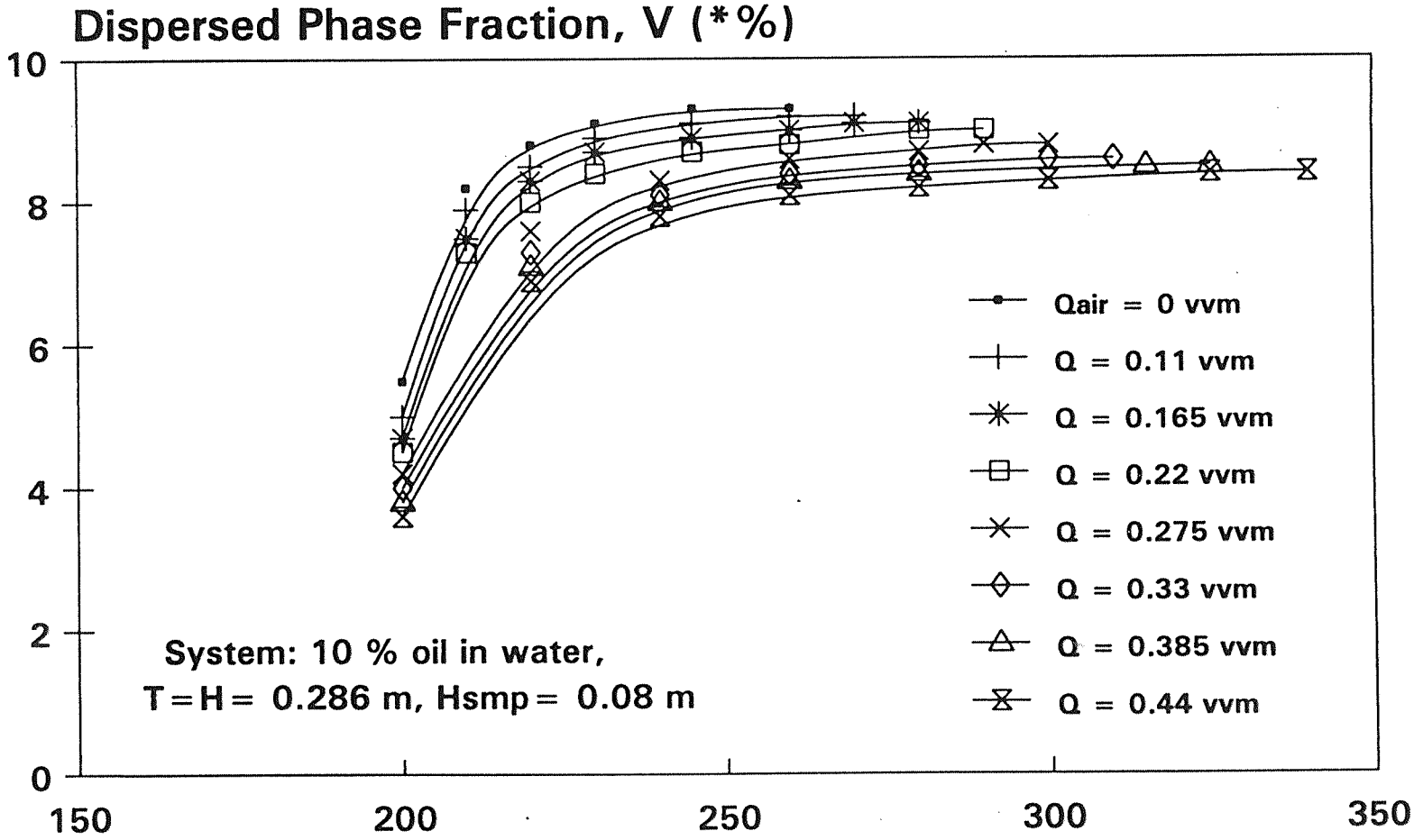

Figre C.10 DT (D= 0.1016 m, C= 0.136 m)

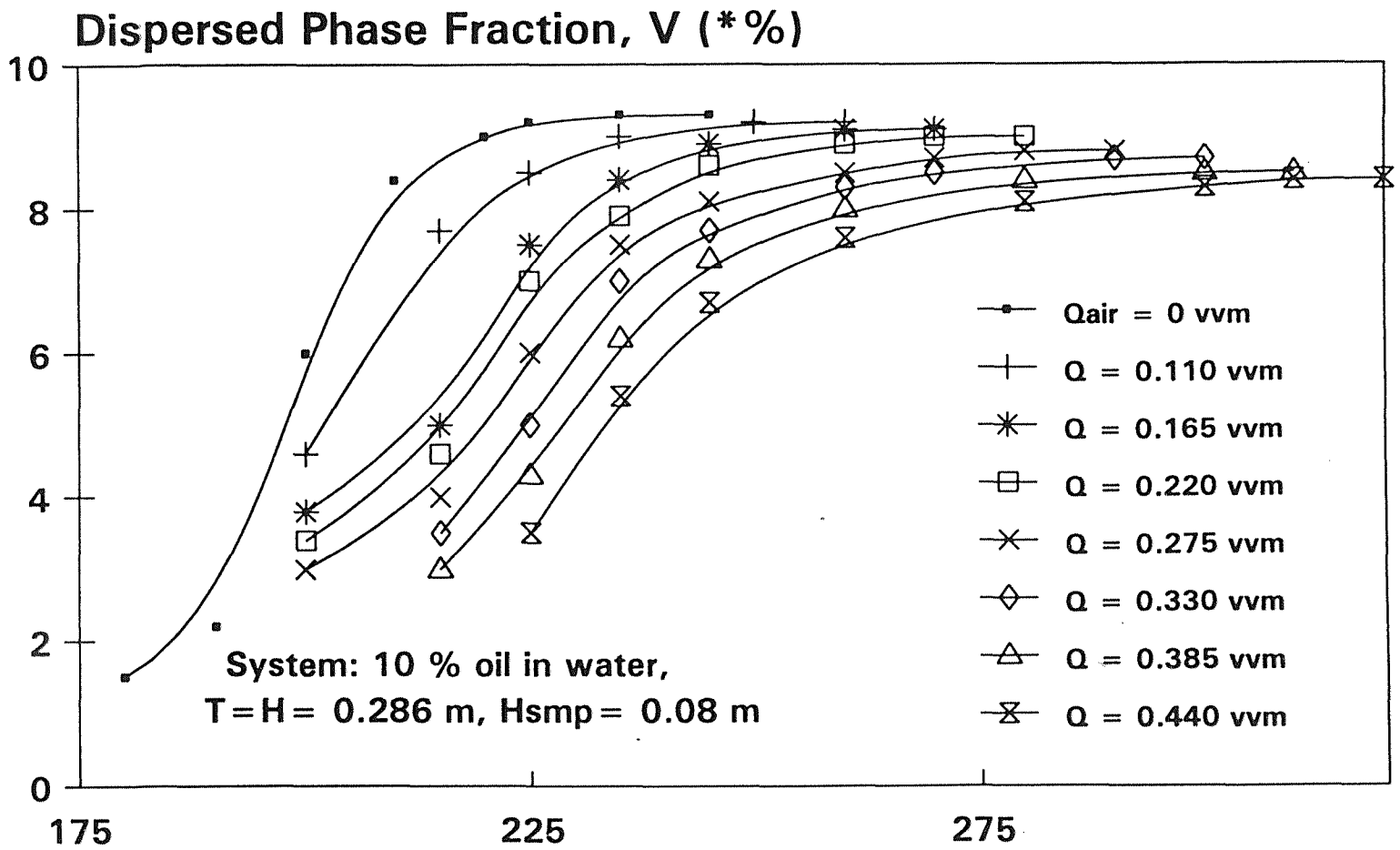

Figure C.11 DT (D=Ct= 0.1016 m)

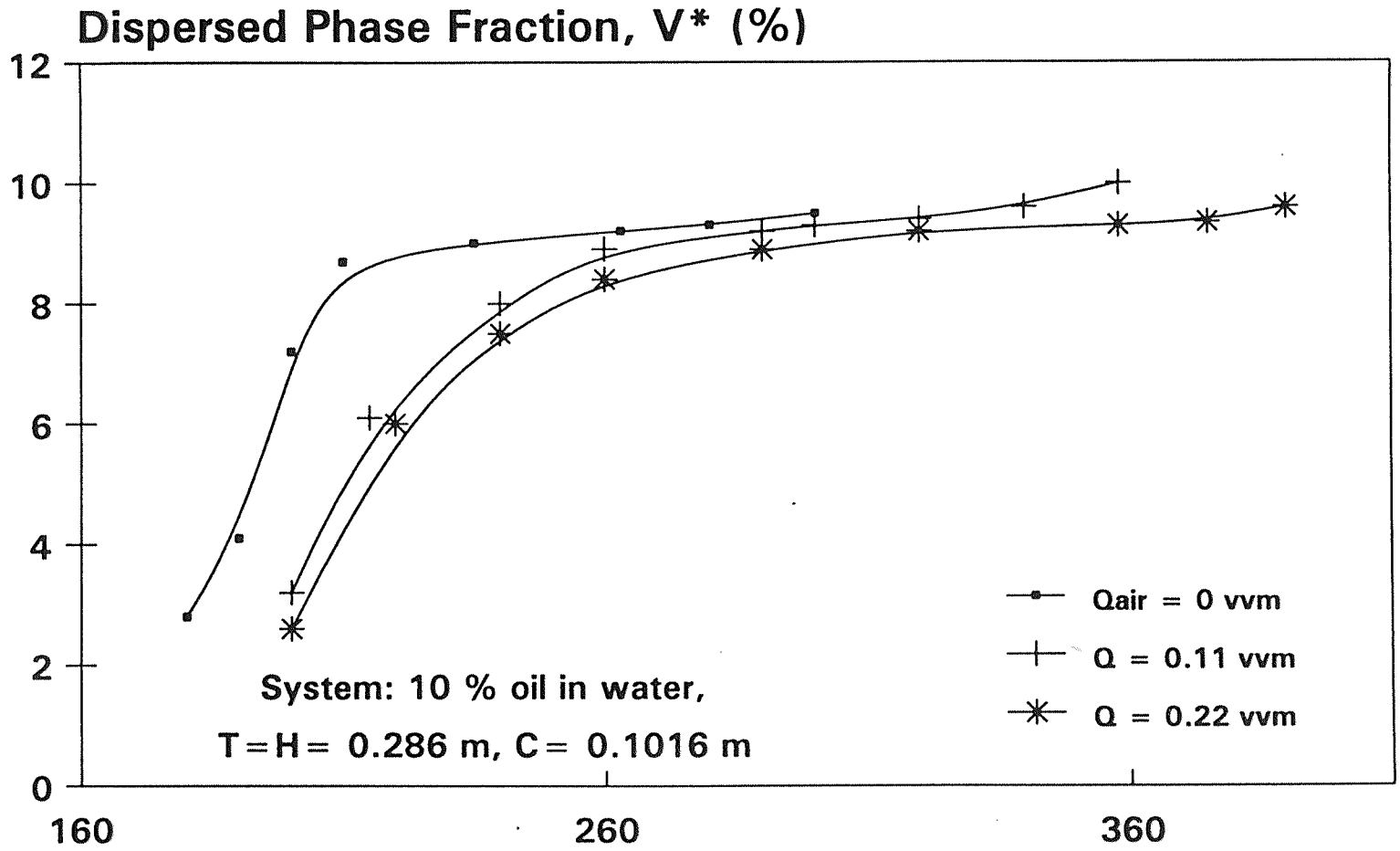

Figure C.12 DT (D = 0.1016 m, Hsmp = 0.12 m)

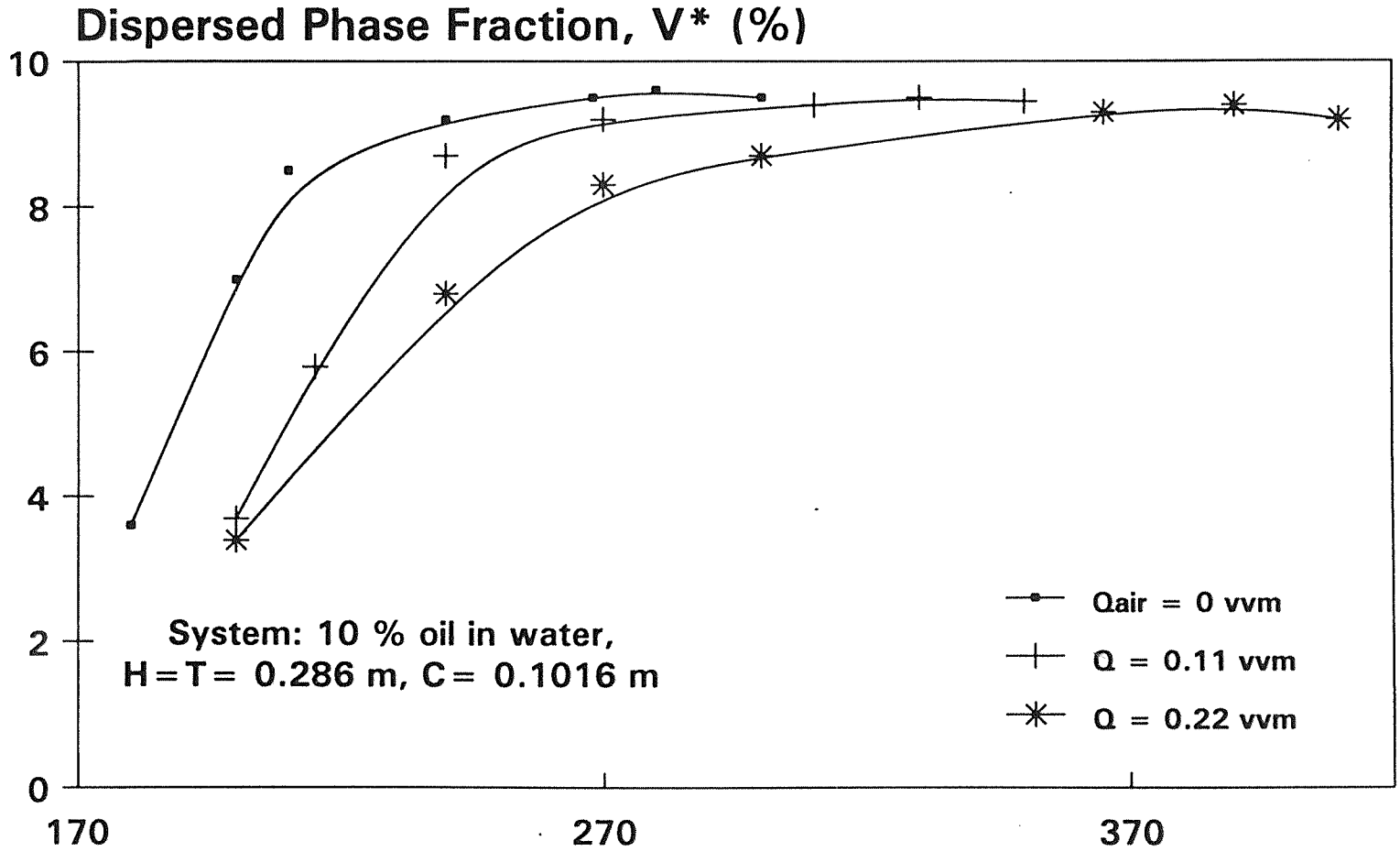

Figure C.13 DT (D=0.1016 m, Hsmp=0.15 m)

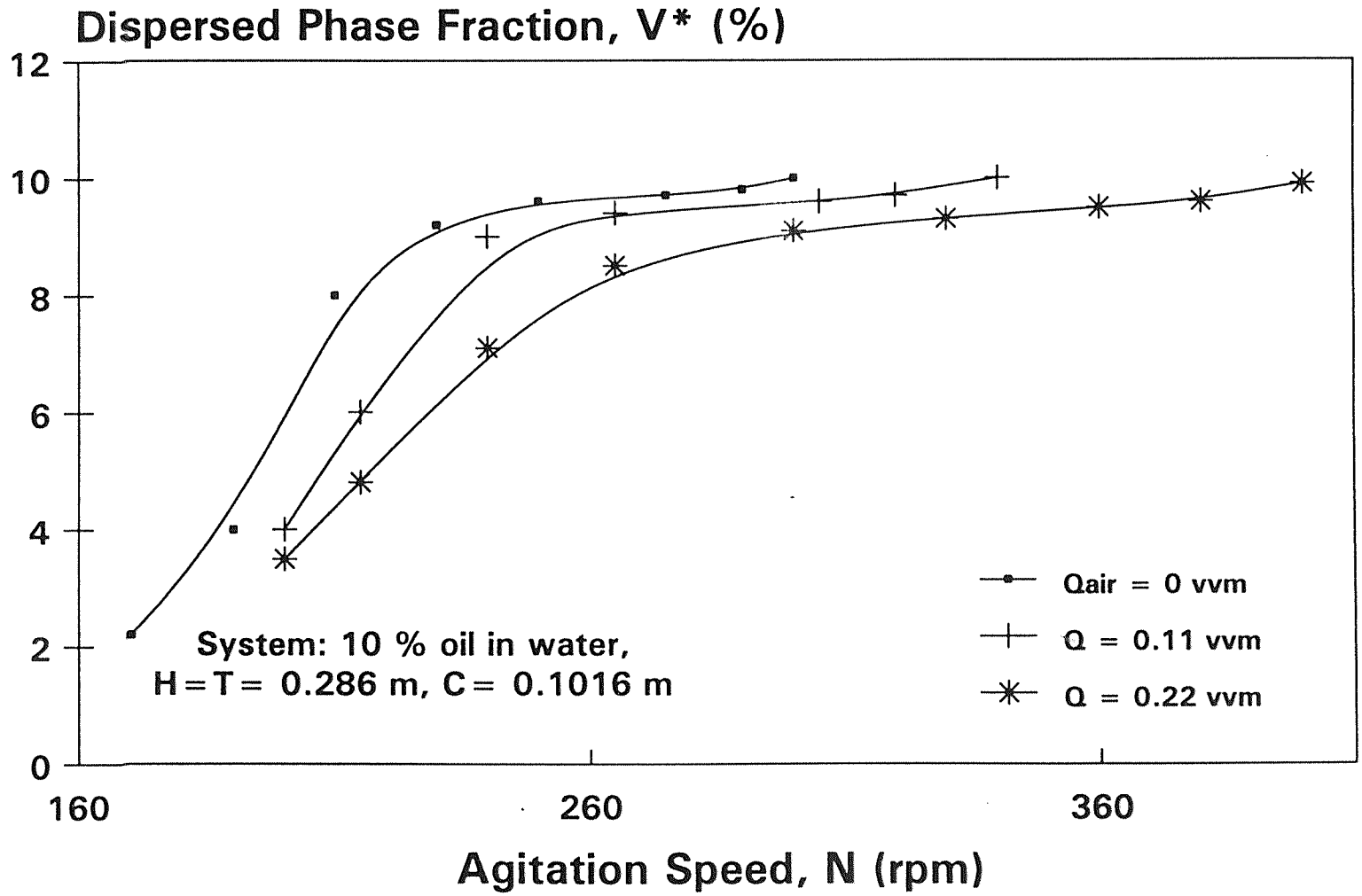

Figure C.14 DT (D = 0.1016 m, Hsmp = 0.20 m)

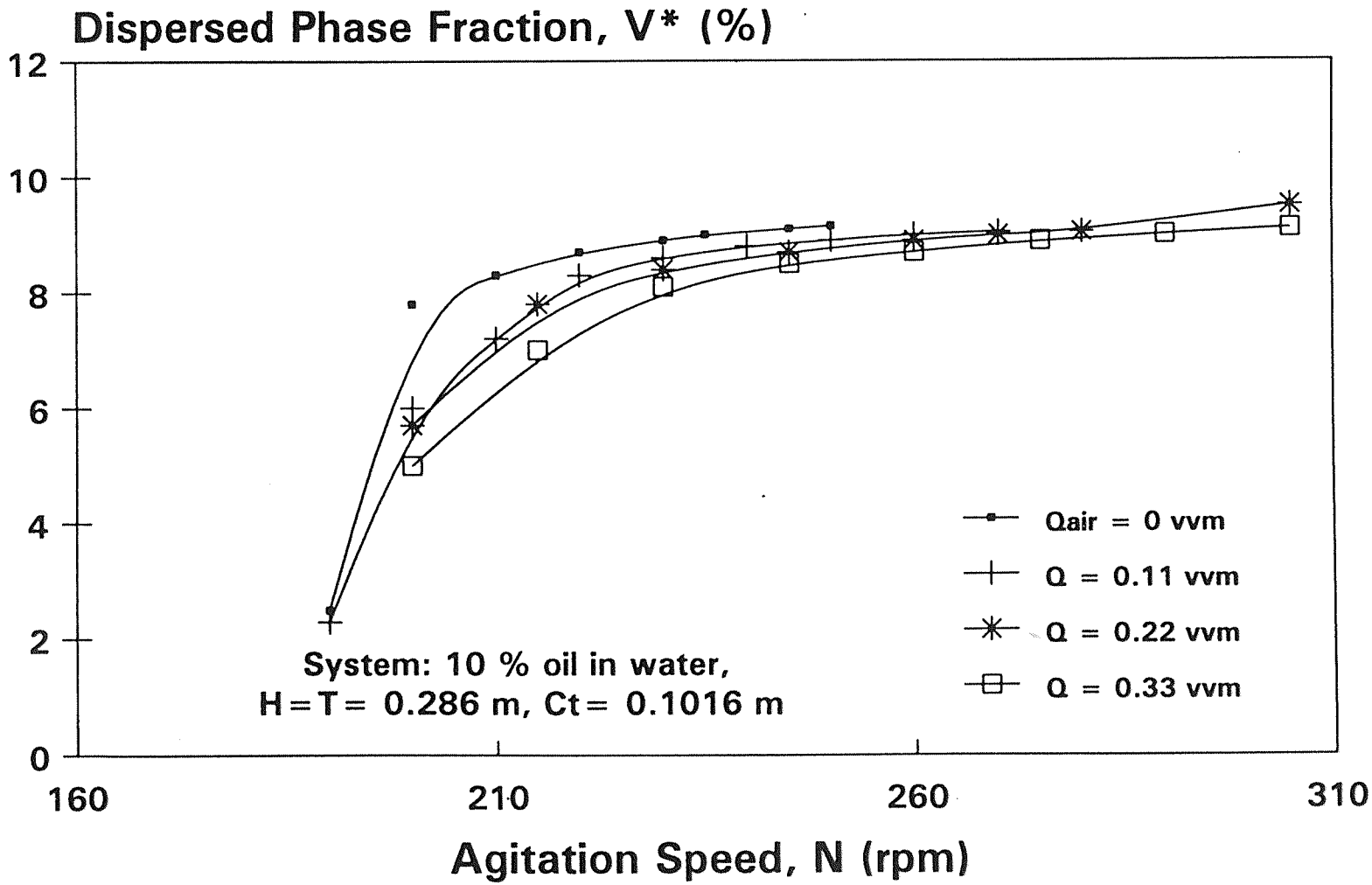

Figure C.15 DT (D=0.1016 m, Hsmp=0.12 m)

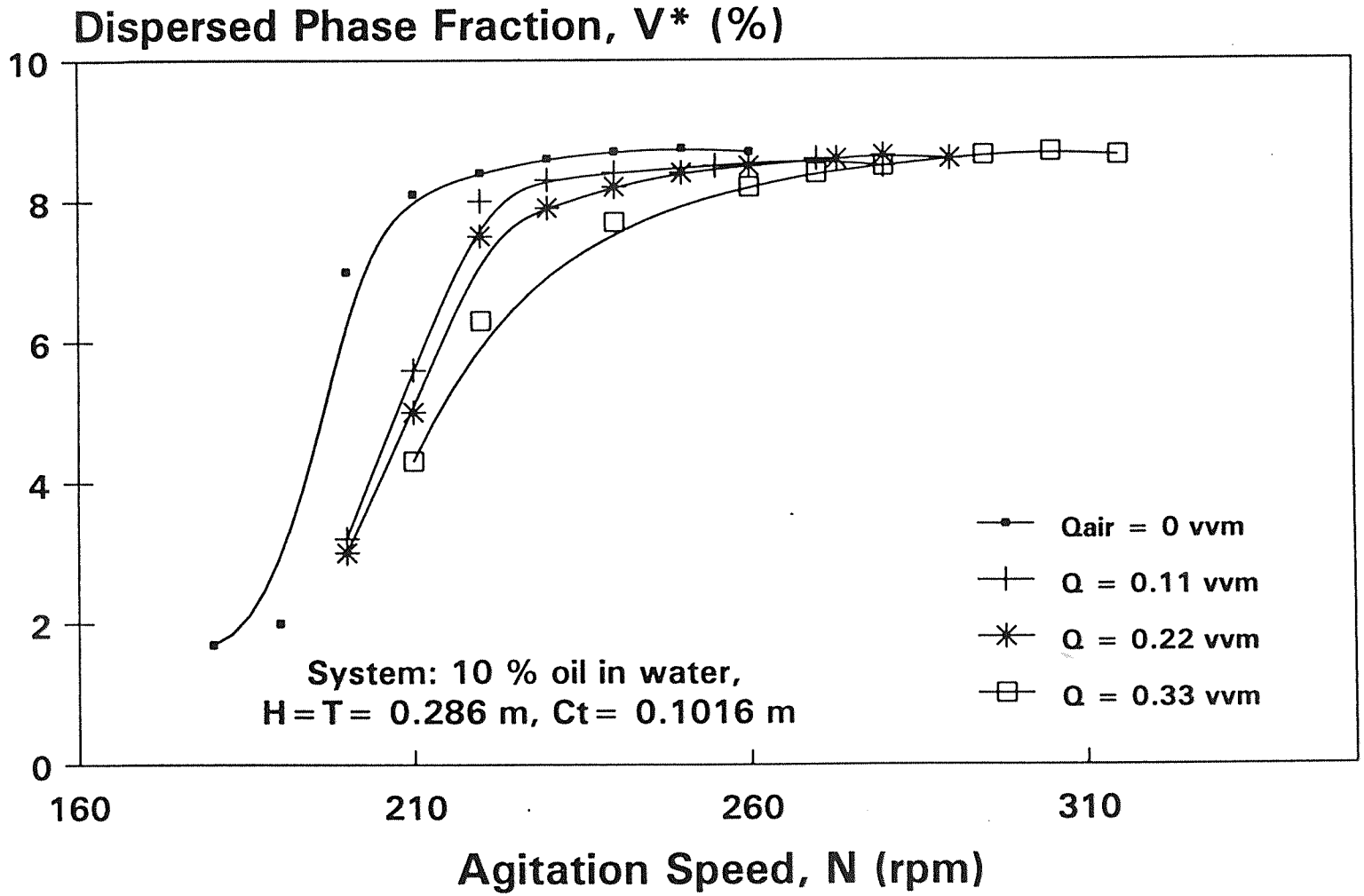

Figure C.16 DT (D = 0.101 m, Hsmp = 0.15 m)

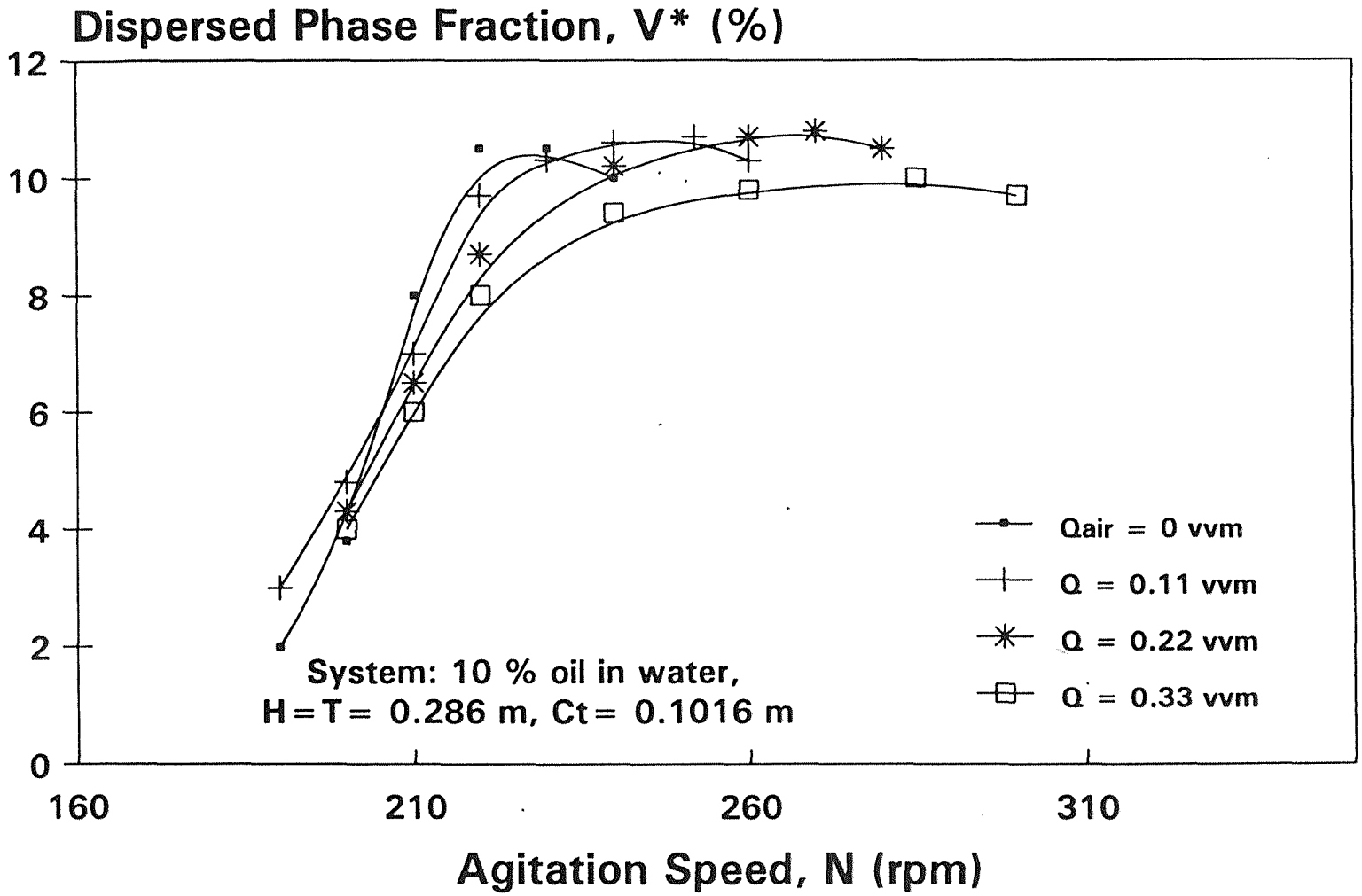

Figure C.17 DT (D = 0.101 m, Hsmp = 0.20 m)

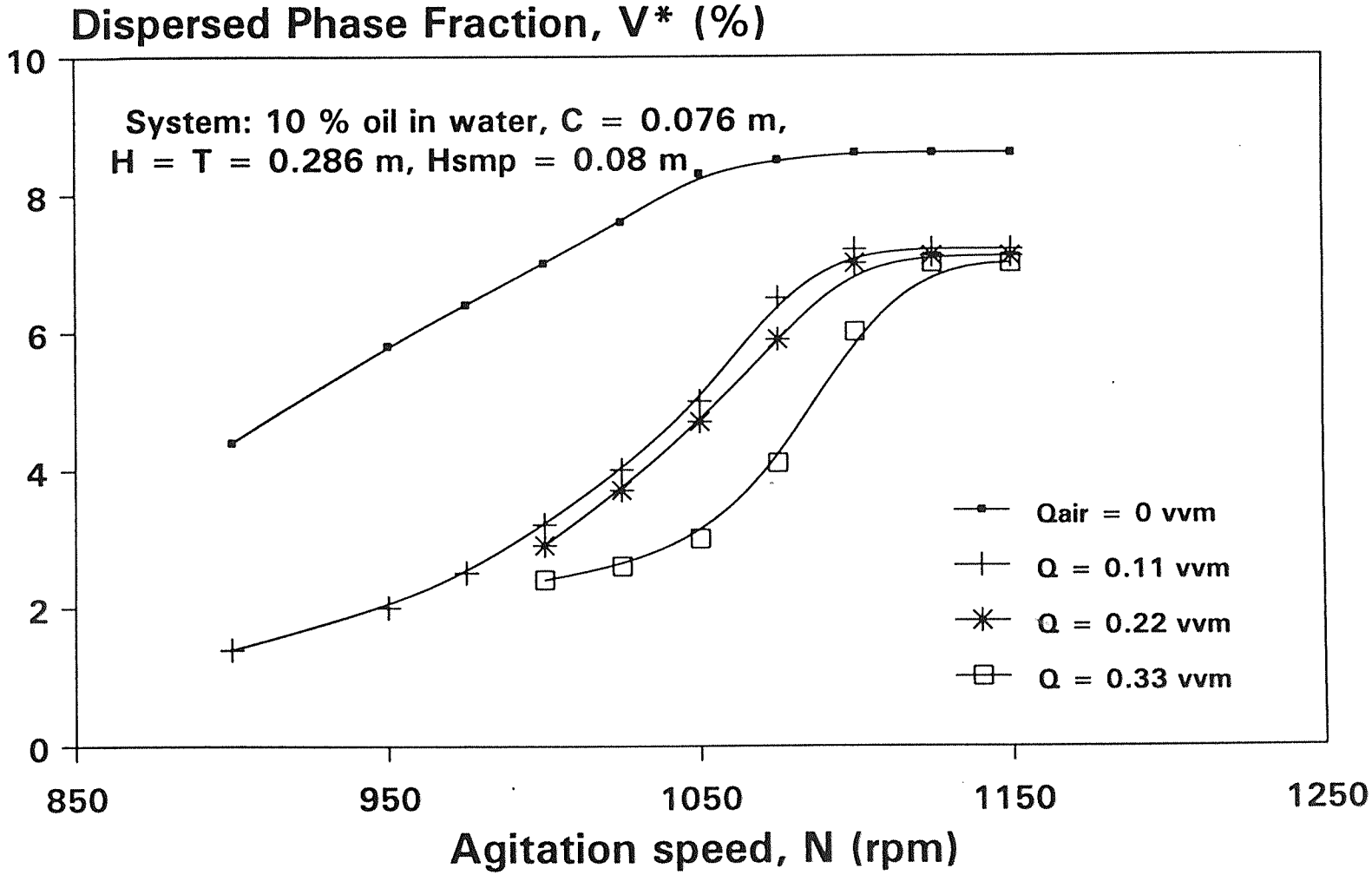

Figure C.18 45-PBT (D = 0.0635 m, Down)

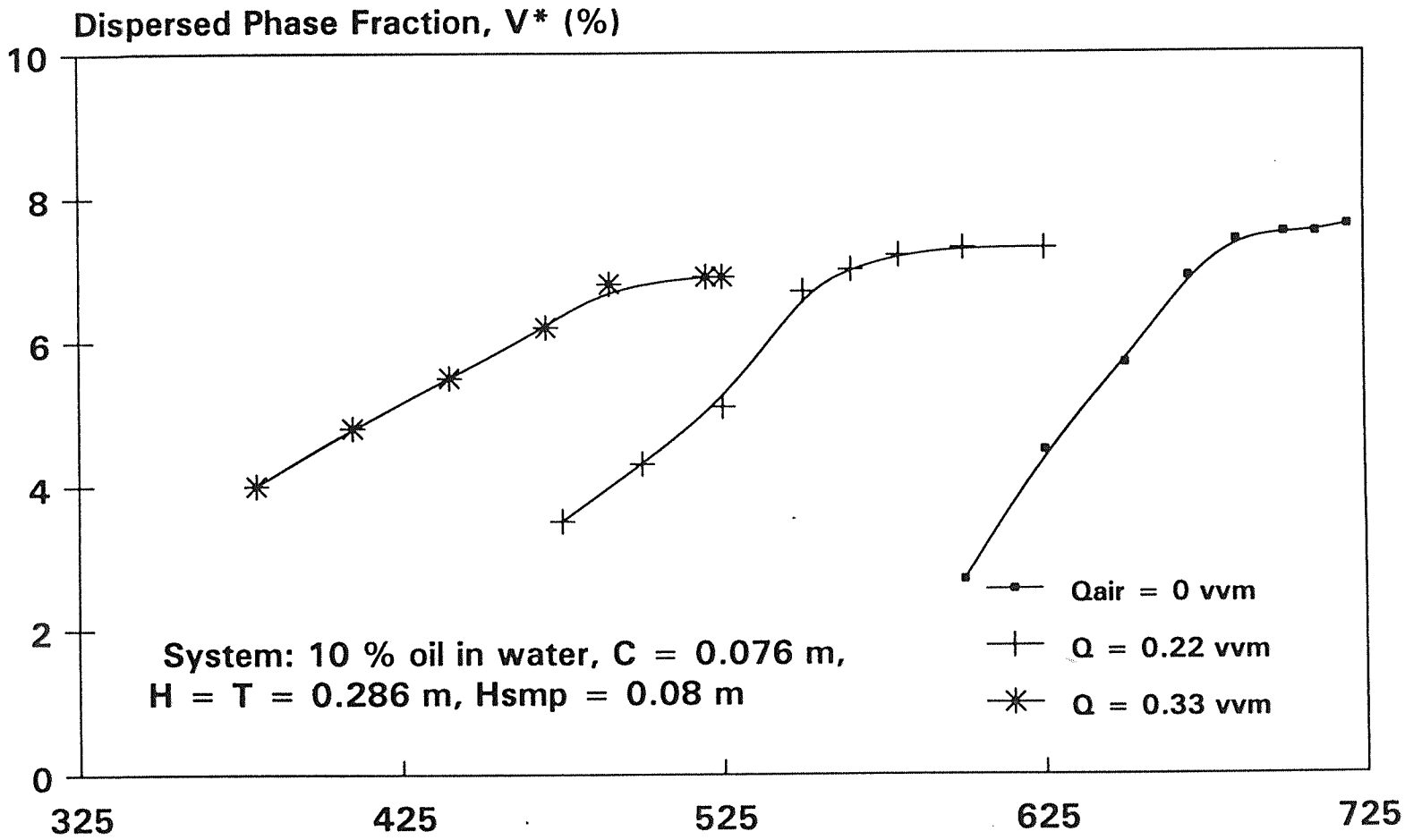

Figure C.19 45-PBT (D = 0.0635 m, Up)

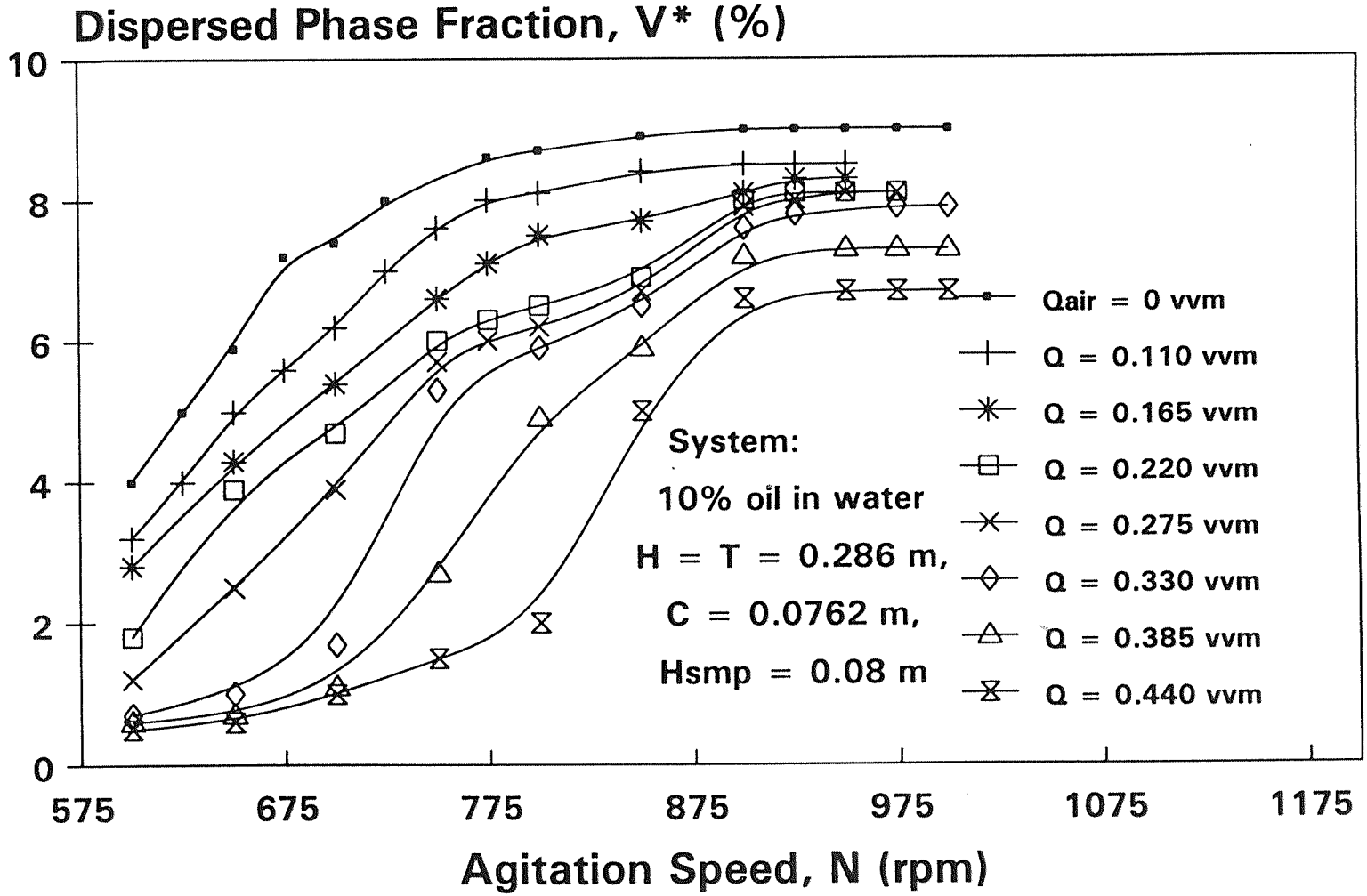

Figure C.20 45-PBT (D = 0.0762 m, Down)

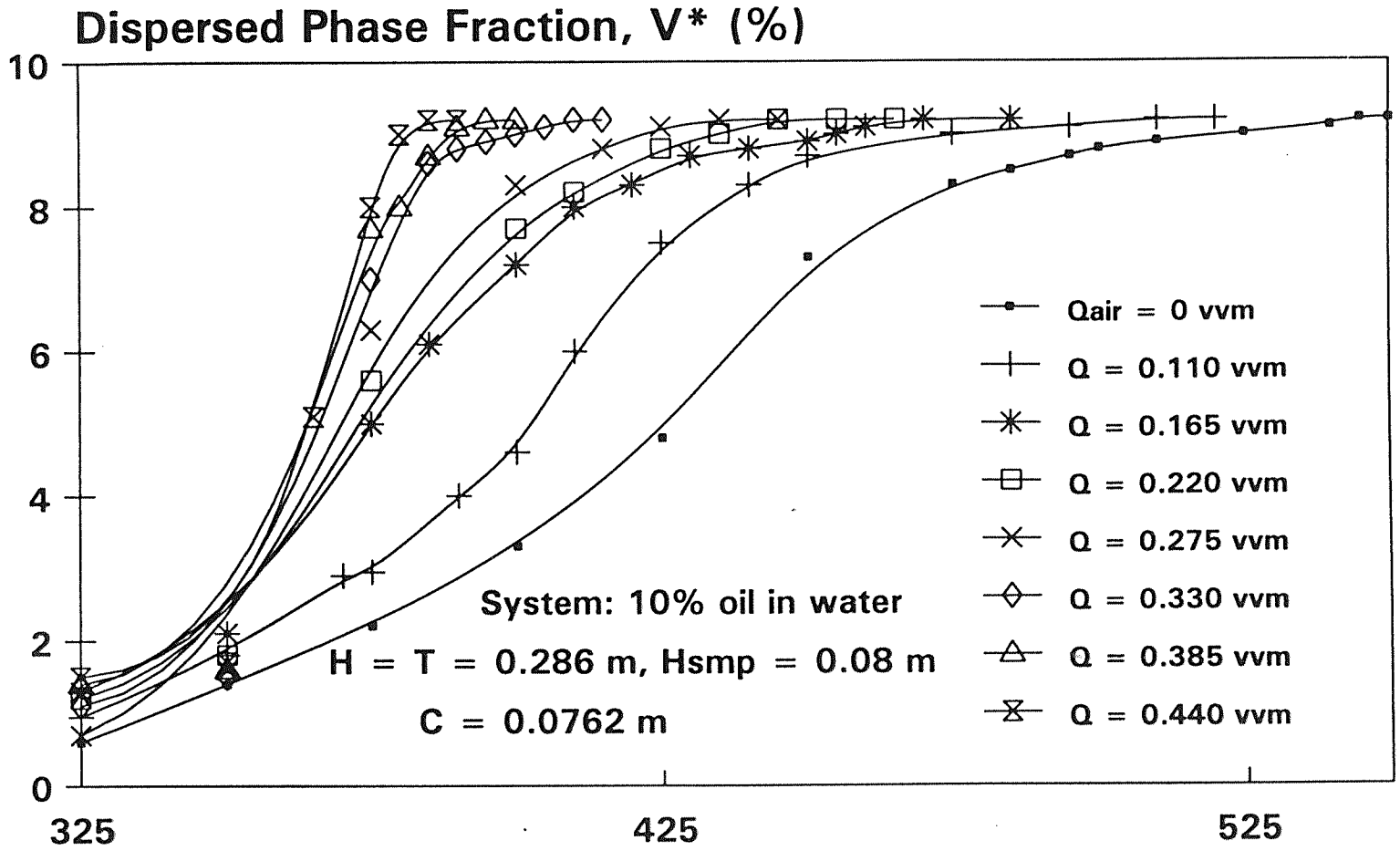

Figure C.21 45-PBT (D = 0.076 m, Up)

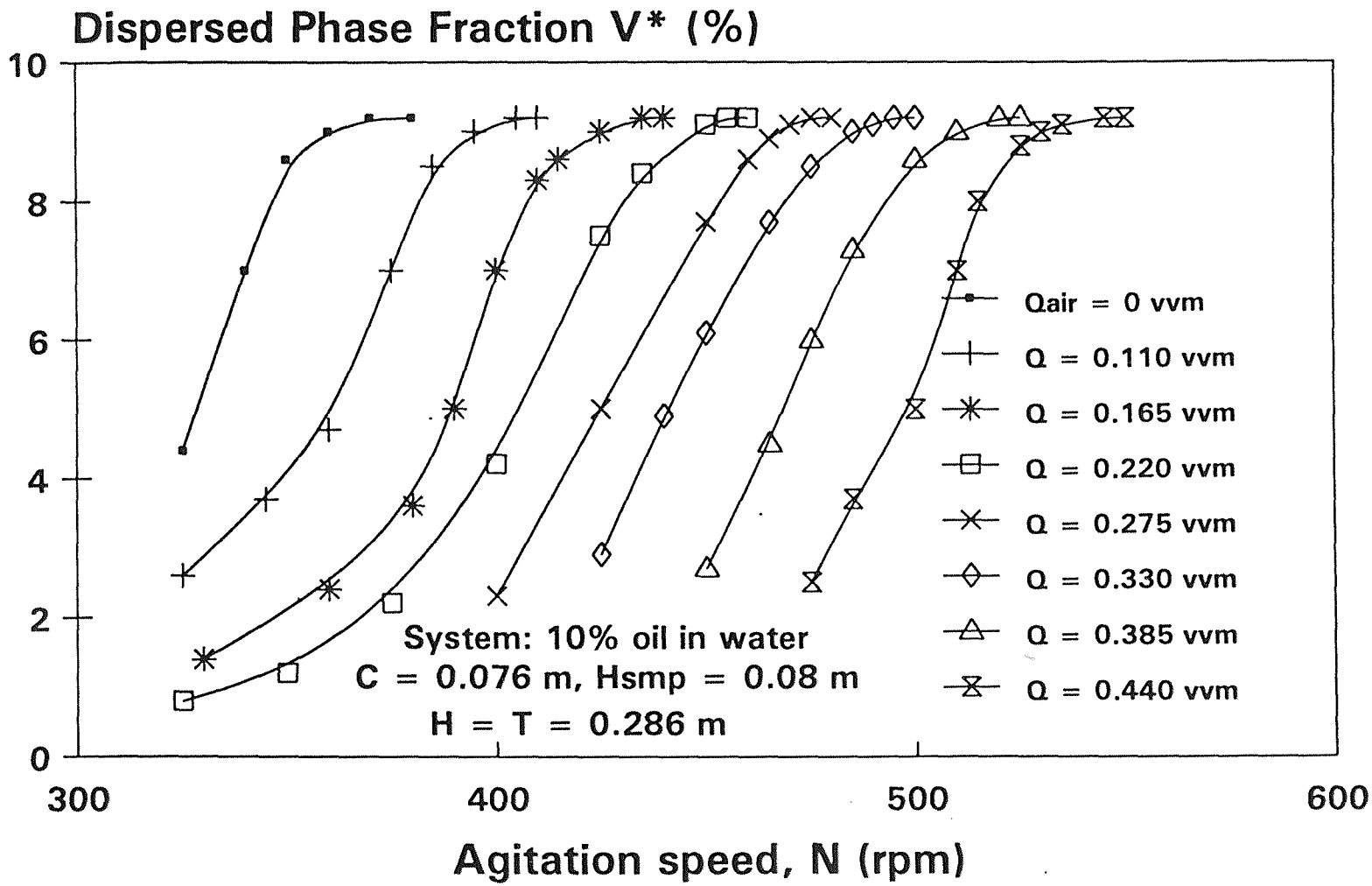

Figure C.22 45-PBT (D = 0.1016 m, Down)

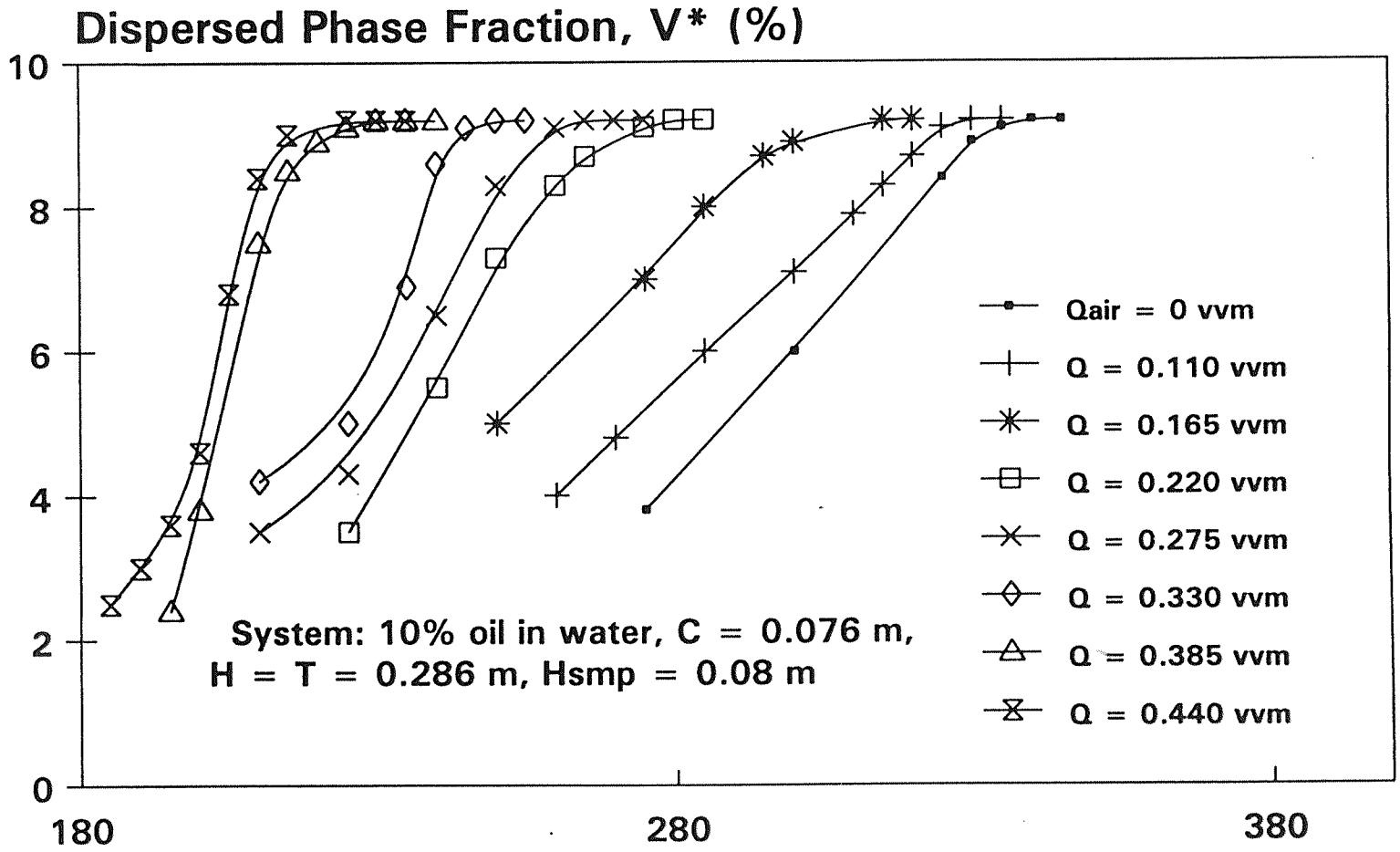

Figure C.23 45-PBT (D = 0.01016 m, UP)

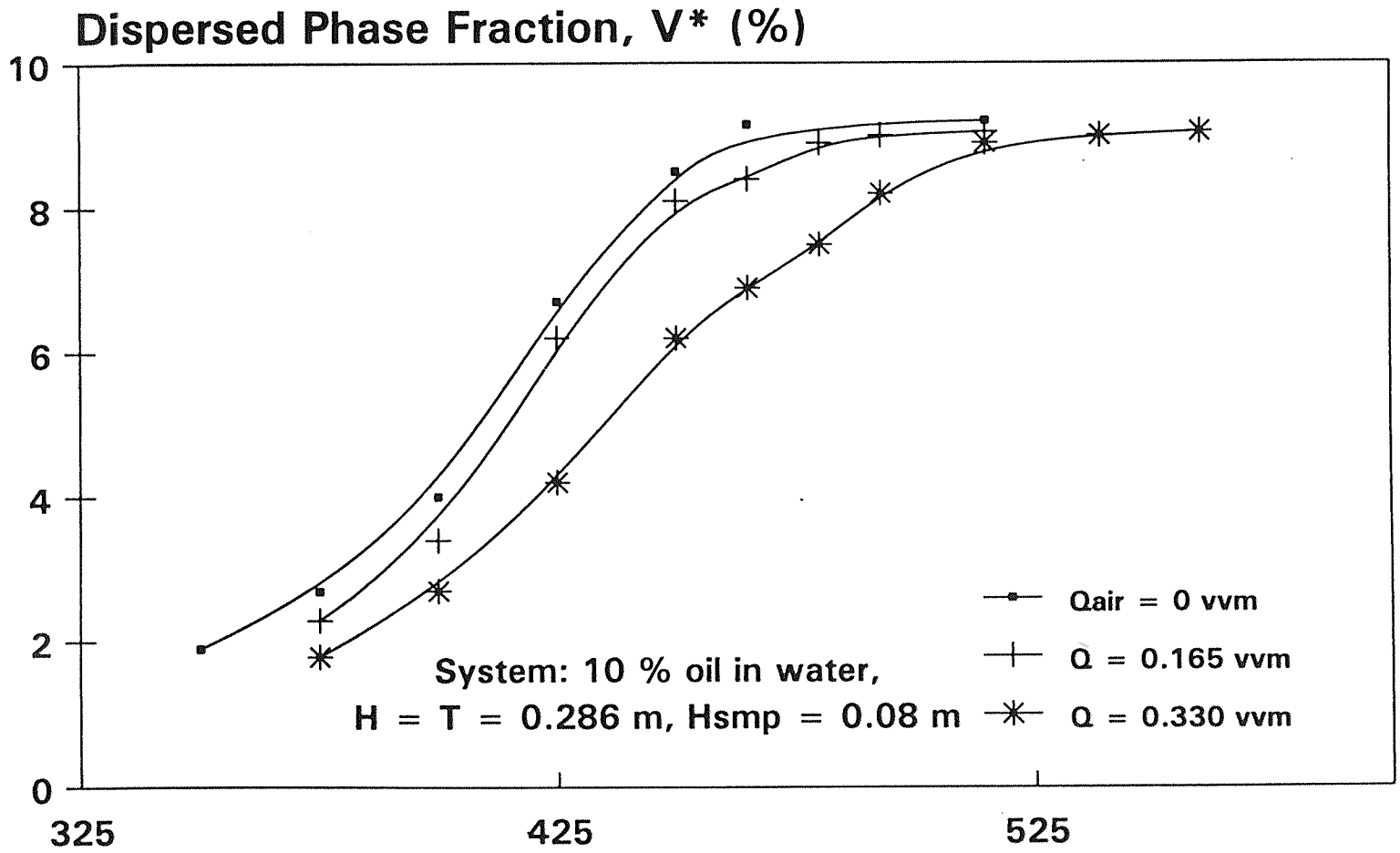

Figure C.24 45-PBT (D = C = 0.1016 m, Dwon)

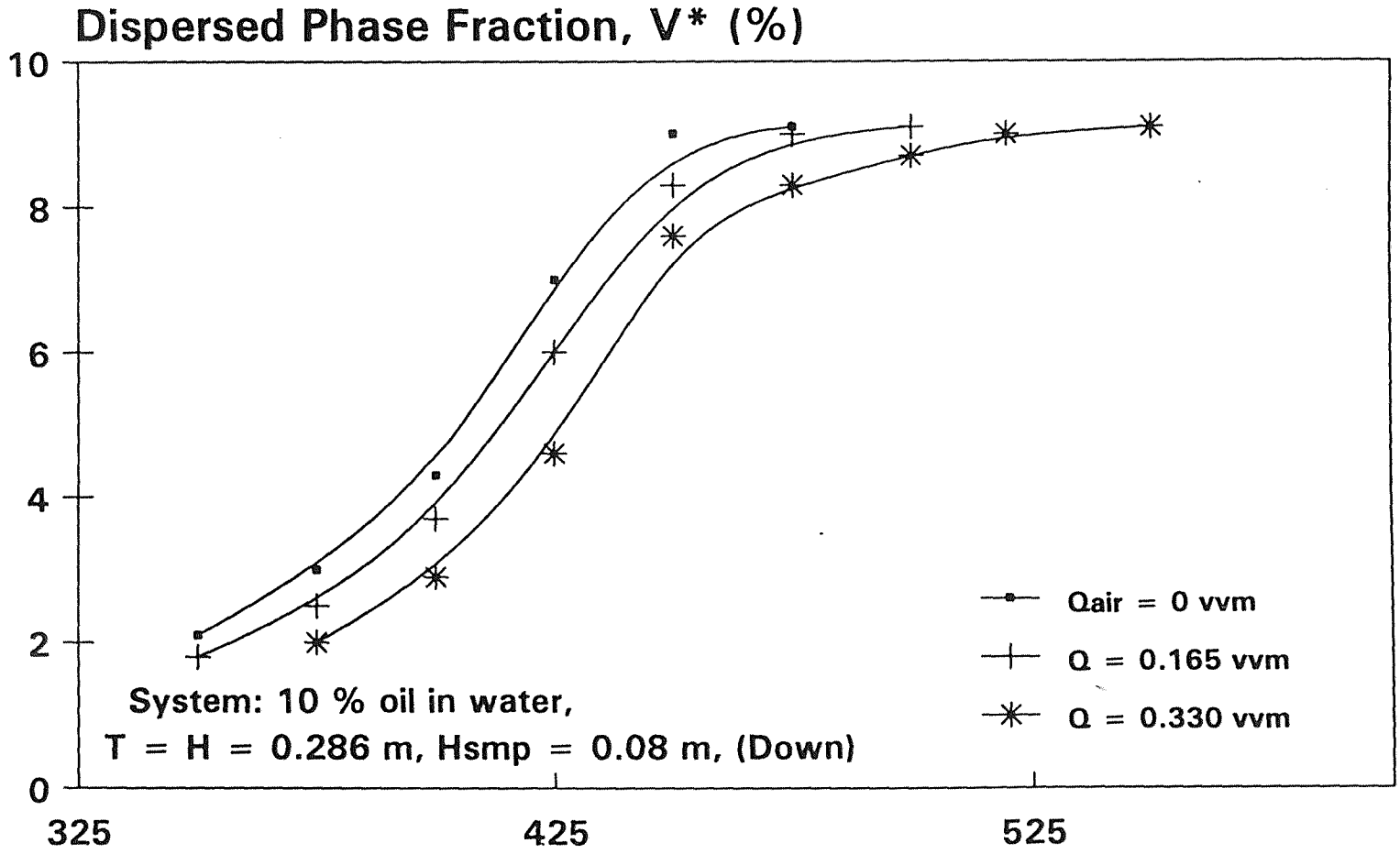

Figure C.25 PBT (D = 0.1016 m, C = 0.136 m)

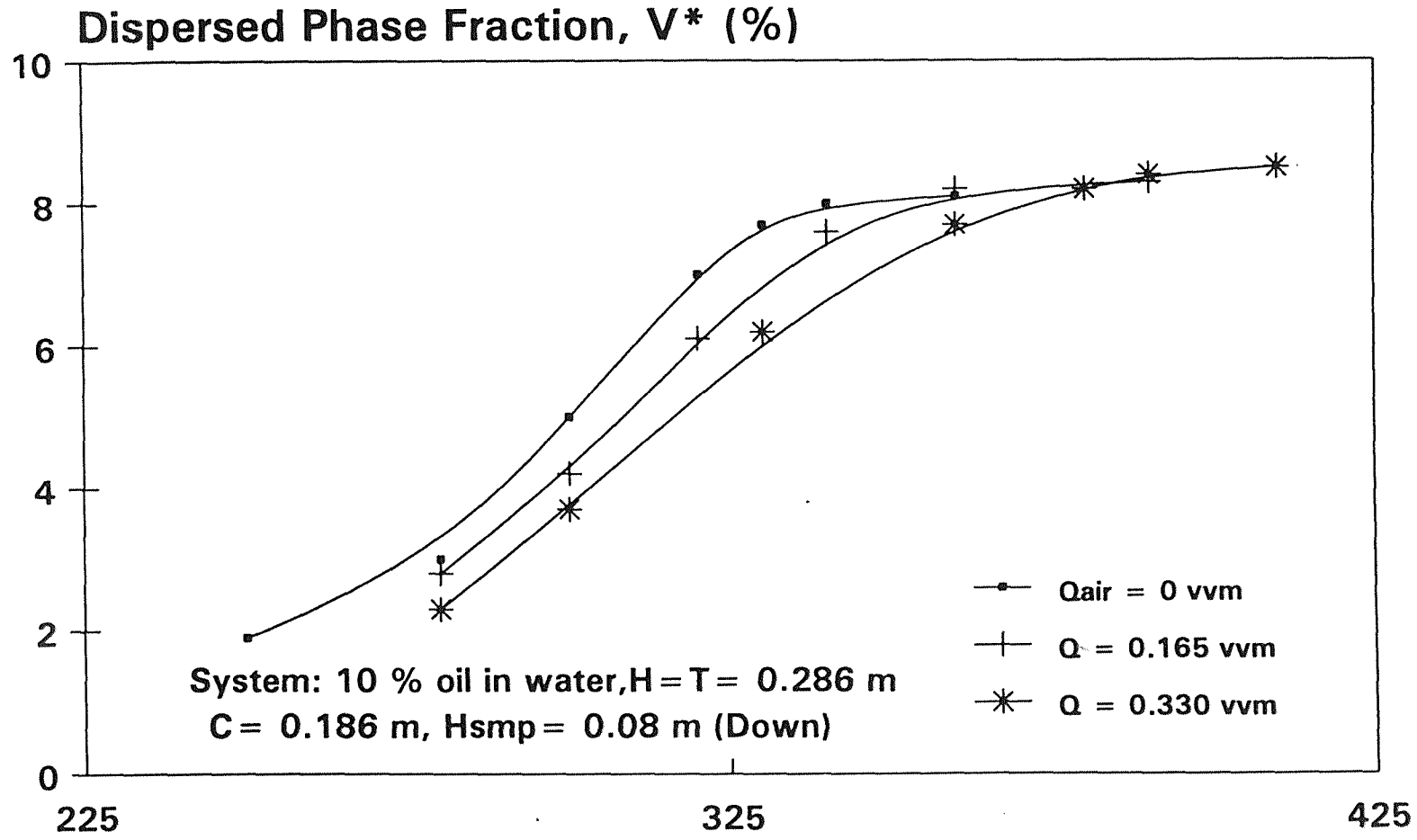

Figure C.26 45-PBT (D = Ct = 0.1016 m)

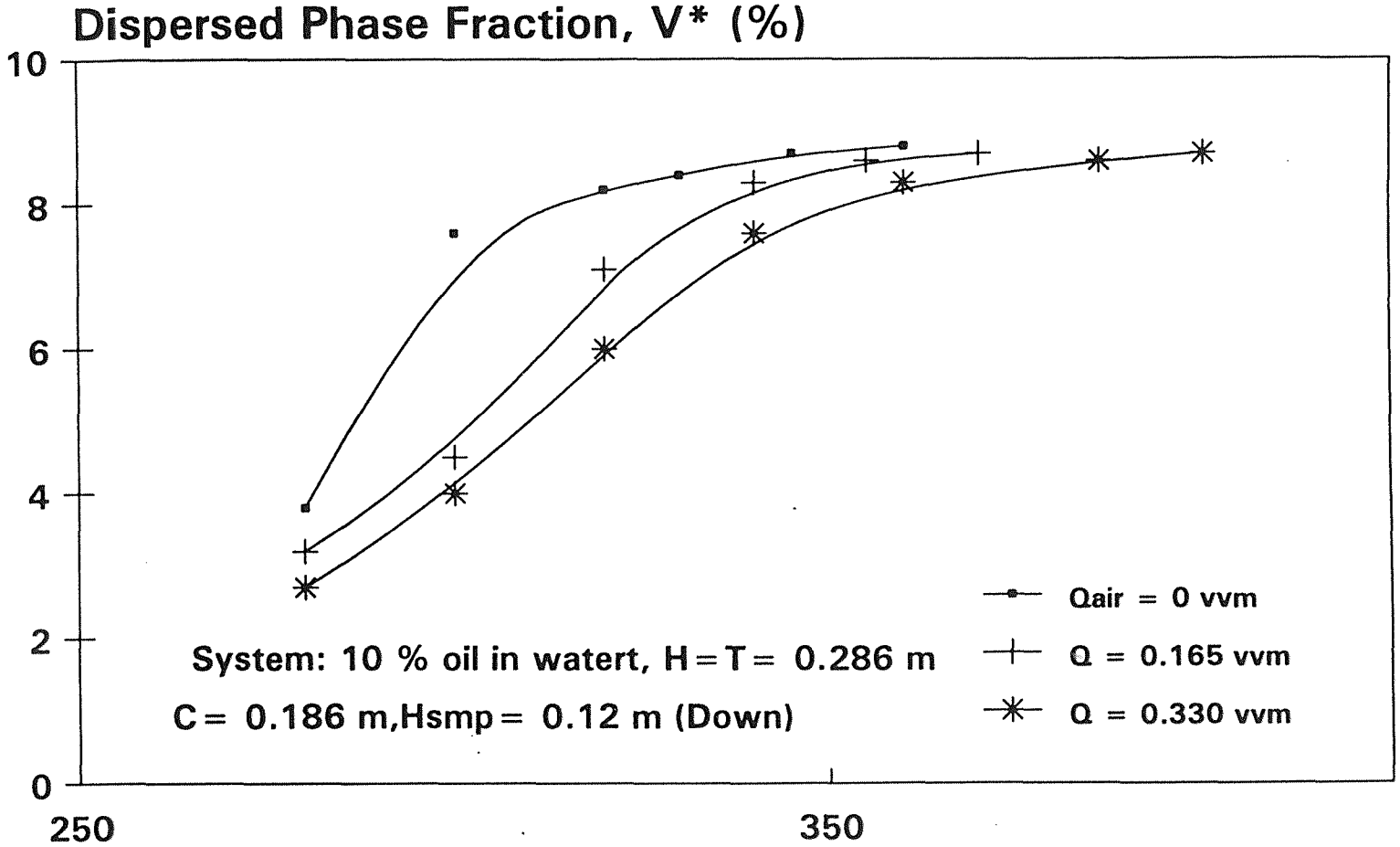

Figure C.27 45-PBT (D = Ct = 0.1016 m)

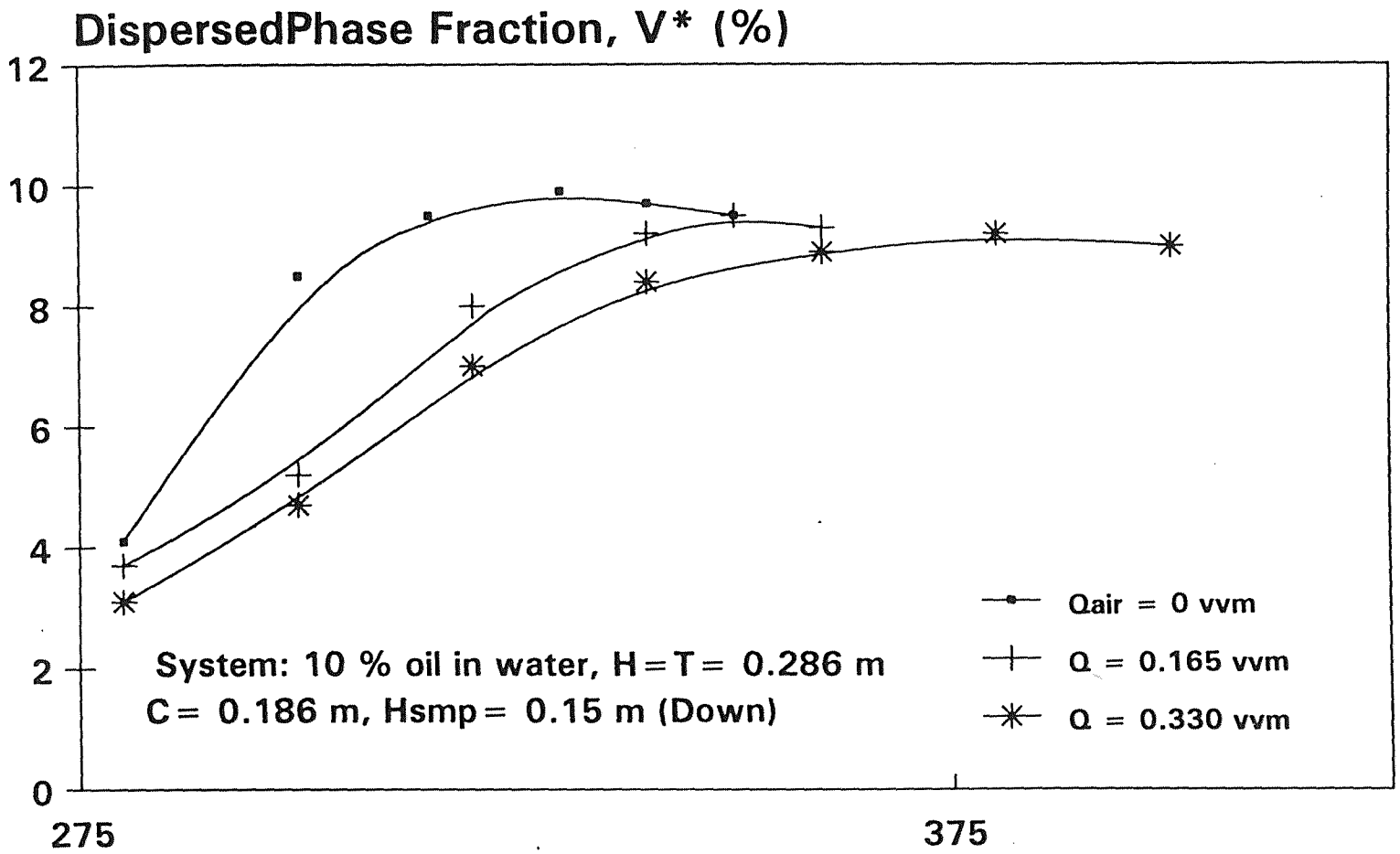

Figure C.28 45-PBT (D = Ct = 0.1016 m)

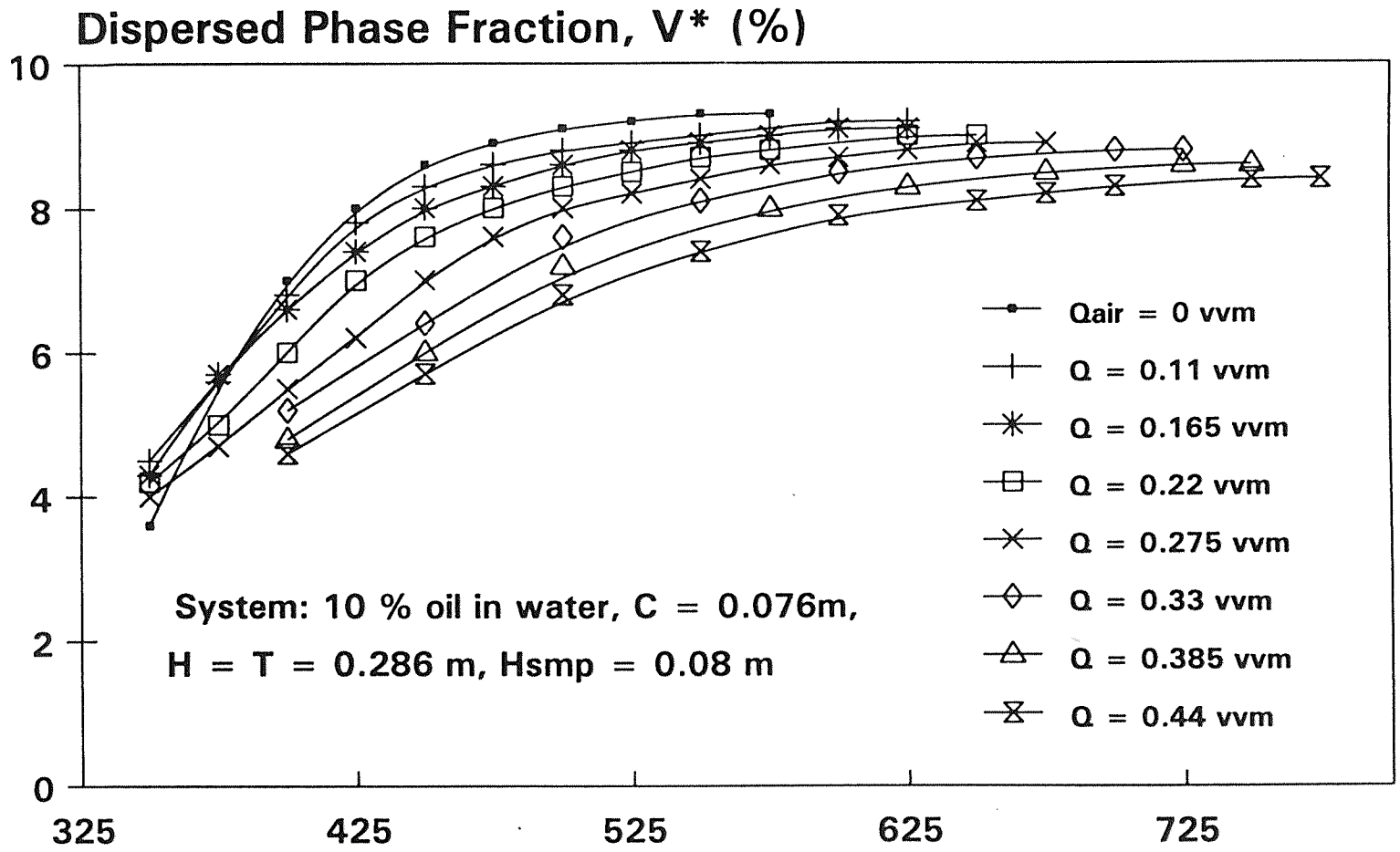

Figure C.29 CBT (D = 0.1016 m)

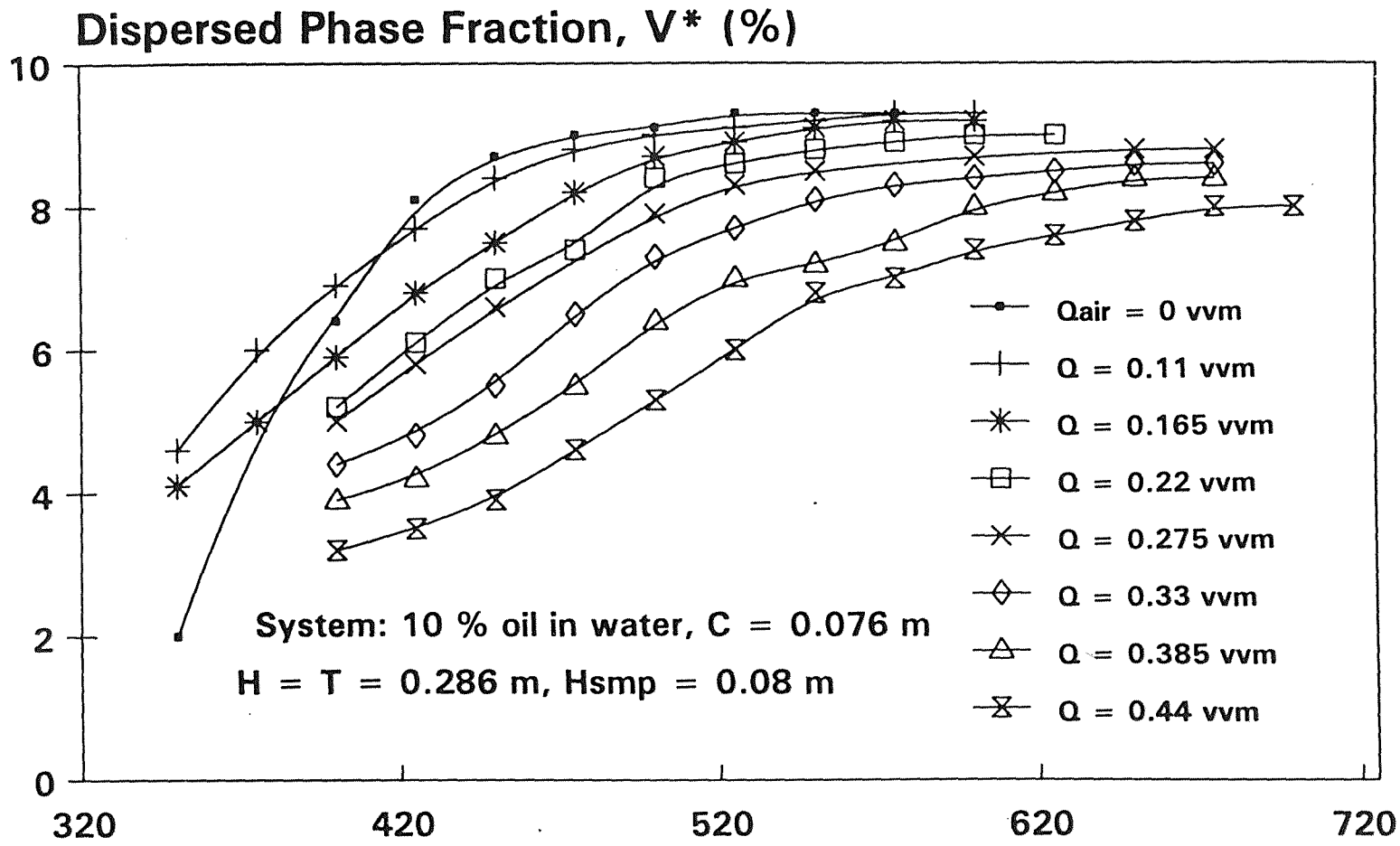

Figure C.30 FBT (D = 0.1016 m)

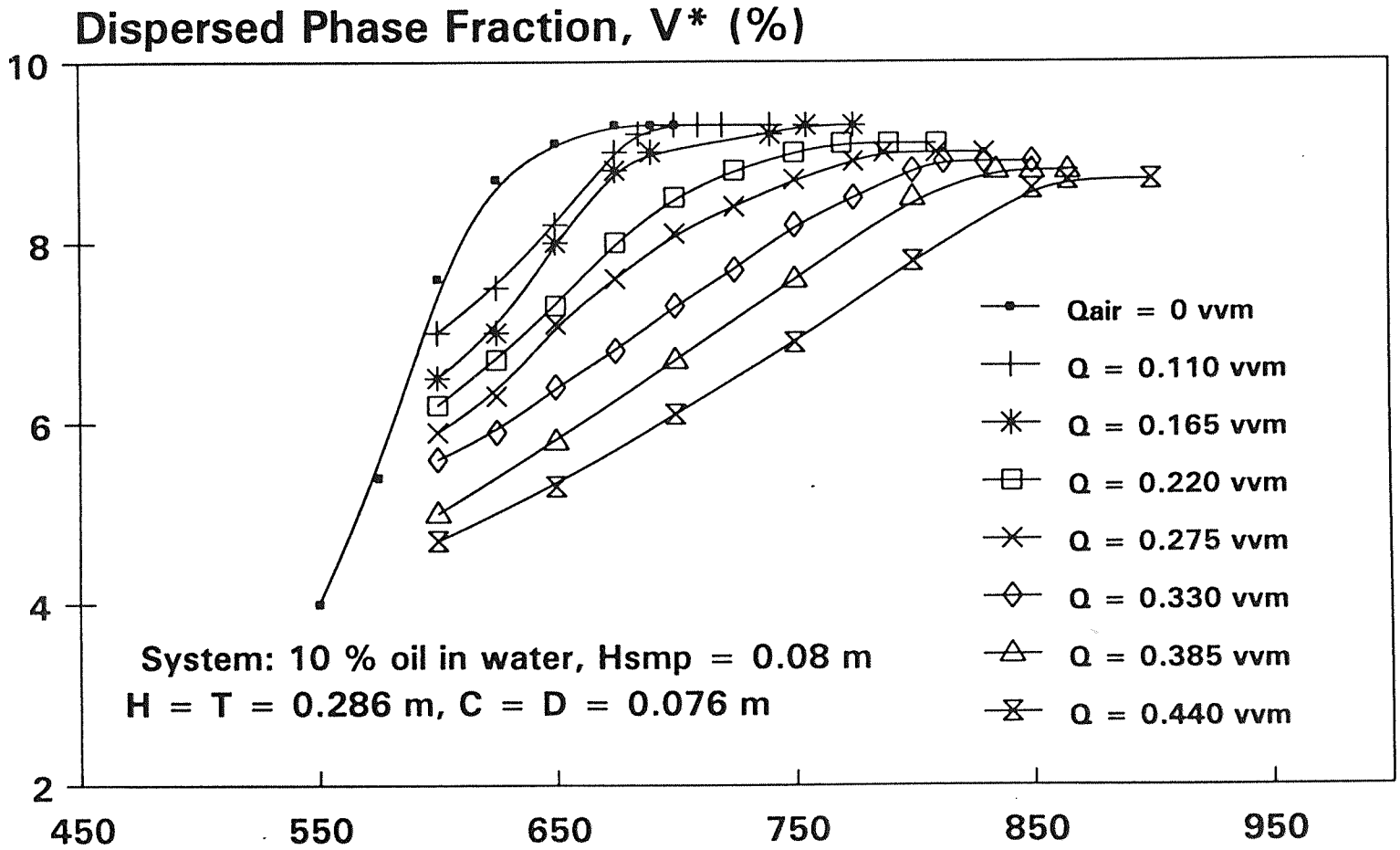

Figure C.31 Propeller (Down)

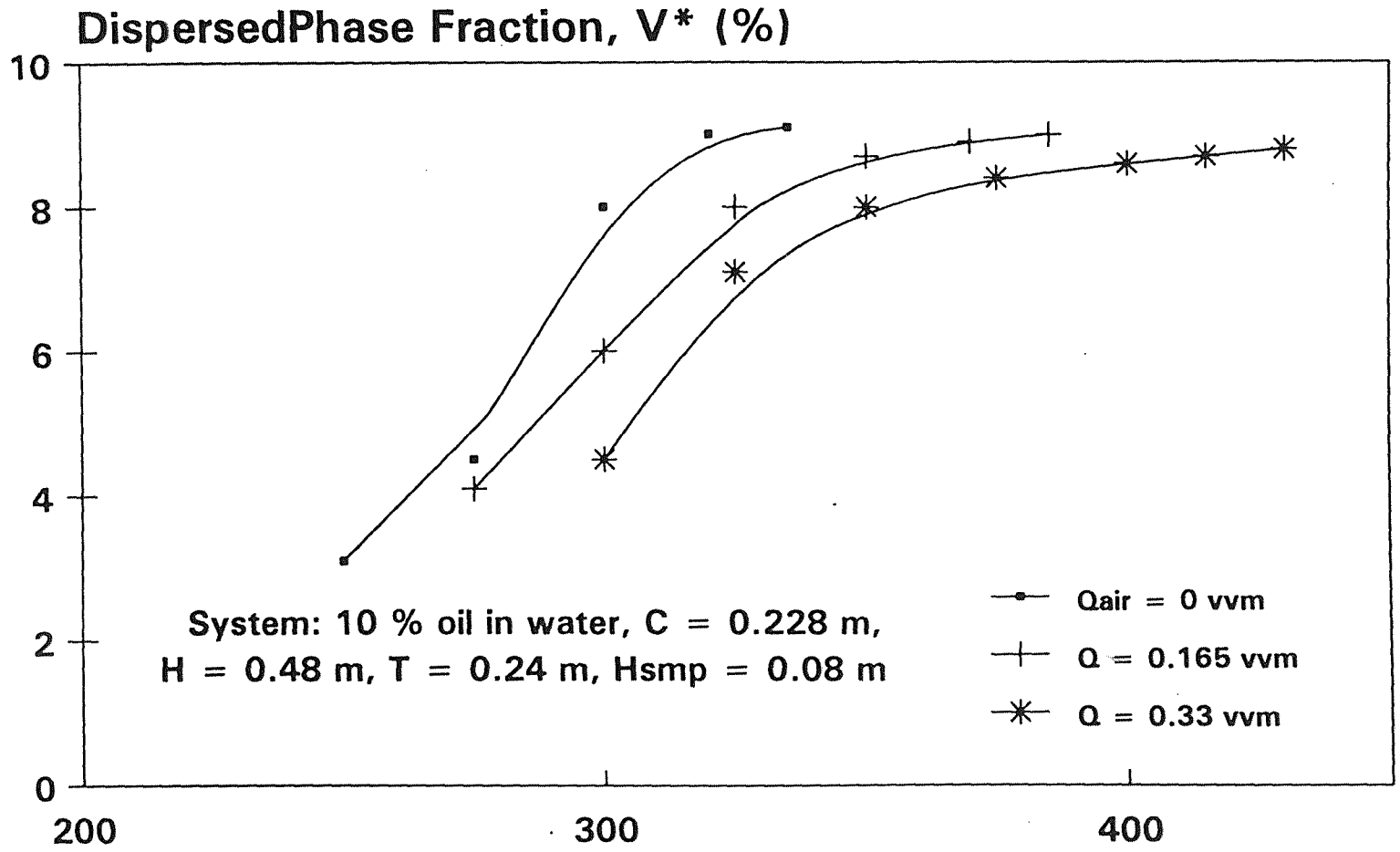

Figure C.32 DT (D = 0.1016 m, H/T = 2)

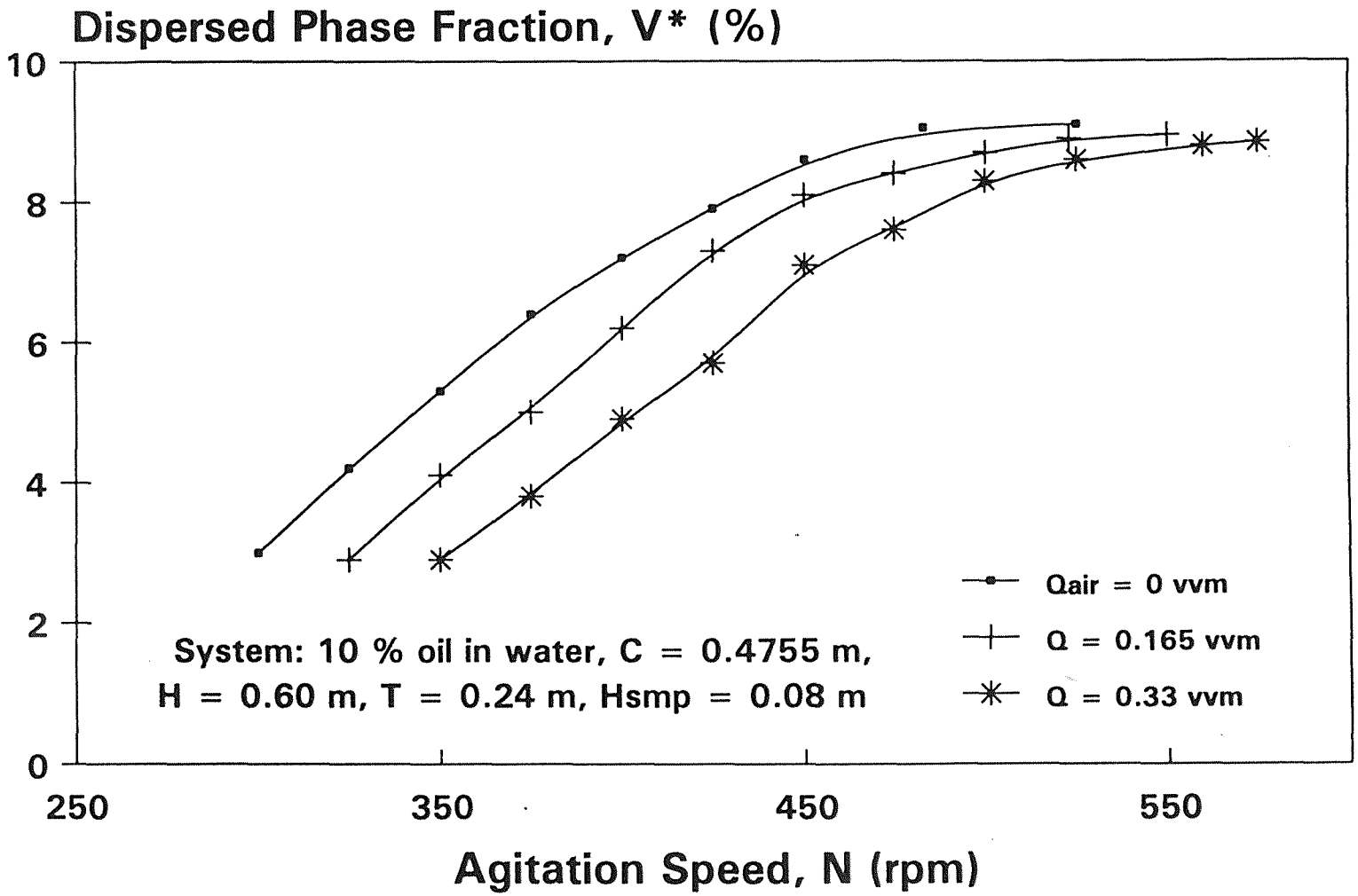

Figure C.33 DT (D = 0.1016 m, H/T = 2.5)

REFERENCES

1. Nagata, S, "Studies on Agitation of two Immiscible Liquids" *Trans. Soc. Chem. Eng.* Japan 8 (1960):43-58

2. Quinn, J. A., and D.B. Sigloh. "Phase Inversion in Mixing of Two Immiscible Liquids." *Can. J. Chem. Eng.* 41 (1963): 15-18.

3. Skelland, A. H. P., and R. Seksaria. "Minimum Impeller Speed for Liquid-Liquid Dispersion in Baffled Vessels." *Ind. Eng. Chem. Process Des. Dev.* 17 (1978): 56-61.

4. Skelland, A. H. P., and J. M. Lee. "Agitator Speed in Baffled Vessels for Uniform Liquid-Liquid Dispersion" *Ind. Eng. Chem. Process Des. Dev.* 17 (1978): 473-478.

5. Skelland, A. H. P., and G. G. Ramsey. "Minimum Agitation Speed for Complete Liquid-Liquid Dispersion." *Ind. Eng. Chem. Res.* 26 (1987): 77-81.

6. van Heuven, J. W. and W. J. Beek. "Power Input, Drop Size and Minimum Stirrer Speed for Liquid-Liquid Dispersion in Stirred Tanks." *Solvent Extr., Proc. Int. Solvent Extr. Conf., Paper* 51 (1971): 70.

7. Armenante, P. M., and Y. T. Huang. "Experimental Determination of the Minimum Agitation Speed for Complete Liquid-Liquid Dispersion in Mechanically Agitated Vessels." *Ind. Eng. Chem. Res.* 31 (1992): 1398-1406.

8. White, A. M., and E. Brenner. "Studies in Agitation v The Correlation of Power Data." *Trans. Ame. Ins. Chem. Eng.* 30 (1934): 585-597.

9. Rushton, J. H., Costich, E. W., and H. J. Everett. "Power Characteristics of Mixing Impellers, Part I." *Chem. Eng. Prog.* 46 (1950): 467-476.

10. Bates, R. L., P. L. Fondy, and R. R. Corpstein. "An Examination of Some Geometric Parameters of Impeller Power." *I&EC Proc. Des. and Dev* 2 (1963): 310-314.

11. Tatterson G. B., *Fluid Mixing and Gas Dispersion in Agitated Tanks. McGraw-Hill, Inc.* NY New York (1991).

12. Smith, J. M. and D. G. F. Verbeek. "Impeller Cavity Development in Nearly Boiling Liquids." *Chem. Eng. Res. Des.* 66 (1988): 39-46.

13. Chapman C. M., A. W. Nienow, M. Cooke, and J. C. Middleton. "Particle-Gas-Liquid Mixing in Stirred Vessel: Part II, Gas-Liquid Mixing." *Trans. Inst. Chem. Eng. (Chem. Eng. Res. Des.)* 61 (1983): 81-84.

14. Michel, B. J, and. and S. A. Miller. "Power Requirements of Gas-Liquid Agitated Systems." *AIChE Journal* 28 (1962): 262-266.

15. Yung, C. N., Wong., C. W., and C. L. Chang. "Gas Holdup and Aerated Power Consumption in Mechanically Stirred Tanks." *Canad. J. Chem. Eng."* 57 (1979): 672-676.

16. Gary, D. J., Treybal, R. E., and S. M. Barnett. "Mixing of Single and Two Phase Systems: Power consumption of Impellers." *AIChE Journal* 28 (1982): 195-199.

17. Warmoeskerken, M. M. C. G., and J. M. Smith. "Flooding of Disc Turbines in Gas-Liquid Dispersion: A New Description of the Phenomenon." *Chem. Eng. Sci.* 40 (1985): 2063-20711.

18. Susanto, J. "Multiphase Solid-Liquid and Solid-Liquid-Gas Mixing." *M S. Thesis,* New Jersey Institute of Technology (1989).

19. Hinze, J. O., *Turbulence, Second Edition. McGraw-Hill Seriese in Mechanical Eng.* (1975)

20. Tsai, D. H., "Agitation Requirement for Complete Dispersion of Emulsion." *M. S. Thesis,* New Jersey Institute of Technology (1988).

21. McCabe, W. L., and C. J. Smith, *Unit Operation of Chemical Engineering, Third Ed. McGraw-Hill Chemical Eng. Series* (1976)

22. ASTM: *D 446-89a* "Standard Specifications and Operating Instruction for Glass Capillary Kinematic Viscometers[1]" (1989)